

**Smart Microgels**  
**for Controlled Uptake and Release**

Yuan Li

**Thesis committee****Thesis supervisors**

Prof. dr. M.A. Cohen Stuart  
Professor of Physical Chemistry and Colloid Science  
Wageningen University

Prof. dr. ir. W. Norde  
Emeritus Professor of Bionanotechnology  
Wageningen University

**Thesis co-supervisor**

Dr. ir. J.M. Kleijn  
Assistant professor, Laboratory of Physical Chemistry and Colloid Science  
Wageningen University

**Other members**

Prof. dr. P. Hansson, Uppsala University, Sweden  
Prof. dr. ir. W.E. Hennink, Utrecht University  
Prof. dr. R.M. Town, University of Southern Denmark, Esbjerg, Denmark  
Prof. dr. ir. M.H. Zwietering, Wageningen University

This research was conducted under the auspices of the Graduate School VLAG

# **Smart Microgels**

## **for Controlled Uptake and Release**

Yuan Li

### **Thesis**

submitted in fulfillment of the requirements for the degree of doctor  
at Wageningen University  
by the authority of the Rector Magnificus  
Prof. dr. M. J. Kropff,  
in the presence of the  
Thesis Committee appointed by the Academic Board  
to be defended in public  
on Friday 21 October 2011  
at 4 p.m. in the Aula.

Yuan Li  
Smart microgels for controlled uptake and release

PhD thesis, Wageningen University, Wageningen, The Netherlands (2011)

ISBN: 978-90-8585-9994



*To my dearest parents*

献给我最最亲爱的父母



## CONTENTS

<b>Chapter 1</b>	Introduction	1
<b>Chapter 2</b>	Preparation and characterization of oxidized starch microgels	17
<b>Chapter 3</b>	Lysozyme uptake by oxidized starch polymer microgels	39
<b>Chapter 4</b>	Mobility of lysozyme inside oxidized starch microgels	63
<b>Chapter 5</b>	Uptake and release kinetics of lysozyme in and from oxidized starch polymer microgels	87
<b>Chapter 6</b>	The antimicrobial activity of lysozyme-loaded oxidized starch microgel	109
<b>Chapter 7</b>	The stabilization of lysozyme-loaded oxidized starch microgel by polyelectrolytes	127
<b>Chapter 8</b>	General discussion	145
	Summary	151
<b>Samenvatting</b>		161
<b>Acknowledgements</b>		165
<b>Curriculum Vitae</b>		171
<b>List of Publication</b>		173



---

# Chapter 1

## Introduction

---

The aim of this thesis is to determine the properties and binding characteristics of a novel biopolymer-based release-on-demand (so-called Bioswitch [1]) microgel. This microgel consists of cross-linked negatively charged potato starch polymer, which interacts with positively charged functional ingredients through electrostatic attraction. The study addresses, in particular, the mechanism of the interaction between microgel and protein (lysozyme) by investigating effects of pH, salt concentration, and amylase degradation on the protein uptake and release process. Before our story begins, this chapter provides a survey of the background and articles review relevant to the topic. It includes polymer gels (emphasizing starch microgels), proteins as functional ingredients (especially antimicrobial peptides and lysozyme), and a short review on electrostatic interactions between (cross-linked) polyelectrolyte and oppositely charged proteins. Finally, the outline of this thesis is presented.

## 1.1 Polymer gels

Gels are diluted cross-linked systems that exhibit interesting mechanical properties ranging from very soft to hard; many gels become fluid-like under stress. Hydrogels are cross-linked polymeric networks capable of absorbing and retaining large quantities of water. Hydrogels are generally classified as two categories based on the nature of the cross-links, either physical or chemical (covalent). Alternatively, depending on the nature of the incorporated functional groups, polymer hydrogels may be classified as neutral [2], cationic [3], anionic [4], amphiphilic [5] or zwitterionic [6]. The use of hydrogels for controlled uptake and release of functional ingredients (e.g., drugs) has been a subject of great interest over the past decades, because their properties allow them to respond to external stimuli, such as temperature [7], pH [8-10], ionic strength [11, 12], solvent [7, 13, 14], or by applying an electric [15] or magnetic field [16]. Hydrogels can be made of both synthetic and natural polymers. Most reported hydrogels are based on synthetic polymers such as poly(N-isopropylacrylamide) (PNIPAM) [16, 17] poly(methacrylic acid) (PMA) [18], poly(N-vinylcaprolactam) (PVCL) [19], poly[2-(diethylamino) ethyl methacrylate] (PDEA) [20] and poly(acrylic acid) (PAA) [21]. Hydrogels from natural polymers such as dextrans [22], pullulan [23], gelatine [24], chitosan [25] and sodium alginate [26] are more attractive for food and biomedical applications, because of their biodegradability and biocompatibility.

Depending on their dimensions hydrogels are often termed macrogels, microgels or nanogels. The notion macrogel usually refers to hydrogels larger than 1 mm. Microgels are commonly meant hydrogels with an average diameter ranging between 50 nm and 100  $\mu$ m [27]. Particles with sizes smaller than about 500 nm are sometimes referred to as nanogels.

Compared to other types of carrier systems, microgels offer unique advantages such as superior colloid stability, fine control over particles size/shape, enhanced responsive behaviour and desired functionality. The first microgels were poly(divinylbenzene) (PDVB) particles prepared by Staudinger and Husemann over 70 years ago [28]. Pelton and Chibante invented the first temperature responsive poly(NIPAM) microgel in 1986 [29]. Since then microgel research started to grow enormously. Microgels are basically prepared by physical and chemical cross-linking methods. Physical cross-linking is usually based on hydrogen bonds, hydrophobic interactions, or electrostatic interactions. Since the crosslink bonds are reversible the resulting gels can restructure and flow during the sol-gel transition. Chemical cross-linking leads to permanent covalent bonds and stable gels. Various heterogeneous polymerization reactions of hydrophilic monomers in the presence of difunctional or

multifunctional cross-linkers have been utilized to prepare well-defined microgels. They include dispersion, precipitation, and suspension (inverse emulsion) polymerization utilizing an uncontrolled free radical polymerization process [30], usually under the conditions of high temperature, or exposure to UV light and radiation.

The most important property of a hydrogel is its swelling capacity. The driving force for swelling of the gel is the free energy of mixing of polymer and solvent. The volume increase is opposed by the elastic energy that results from stretching of the polymer chains in the gel. At equilibrium, these two effects balance each other [31]. Since a large volume change of the gel can be triggered by a change in external conditions, this gives the responsive swelling properties of microgel. For instance, addition of salt can cause polyelectrolyte gels to de-swell. This is because of screening of the charges in the gel by the salt ions. The gel stops de-swelling when all the charges on the gel are screened and the polyelectrolyte gel behaves as a neutral gel. The pH can also affect the swelling of a gel by changing the dissociation of weak acid or base groups on the polyelectrolyte chains. If the total charge on the gel increases, the swelling will increase accordingly due to the repulsion between the polymer chains [32]. The swelling-deswelling transition allows small drug molecules to be incorporated and then released from their interior.

The unique properties of “smart” (i.e., stimuli-responsive) microgel particles make them very useful in all kinds of advanced technological applications such as targeted drug delivery [33, 34], microreactors [35], semiconductors [36], immunosensors [37], optical sensitizers [38] and molecular imprinting [39]. The porous structure of microgels facilitates inclusion of all kinds of functional ingredients. For example, the group of Malmsten encapsulated several positively charged peptides and proteins into negatively charged poly(acrylic acid) and poly(NIPAM-*co*-acrylic acid) microgels, hereby using these microgels as protein/peptides drug carriers [40]. One of the highlights in the research of the group of Hennink, active in the field of drug delivery, is incorporating DNA into polymeric carriers for gene therapy applications [41]. Ballauff and co-workers included metal ions (e.g., Au and Pd) into thermosensitive core-shell microgel particles. They found that the catalytic activity of the incorporated metal ions can be switched on and off through the volume transition of the microgel. In this way it can be used as a controlled microreactor [42]. Apart from the possibility of loading functional ingredients into microgels, the mechanical and rheological properties of a microgel dispersion are potentially interesting for a number of applications, in particular tissue engineering. Saunders et al. [43, 44] studied the fluid-to-gel transitions of pH-responsive microgel dispersions. They showed that the microgel dispersion can be used as

a matrix for load-bearing tissue regeneration. Various other applications for microgels have recently been reviewed by Oh et al. [30], Pich et al. [45] and Das et al. [34]. In the following section, the possible applications of our oxidized starch microgels, e.g., for antimicrobial packaging, will be addressed.

### ***Oxidized potato starch microgels***

Potato is a cheap source for starch. Microgels based on this natural biopolymer are biocompatible and biodegradable. In addition, producing them is generally more environmental friendly than other synthetic polymer gels. Our Bioswitch microgel particles, prepared from oxidized potato starch polymers, are the first of their kind reported in literature. In short the preparation of these microgels is as follows. The starch polymer is first selectively oxidized at the 6-position to obtain a polyglucuronate; the oxidation catalyst is 2,2,6,6-tetramethyl-1-piperidinyloxy (TEMPO). For complete conversion of the primary alcohol groups into carboxyl groups a selectivity of more than 95% was established [46]. Following the procedure developed at TNO (Zeist, The Netherlands) [47], starch polymers of 30%, 50%, 70% and 100% degree of oxidation (DO) were prepared. The DO was controlled by the amount of sodium hypochlorite added during oxidation. Spherical microgel particles (10 – 20  $\mu\text{m}$  in diameter) of cross-linked oxidized starch polymer were synthesized by inverse emulsion cross-linking (see Figure 1.1) [48]. Hexane was used as the continuous phase and Span 80 as the surfactant. Firstly, the starch polymer and the cross-linker sodium trimetaphosphate (STMP) were added to a Span 80 containing hexane solution for pre-emulsification. Then the mixture was passed through a 10  $\mu\text{m}$  (pore diameter) filter membrane in order to obtain a homogeneous size distribution around 10  $\mu\text{m}$ . Subsequently, the starch in the emulsion droplets was cross-linked to make microgel particles by heating to 40  $^{\circ}\text{C}$  while mildly stirring for 40 minutes. Finally, the microgel particles were washed with

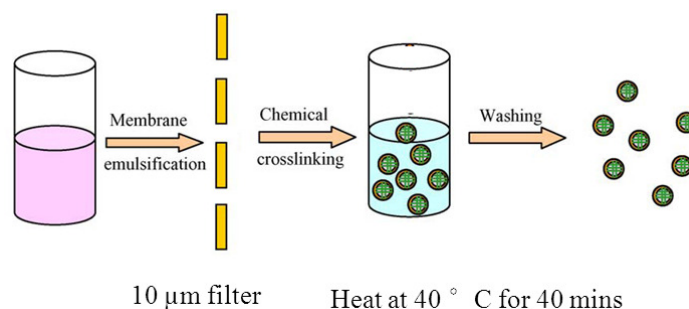


Figure 1.1 Preparation of oxidized starch microgels by inverse emulsion polymerization



methanol by dispersion and centrifugation, followed by decantation of methanol and equilibration in excess water.

Advantages of the Bioswitch microgel are the controlled charge- and cross-linking density, and hence controlled swelling and functional ingredient uptake capacity. As shown in Figure 1.2, the microgel is responsive to environmental changes, such as pH and salt concentration; hence uptake and release of functional ingredients by the gel can also be tuned through solvent conditions.

In this thesis focus is on the protein lysozyme as a functional ingredient. It is anticipated that the lysozyme-starch system has great potential for antimicrobial food packaging [49]. The idea is that exposing lysozyme-containing starch particles to a microbially contaminated environment leads to hydrolysis of the starch by microbial enzymes. As a result, lysozyme is released in the environment where it inhibits microbial growth.

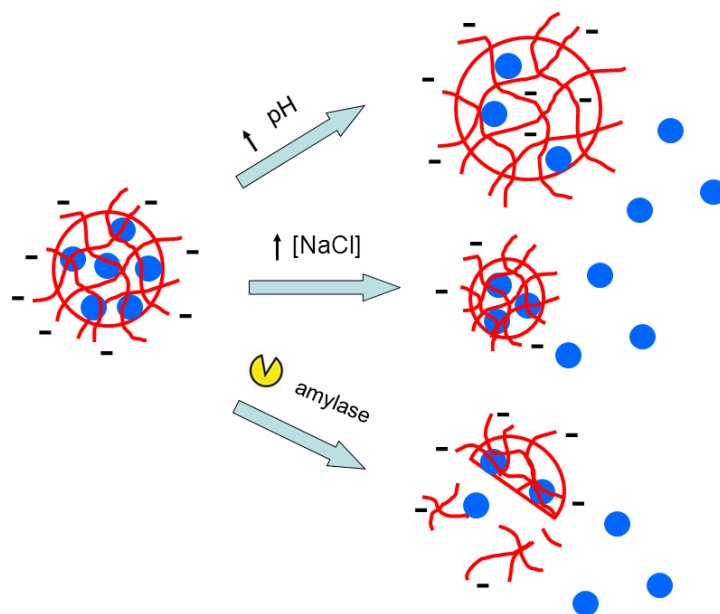


Figure 1.2 Schematic presentation of protein release from oxidized starch microgel triggered by increasing the pH or salt concentration, or by amylase degradation. Responsive gel structure: gel swelling after increasing pH; gel shrinkage after increasing salt; gel break-down after amylase.

## 1.2 Proteins

Proteins are the most diverse and complicated natural polymers, composed of only about twenty different amino acids. A protein consists of one or more long chain molecules made up of amino acids linked by peptide bonds between their carboxyl and amine groups. Depending

on their primary structure (the amino acid sequence encoded by DNA), proteins can organize into a secondary structure ( $\alpha$ -helix,  $\beta$ -sheet,  $\beta$ -turn *etc.*) and then into more complex three-dimensional (tertiary) and multi-molecular (quaternary) structures. The protein structure is stabilized by non-covalent interactions such as hydrogen bonds, electrostatic and hydrophobic interactions, and sometimes also by covalent bonds such as disulfide bridges.

Proteins provide essential functions for every living organism. To name a few, they serve as enzymes for catalysis of biochemical reactions, form structural elements such as collagens, take care of transport of for example oxygen (hemoglobin and myoglobin), of muscle contraction (actin and myosin), and are involved in signalling and regulation (hormones) and the immune system (immunoglobulins).

### ***Antimicrobial peptides***

Antimicrobial peptides (AMPs) are small (12 - 60 amino acid residues) peptides, which are effective defensive weapons for animals and plants against a wide range of microbes, including bacteria, fungi, virus and protozoa [50, 51]. These peptides are composed of hydrophilic, hydrophobic and cationic amino acids arranged in a molecule that can organize into an amphiphilic structure [52]. This structure allows them to attach to and insert into lipid membrane bilayers. The mechanism of AMPs killing bacteria is complex, and a commonly recognized model is the Shai-Matsuzaki-Huang (SMH) model [53-55]. This model proposes that positively charged AMPs interact with the negatively charged lipid cell membrane of bacteria through electrostatic interactions, followed by alteration of the membrane structure, and entry of the peptide into the interior of the cell. Investigation of AMPs is extremely relevant for designing new anti-infective drugs. However, AMPs may suffer from chemical and proteolytic degradation in many conditions associated with bacterial infections. Therefore encapsulation of AMPs by protective carriers, e.g., polyelectrolyte gels, can improve the efficacy of these antimicrobial drugs. Extensive and excellent work on the interaction between AMPs and oppositely charged polyelectrolyte microgels has been performed by Malmsten and co-workers [56-59].

### ***Lysozyme***

Lysozymes are hydrolytic enzymes, able to cleave the  $\beta$ -(1,4)-glycosidic bond between *N*-acetylmuramic acid and *N*-acetylglucosamine in peptidoglycan, the major bacterial cell wall polymer. Because of this antimicrobial activity they are widely used as a preservative in foods and pharmaceuticals [60]. Lysozyme is abundant in a number of animal secretions [61],

such as tears, saliva, milk and mucus, and also exists in cells and tissues of virtually all living organisms and viruses [62]. Large amounts of lysozyme can be found in hen egg white (HEWL), which is the primary source for lysozyme production in industry. All of its polar groups are at the outside of the compact globular molecule and the majority of the hydrophobic groups are buried in the interior. Four disulfide bonds make this small single-polypeptide chain enzyme unusually compact and highly stable. At least two of the S–S bonds must be intact to maintain its enzymatic activity and thermal stability [63].

Lysozyme (HEWL) has a very high isoelectric point of pH 11 (below pH 11 it carries a net positive charge). Its molar mass is 14.6 kDa and its dimensions are  $4.5 \times 3 \times 3 \text{ nm}^3$  [64]. Because of its well-known and unique physical chemical properties lysozyme has been used as a model protein in a variety of studies in the areas of physical-chemistry, protein chemistry, crystallography, enzymology and molecular biology. Because of its antimicrobial action and since lysozyme is highly positively charged over a wide pH range, we use lysozyme as model protein to investigate the interaction with the negatively charged starch microgel. After encapsulation of the lysozyme by the starch microgel particles, their antimicrobial activity on some amylase-producing bacteria strains has been tested.

### **1.3 Electrostatic interactions between (cross-linked) polyelectrolytes and proteins**

#### ***Polyelectrolyte complex coacervate***

When polycations and polyanions are mixed polyelectrolyte complexes are formed. Depending on the relative concentrations this may lead to two separated phases, a condensed polyelectrolyte coacervate phase in equilibrium with a dilute polymer phase. The electrostatic attraction between oppositely charged polyelectrolytes contributes significantly to the complex formation, and for weak polyelectrolytes proton exchange also contributes. The behaviour of such complexes and the latest research in this field were recently reviewed by Van der Gucht et al.[65].

Proteins may be considered as weakly charged polyelectrolytes. The interaction between proteins and oppositely charged polyelectrolytes is important in food formulation. For example, systems of gum Arabic/gelatin [66], xanthan/gelatin [67], pectin/ $\beta$ -lactoglobulin [68], and carrageenan/whey protein [69] have been studied extensively because they are of practical interest. The stoichiometry of the complexes is (mainly) ruled by the charge

densities of the polyanions and polycations, which are generally pH dependent. Girod et al. [70] found that complexes of poly (L-lysine) and  $\iota$ -carrageenan have a charge ratio of 1:1. The salt concentration is critical for the complex formation. Salt screens the electrostatic interactions between the oppositely charged macromolecules. At high salt concentration, the complexes dissociate completely and no phase separation occurs. On the other hand, also at very low salt concentration ( $< 10$  mM), complex formation may sometimes be suppressed. The reason may be that when the Debye length ( $\kappa^{-1}$ ) is larger than the protein (radius about 3 nm), which is the case at low salt concentrations, an effective electrostatic repulsion between protein molecules exists [71]. Weinbreck et al. [72] studied the complex formation in gum Arabic/whey protein systems by light scattering techniques, and they found that phase transitions occurred at three specific pH values. Other experimental results [73] and Monte Carlo simulations [74] showed two critical pH values ( $\text{pH}_c$  and  $\text{pH}_\phi$ ) for the process of complex coacervate formation: at  $\text{pH}_c$  intrapolymeric soluble complexes form, between  $\text{pH}_c$  and  $\text{pH}_\phi$  soluble and insoluble complexes exist, and at  $\text{pH}_\phi$  coacervates form and give rise to macroscopic phase separation. Weinbreck et al. [75] studied the microstructure of coacervate suspensions from whey protein and gum Arabic. They described the coacervate as a concentrated dispersion of gum Arabic chains electrostatically crosslinked with whey proteins. They found a high maximum in viscosity as a function of pH and this was attributed to a maximum in the attractive electrostatic interactions between protein and polyelectrolyte.

Complexes are not only formed between oppositely charged proteins and polyelectrolytes. Wittemann et al. [76] found that anionic polyelectrolytes and proteins can form soluble complexes even above (“at the wrong side of”) the iso-electric point of the proteins. They argued that this is due to patches of positive charges on the surface of the proteins. An alternative (or additional) explanation is that charge regulation takes place [77]: one of the macromolecules adapts its charge as a response to the potential of the other so that the electric repulsion turns into an attraction. Complex coacervation of proteins and anionic polysaccharides have been excellently reviewed by de Kruif et al. [78], with respect to phase behaviour, composition and complex structures, rheological properties and with emphasis on complexes formed by milk proteins and polysaccharides. The review of Turgeon et al. [79] focuses on phase-ordering kinetics, thermodynamics and structural aspects of protein and polysaccharides, in order to identify important parameters to control phase separation of proteins and polysaccharides in complex mixtures. De Vries and Cohen Stuart [80] reviewed theories and simulations of macro-ion complex formation, emphasising linear/cylindrical (flexible, semi flexible polyelectrolyte) and spherical/globular macro-ions (colloids, micelles,

globular proteins). They discussed soluble complexes, dense complex phases, and micelles with dense complex coacervate cores, stabilized by neutral hydrophilic chains. In their review Cooper et al. [81] put more stress on the heterogeneity of charges in both macro-ions, arguing that this provides a more realistic depiction of proteins. They also discussed the interaction between proteins and polyelectrolyte multilayers and brushes. In addition, they described recent developments in investigation methods and novel applications of protein/polyelectrolyte complexes.

### ***Interaction between cross-linked polyelectrolyte and proteins***

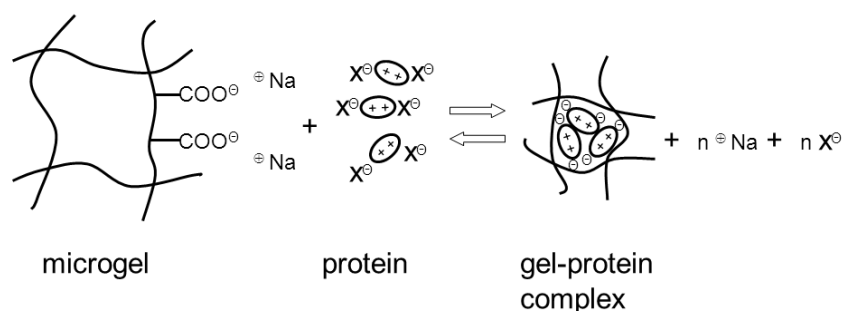


Figure 1.3 Schematic representation of the complex formation between a microgel and an oppositely charged protein at a pH value below the isoelectric point of the protein. An equivalent number of simple counterions originally neutralizing the protein molecules ( $X^-$ ) and the microgel network ( $Na^+$ ), is released.

As compared to complex formation between polyelectrolytes and proteins in solution, protein uptake by cross-linked polyelectrolytes (i.e., gels) involves a number of additional aspects, such as the swelling and de-swelling of the network, changes in excluded volume interactions, and osmotic pressure. Figure 1.3 demonstrates the interaction between a microgel and an oppositely charged protein. As a result of protein binding to the gel network, and (partial) neutralization of its charges, the gel de-swells to a certain degree. For a slightly cross-linked hydrogel system, Kabanov et al. [82] concluded that the driving force for protein uptake is similar to that for a linear polyelectrolyte: it is the increase in entropy of released counterions that drives formation of the cross-linked polyelectrolyte-protein complex. However, the combination of phase separation and gel elasticity may give rise to complicated effects: at intermediate stages of complex formation these authors [82] found a morphology consisting of an outer weakly swollen complex shell and a highly swollen hydrogel core. For slightly cross-linked poly (acrylic acid) microgels (60 - 80  $\mu m$ ), such a “core-shell” formation

was also found by Johansson et al. [83, 84]. They found that the uptake process of lysozyme could be divided into two steps, firstly the shell formation combined with de-swelling of the outer part of the microgel and with no protein diffusing into the core. In the second phase, microgel de-swelling is negligible and lysozyme diffuses into the microgel core. Bysell and Malmsten [85] studied the uptake of poly-L-lysine by poly(acrylic acid) (PAA) microgels (50 - 150  $\mu\text{m}$ ) as a function of pH, ionic strength, size of the peptides and peptide concentration. They found that shell formation and de-swelling occurred, but only for poly-lysine sizes above 28 kDa. Eichenbaum et al. [86] reported that protein loading of poly (methacrylic acid-co-acrylic acid) microgels (4 - 10  $\mu\text{m}$ ) strongly depends on the cross-link density and the pore size of the microgel. They showed that the protein cannot enter the gel if its size is larger than the average pore size of the network. Environmental conditions such as the pH and salt concentration affect the interaction between microgel and protein. Johansson et al. [83] found that the lysozyme binding capacity of their poly (acrylic acid) microgel is higher at pH 7 than that at pH 4.5 as a result of the higher charge contrast between the protein and microgel at pH 7. They also found that the binding capacity increases with decreasing ionic strength, due to the electrostatic screening at high ionic strength.

## 1.4 Outline of this thesis

The work described in this thesis focuses on the uptake of the protein lysozyme in and its release from the Bioswitch oxidized starch microgels, the control over these processes by variation of environmental conditions (pH, salt concentration) and the release by (microbial) amylase activity. The results provide important guidelines for efficient loading and controlled release of functional ingredients from these novel carrier systems.

In **Chapter 2** we describe the preparation of the oxidized starch microgels; its physical-chemical properties are characterized in terms of charge density, electrophoretic mobility and swelling capacity as a function of cross-link density, pH and salt concentration.

In **Chapter 3** the optimum conditions for lysozyme uptake by oxidized starch microgels are explored. We first determined the binding affinity of lysozyme to microgels of various degrees of oxidation (DO). Then we focus on the DO100% microgel, of which we measured the saturation uptake capacity at various pH values and salt concentrations. In addition, the de-swelling ratio of the gel particles as a result of protein absorption and the colloidal stability of the gel-protein complexes at different pH values were investigated. Finally, the charge regulation between microgel and protein during absorption process has been determined.

In **Chapter 4** we extend our study to the mobility of lysozyme inside spherical DO30% oxidized starch microgels. For this we made use of fluorescently labelled protein and studied the exchange reaction between bleached and unbleached protein molecules inside the gel. To analyse the results we developed a model and we identified several protein fractions of different exchange rates. It was found that increasing the salt concentration (NaCl) or the pH causes a shift in the distribution towards the more mobile fractions. This is consistent with the binding affinity and uptake results described in Chapter 3.

The subject of **Chapter 5** is the kinetics of lysozyme uptake in and release from the microgel particles. The results were analysed using a model based on diffusion, taking into account the equilibrium exchange between protein bound to the gel matrix and free protein in the pores of the gel. The results are in line with the findings from the absorption and mobility studies in Chapter 3 and 4, showing a sharply decreasing affinity and increasing mobility with increasing ionic strength. We also briefly explored the effect of amylase. This enzyme was found to completely break down the oxidized starch microgel, which results in the release of the embedded protein into solution.

In **Chapter 6** we studied the antimicrobial activity of lysozyme release from amylase-degradable DO30% microgel against several bacteria strains. The starch gel-lysozyme particles exhibit an antibacterial activity and they were successfully employed in both solid agar plates and in liquid suspension media. The promising results confirm the original hypothesis that the use of starch gel-lysozyme particles opens a new approach in antimicrobial applications. The previous studies indicate that protein release by increasing the salt concentration is quite fast (see minutes time scale), which is not always desirable in application. To slow down the protein release from the gel, we successfully built a poly-lysine/poly-glutamic acid complex layer around lysozyme-loaded microgel. This is described in **Chapter 7**. It was found that the layer also protects the gel-lysozyme particles against amylase-degradation. This is extremely useful for applications where the release kinetics have to be controlled, and incorporated functional ingredients have to be protected from enzymatic degradation. **Chapter 8** gives a general discussion on the results of this thesis. A summary of this dissertation is presented in the end.

## References

- [1] H.M.W.M. Thijssen, R. C. ;Timmermans, J. W. ;Van Veen, J. J. F. , Inducible release vehicles. Eur.Patent EP1628529, 2006.
- [2] M. Andersson, S.L. Maunu, Structural studies of Poly(N-isopropylacrylamide) microgels: Effect of SDS surfactant concentration in the microgel synthesis, *J. Polym. Sci. Pt. B-Polym. Phys.*, 44 (2006) 3305-3314.
- [3] K.S. Kim, B. Vincent, pH and temperature-sensitive behaviors of poly(4-vinyl pyridine-co-N-isopropyl acrylamide) microgels, *Polym. J.*, 37 (2005) 565-570.
- [4] T. Hoare, R. Pelton, Functional group distributions in carboxylic acid containing poly(N-isopropylacrylamide) microgels, *Langmuir*, 20 (2004) 2123-2133.
- [5] H. Ni, H. Kawaguchi, T. Endo, Preparation of amphoteric microgels of poly(acrylamide/methacrylic acid/dimethylamino ethylene methacrylate) with a novel pH-volume transition, *Macromolecules*, 40 (2007) 6370-6376.
- [6] S. Nayak, L.A. Lyon, Synthesis and characterization of zwitterionic thermosensitive microgels, *Abstr. Pap. Am. Chem. Soc.*, 226 (2003) 279-287.
- [7] Q.F. Luo, P.X. Liu, Y. Guan, Y.J. Zhang, Thermally Induced Phase Transition of Glucose-Sensitive Core-Shell Microgels, *ACS Appl. Mater. Interfaces*, 2 (2010) 760-767.
- [8] S. Schachschal, A. Balaceanu, C. Melian, D.E. Demco, T. Eckert, W. Richtering, A. Pich, Polyampholyte Microgels with Anionic Core and Cationic Shell, *Macromolecules*, 43 (2010) 4331-4339.
- [9] S. Fujii, S. Kameyama, S.P. Armes, D. Dupin, M. Suzuki, Y. Nakamura, pH-responsive liquid marbles stabilized with poly(2-vinylpyridine) particles, *Soft Matter*, 6 (2010) 635-640.
- [10] G.X. Sun, M.Z. Zhang, Y. Xu, Y.M. Lu, P.H. Ni, Synthesis and Properties of pH-Responsive Cationic Microgels, *Acta Chim. Sin.*, 67 (2009) 1685-1690.
- [11] W.J. Liu, Y. Zhou, H.Y. Chen, Y.M. Huang, H.L. Liu, Flocculation and aggregation Behavior of doubly responsive microgel, *Acta Chim. Sin.*, 66 (2008) 449-453.
- [12] Y.R. Ren, X.S. Jiang, J. Yin, Copolymer of poly(4-vinylpyridine)-g-poly(ethylene oxide) respond sharply to temperature, pH and ionic strength, *Eur. Polym. J.*, 44 (2008) 4108-4114.
- [13] V. Lapeyre, C. Ancla, B. Catargi, V. Ravaine, Glucose-responsive microgels with a core-shell structure, *J. Colloid Interface Sci.*, 327 (2008) 316-323.
- [14] T. Hoare, R. Pelton, Charge-switching, amphoteric glucose-responsive microgels with physiological swelling activity, *Biomacromolecules*, 9 (2008) 733-740.
- [15] H. Li, R.M. Luo, K.Y. Lam, Multiphysics Modeling of Electrochemomechanically Smart Microgels Responsive to Coupled pH/Electric Stimuli, *Macromol. Biosci.*, 9 (2009) 287-297.
- [16] S. Bhattacharya, F. Eckert, V. Boyko, A. Pich, Temperature-, pH-, and magnetic-field-sensitive hybrid microgels, *Small*, 3 (2007) 650-657.
- [17] R. Pelton, Temperature-sensitive aqueous microgels, *Advances in colloid and interface science*, 85 (2000) 1-33.
- [18] G.M. Eichenbaum, Alkali earth metal binding properties of ionic microgels, *Macromolecules*, 33 (2000) 4087-4093.
- [19] V. Boyko, Thermo-sensitive poly(N-vinylcaprolactam-co-acetoacetoxyethyl methacrylate) microgels: 1 - Synthesis and characterization, *Polymer*, 44 (2003) 7821-7827.



- 
- [20] J.I. Amalvy, Synthesis and characterization of novel pH-responsive microgels based on tertiary amine methacrylates, *Langmuir*, 20 (2004) 8992-8999.
- [21] L. Bromberg, Dually responsive microgels from polyether-modified poly(acrylic acid): Swelling and drug loading, *Langmuir*, 18 (2002) 4944-4952.
- [22] T.G. Van Thienen, Protein release from biodegradable dextran nanogels, *Langmuir*, 23 (2007) 9794-9801.
- [23] G. Fundueanu, M. Constantin, P. Ascenzi, Preparation and characterization of pH- and temperature-sensitive pullulan microspheres for controlled release of drugs, *Biomaterials*, 29 (2008) 2767-2775.
- [24] C.A. Farrugia, Gelatin behaviour in dilute aqueous solution: Designing a nanoparticulate formulation, *Journal of Pharmacy and Pharmacology*, 51 (1999) 643-649.
- [25] S.A. Agnihotri, N.N. Mallikarjuna, T.M. Aminabhavi, Recent advances on chitosan-based micro- and nanoparticles in drug delivery, *Journal of Controlled Release*, 100 (2004) 5-28.
- [26] D.B. Shenoy, G.B. Sukhorukov, Microgel-based engineered nanostructures and their applicability with template-directed layer-by-layer polyelectrolyte assembly in protein encapsulation, *Macromolecular Bioscience*, 5 (2005) 451-458.
- [27] A.Z. Pich, Composite aqueous microgels: An overview of recent advances in synthesis, characterization and application, *Polymer international*, 56 (2007) 291-307.
- [28] H. Staudinger, E. Huseman, One highly polymeric compounds, 116(th) Announcement - On the limite swellable poly-styrene *Berichte der deutschen chemischen gesellschaft* 68 (1935) 1618.
- [29] R.H. Pelton, P. Chibante, Preparation of aqueous lattices with N-isopropylacrylamide *Colloids and Surfaces*, 20 (1986) 247-256.
- [30] J.K. Oh, R. Drumright, D.J. Siegwart, K. Matyjaszewski, The development of microgels/nanogels for drug delivery applications, *Prog. Polym. Sci.*, 33 (2008) 448-477.
- [31] J. van der Gucht, Advanced soft matter, Wageningen university lecture book, 2009, pp140-143
- [32] Y. Li, R. De Vries, T. Slaghek, J. Timmermans, M.A. Cohen Stuart, W. Norde, Preparation and characterization of oxidized starch polymer microgels for encapsulation and controlled release of functional ingredients, *Biomacromolecules*, 10 (2009) 1931-1938.
- [33] B.G. De Geest, S. De Koker, J. Demeester, S.C. De Smedt, W.E. Hennink, Self-exploding capsules, *Polym. Chem.*, 1 (2010) 137-148.
- [34] M. Das, S. Mardyani, W.C.W. Chan, E. Kumacheva, Biofunctionalized pH-responsive microgels for cancer cell targeting: Rational design, *Adv. Mater.*, 18 (2006) 80-83.
- [35] Y. Lu, Y. Mei, M. Drechsler, M. Ballauff, Thermosensitive core-shell particles as carriers for Ag nanoparticles: Modulating the catalytic activity by a phase transition in networks, *Angew. Chem.-Int. Edit.*, 45 (2006) 813-816.
- [36] W. Park, J.S. King, C.W. Neff, C. Liddell, C.J. Summers, ZnS-based photonic crystals, *Phys. Status Solidi B-Basic Res.*, 229 (2002) 949-960.
- [37] H. Yang, L.W. Qu, A. Wimbrow, X.P. Jiang, Y.P. Sun, Enhancing antimicrobial activity of lysozyme against *Listeria monocytogenes* using immunonanoparticles, *J. Food Prot.*, 70 (2007) 1844-1849.
- [38] G. Horner, P. Johne, R. Kunneth, G. Twardzik, H. Roth, T. Clark, H. Kisch, Heterogeneous photocatalysis, part XIX - Semiconductor type A photocatalysis: Role of substrate adsorption and the nature of photoreactive surface sites in zinc sulfide catalyzed C-C coupling reactions, *Chem.-Eur. J.*, 5 (1999) 208-217.
- [39] L. Ye, P.A.G. Cormack, K. Mosbach, Molecular imprinting on microgel spheres, *Anal. Chim. Acta*, 435 (2001) 187-196.

- [40] M. Malmsten, H. Bysell, P. Hansson, Biomacromolecules in microgels - Opportunities and challenges for drug delivery, *Curr. Opin. Colloid Interface Sci.*, 15 (2010) 435-444.
- [41] E. Mastrobattista, W.E. Hennink, R.M. Schiffelers, Delivery of nucleic acids, *Pharm. Res.*, 24 (2007) 1561-1563.
- [42] M. Ballauff, Y. Lu, "Smart" nanoparticles: Preparation, characterization and applications, *Polymer*, 48 (2007) 1815-1823.
- [43] J.M. Saunders, T. Tong, C.L. Le Maitre, T.J. Freemont, B.R. Saunders, A study of pH-responsive microgel dispersions: from fluid-to-gel transitions to mechanical property restoration for load-bearing tissue, *Soft Matter*, 3 (2007) 486-494.
- [44] B.R. Saunders, N. Laajam, E. Daly, S. Teow, X.H. Hu, R. Stepto, Microgels: From responsive polymer colloids to biomaterials, *Adv. Colloid Interface Sci.*, 147-48 (2009) 251-262.
- [45] A.Z. Pich, H.J.P. Adler, Composite aqueous microgels: an overview of recent advances in synthesis, characterization and application, *Polym. Int.*, 56 (2007) 291-307.
- [46] A.E.J. De Nooy, A.C. Besemer, H. vanBekkum, Highly selective nitroxyl radical-mediated oxidation of primary alcohol groups in water-soluble glucans *Carbohydrate Research*, 269 (1995) 89-98.
- [47] A.E.J. De Nooy, Selective Oxidation of Primary Alcohol Groups in Polysaccharides, in, Technical University of Delft, Delft, The Netherlands, 1997.
- [48] Y. Li, J.M. Kleijn, T. Slaghek, J. Timmermans, M.A. Cohen Stuart, W. Norde, Mobility of lysozyme inside oxidized starch polymer microgels, *Soft Matter*, 7 (2011) 1926-1935.
- [49] J.W.M. Timmermans, R. C. ;Thijssen, H. M. W. M. , Antimicrobial Envelopes. Patent. WO 03101196, 2003.
- [50] K.A. Brogden, Antimicrobial peptides: Pore formers or metabolic inhibitors in bacteria?, *Nat. Rev. Microbiol.*, 3 (2005) 238-250.
- [51] N.Y. Yount, A.S. Bayer, Y.Q. Xiong, M.R. Yeaman, Advances in antimicrobial peptide immunobiology, *Biopolymers*, 84 (2006) 435-458.
- [52] M. Zasloff, Antimicrobial peptides of multicellular organisms, *Nature*, 415 (2002) 389-395.
- [53] K. Matsuzaki, Why and how are peptide-lipid interactions utilized for self-defense? Magainins and tachyplesins as archetypes, *Biochim. Biophys. Acta-Biomembr.*, 1462 (1999) 1-10.
- [54] L. Yang, T.M. Weiss, R.I. Lehrer, H.W. Huang, Crystallization of antimicrobial pores in membranes: Magainin and protegrin, *Biophys. J.*, 79 (2000) 2002-2009.
- [55] Y. Shai, Mechanism of the binding, insertion and destabilization of phospholipid bilayer membranes by alpha-helical antimicrobial and cell non-selective membrane-lytic peptides, *Biochim. Biophys. Acta-Biomembr.*, 1462 (1999) 55-70.
- [56] R. Mansson, H. Bysell, P. Hansson, A. Schmidtchen, M. Malmsten, Effects of Peptide Secondary Structure on the Interaction with Oppositely Charged Microgels, *Biomacromolecules*, 12 (2011) 419-424.
- [57] H. Bysell, P. Hansson, M. Malmsten, Effect of Charge Density on the Interaction between Cationic Peptides and Oppositely Charged Microgels, *J. Phys. Chem. B*, 114 (2010) 7207-7215.
- [58] H. Bysell, P. Hansson, A. Schmidtchen, M. Malmsten, Effect of Hydrophobicity on the Interaction between Antimicrobial Peptides and Poly(acrylic acid) Microgels, *J. Phys. Chem. B*, 114 (2010) 1307-1313.
- [59] H. Bysell, A. Schmidtchen, M. Malmsten, Binding and Release of Consensus Peptides by Poly(acrylic acid) Microgels, *Biomacromolecules*, 10 (2009) 2162-2168.
- [60] N. Benkerroum, Antimicrobial activity of lysozyme with special relevance to milk, *Afr. J. Biotechnol.*, 7 (2008) 4856-4867.

- 
- [61] L. Callewaert, C.W. Michiels, Lysozymes in the animal kingdom, *J. Biosci.*, 35 (2010) 127-160.
- [62] B. Masschalck, C.W. Michiels, Antimicrobial properties of lysozyme in relation to foodborne vegetative bacteria, *Crit. Rev. Microbiol.*, 29 (2003) 191-214.
- [63] R. Huopalahti, R. López-Fandiño, M. Anton, R. Schade, G. Lesniewski, J. Kijowski, Lysozyme, in: *Bioactive Egg Compounds*, Springer Berlin Heidelberg, 2007, pp. 33-42.
- [64] W. Norde, F.G. Gonzalez, C.A. Haynes, Protein adsorption on polystyrene latex-particles, *Polym. Adv. Technol.*, 6 (1995) 518-525.
- [65] J. van den Gucht, E. Spruijt, M. Lemmers, A.M. Cohen Stuart, Polyelectrolyte complexes: bulk phases and colloidal systems, *J. Colloid Interface Sci.*, 361 (2011) 407-422.
- [66] D.J. Burgess, J.E. Carless, Microelectrophoretic studies of gelatin and acacia for the prediction of complex coacervation, *J. Colloid Interface Sci.*, 98 (1984) 1-8.
- [67] C.Y. Lii, S.C. Liaw, V.M.F. Lai, P. Tomasik, Xanthan gum-gelatin complexes, *Eur. Polym. J.*, 38 (2002) 1377-1381.
- [68] M. Girard, S.L. Turgeon, S.F. Gauthier, Interbiopolymer complexing between beta-lactoglobulin and low- and high-methylated pectin measured by potentiometric titration and ultrafiltration, *Food Hydrocolloids*, 16 (2002) 585-591.
- [69] F. Weinbreck, H. Nieuwenhuijse, G.W. Robijn, C.G. de Kruif, Complexation of whey proteins with carrageenan, *J. Agric. Food Chem.*, 52 (2004) 3550-3555.
- [70] S. Girod, M. Boissere, K. Longchambon, S. Begu, C. Tourne-Petheil, J.M. Devoisselle, Polyelectrolyte complex formation between iota-carrageenan and poly(L-lysine) in dilute aqueous solutions: a spectroscopic and conformational study, *Carbohydr. Polym.*, 55 (2004) 37-45.
- [71] E. Seyrek, P.L. Dubin, C. Tribet, E.A. Gamble, Ionic strength dependence of protein-polyelectrolyte interactions, *Biomacromolecules*, 4 (2003) 273-282.
- [72] F. Weinbreck, R. de Vries, P. Schrooyen, C.G. de Kruif, Complex coacervation of whey proteins and gum arabic, *Biomacromolecules*, 4 (2003) 293-303.
- [73] D. Leisner, T. Imae, Interpolyelectrolyte complex and coacervate formation of poly(glutamic acid) with a dendrimer studied by light scattering and SAXS, *J. Phys. Chem. B*, 107 (2003) 8078-8087.
- [74] M. Skepo, P. Linse, Complexation, phase separation, and redissolution in polyelectrolyte-macroion solutions, *Macromolecules*, 36 (2003) 508-519.
- [75] F. Weinbreck, R.H.W. Wientjes, Rheological properties of whey protein/gum arabic coacervates, *J. Rheol.*, 48 (2004) 1215-1228.
- [76] A. Wittemann, B. Haupt, M. Ballauff, Polyelectrolyte-mediated protein adsorption, in: W. Richtering (Ed.) *Smart Colloidal Materials*, Springer-Verlag Berlin, Berlin, 2006, pp. 58-64.
- [77] W.M. De Vos, P.M. Biesheuvel, A. De Keizer, J.M. Kleijn, M.A.C. Stuart, Adsorption of the protein bovine serum albumin in a planar poly(acrylic acid) brush layer as measured by optical reflectometry, *Langmuir*, 24 (2008) 6575-6584.
- [78] C.G. de Kruif, F. Weinbreck, R. de Vries, Complex coacervation of proteins and anionic polysaccharides, *Curr. Opin. Colloid Interface Sci.*, 9 (2004) 340-349.
- [79] S.L. Turgeon, M. Beaulieu, C. Schmitt, C. Sanchez, Protein-polysaccharide interactions: phase-ordering kinetics, thermodynamic and structural aspects, *Curr. Opin. Colloid Interface Sci.*, 8 (2003) 401-414.
- [80] R. de Vries, M.A. Cohen Stuart, Theory and simulations of macroion complexation, *Curr. Opin. Colloid Interface Sci.*, 11 (2006) 295-301.

- [81] C.L. Cooper, P.L. Dubin, A.B. Kayitmazer, S. Turksen, Polyelectrolyte-protein complexes, *Curr. Opin. Colloid Interface Sci.*, 10 (2005) 52-78.
- [82] V.A. Kabanov, V.B. Skobeleva, V.B. Rogacheva, A.B. Zezin, Sorption of proteins by slightly cross-linked polyelectrolyte hydrogels: Kinetics and mechanism, *Journal of Physical Chemistry B*, 108 (2004) 1485-1490.
- [83] C. Johansson, P. Hansson, M. Malmsten, Interaction between lysozyme and poly(acrylic acid) microgels, *J. Colloid Interface Sci.*, 316 (2007) 350-359.
- [84] C. Johansson, P. Hansson, M. Malmsten, Mechanism of lysozyme uptake in poly(acrylic acid) microgels, *Journal of Physical Chemistry B*, 113 (2009) 6183-6193.
- [85] H. Bysell, M. Malmsten, Visualizing the interaction between poly-L-lysine and poly(acrylic acid) microgels using microscopy techniques: Effect of electrostatics and peptide size, *Langmuir*, 22 (2006) 5476-5484.
- [86] G.M. Eichenbaum, P.F. Kiser, A.V. Dobrynin, S.A. Simon, D. Needham, Investigation of the swelling response and loading of ionic microgels with drugs and proteins: the dependence on cross-link density, *Macromolecules*, 32 (1999) 4867-4878.

---

# Chapter 2

## Preparation and characterization of oxidized starch microgels

---

### *Abstract*

A novel biocompatible and biodegradable microgel system has been developed for controlled uptake and release of especially proteins. It contains TEMPO-oxidized potato starch polymers which are chemically cross-linked by sodium trimetaphosphate (STMP). Physical chemical properties have been determined for microgels of different weight ratio of cross-linker to polymer (0.10, 0.15, 0.20, 0.30, and 0.40) and degree of oxidation (30%, 50%, 70%, and 100%). The charge density of the microgels as determined by proton titration is found to be in good agreement with the expected degree of oxidation (DO). The electrophoretic mobility of the microgel particles is used as a qualitative indicator of the pore size, and scales with microgel swelling capacity as expected. The swelling capacity increases with increasing pH and decreasing salt concentration. Preliminary data for the uptake of the globular protein lysozyme by the microgels show it increases with increasing DO and decreasing cross-linker to polymer ratio. Highly charged microgels with intermediate cross-linker to polymer ratios (0.15 and 0.2) are found to be optimal for encapsulating lysozyme.

## 2.1 Introduction

Microgels are widely used as drug delivery vehicles [1, 2], in coatings of functional ingredients [3], sensing devices [4], in biomaterials [5] and for catalysis [6]. The use of microgels for controlled uptake and release has been a subject of great interest over the past decades, since their properties allow them to respond to external stimuli, such as temperature [7, 8], pH [9], light [10], ionic strength [11], solvent [12], applied electric [13] or magnetic fields [14]. Microgels can be made of both synthetic and natural polymers. Most of the microgel particles are based on synthetic polymers such as poly(N-isopropylacrylamide) (PNIPAAm) [15], poly(methacrylic acid) (PMA) [16], poly(N-vinylcaprolactam) (PVCL) [17], poly[2-(diethylamino)ethyl methacrylate] (PDEA) [18] or poly(acrylic acid) (PAA) [19].

Microgels from natural polymers such as dextrans [20], pullulan [21], gelatin [22], chitosan [23] and sodium alginate [24] are more attractive for food and biomedical applications, because of their biodegradability and biocompatibility. There is an increasing demand for effective encapsulation systems consisting of natural polymers, in which the active compounds are well-protected, and can be released at the time and place where they are needed.

We have developed a biopolymer-based release-on-demand BioSwitch [25] microgel, that consists of cross-linked negatively charged potato starch polymers, which interacts with charged functional ingredients through electrostatic interactions [26, 27]. The gel may be degraded by external conditions, e. g., enzymatic attacked by amylase, which switches on the release of the functional ingredients from the gel. Advantages of the Bioswitch microgel are the controlled charge- and cross-linking density, and hence controlled swelling and functional ingredient uptake capacity. The microgels are responsive to environmental changes, such as pH and salt concentration, hence uptake and release of functional ingredients inside the gels can also be tuned through solvent conditions.

For the case of lysozyme (that we consider here as an example of functional ingredient), the starch microgel is an appropriate absorbent because the overall charges of the protein and gel have opposite signs. The lysozyme-starch system has great potential for antimicrobial food packaging [28]. Exposing lysozyme-containing starch particles to an initial microbially contaminated environment leads to hydrolysis of the starch by microbial enzymes. As a result, lysozyme is released in the environment where it inhibits microbial growth.

To design such applications, it is essential to establish basic physical-chemical properties of the microgels, in order to select optimum parameter values. In this chapter, we first present the TEMPO-mediated oxidization of starch polymers and the synthesis of different types of microgels. Next, we physically-chemically characterize the microgels, with the ultimate aim to select optimal gels for encapsulation applications. Potentiometric titrations are used for quantitative evaluation of charge densities of the microgels. Swelling capacities are determined as a function of degree of oxidation (DO), cross-link density, pH and salt concentration. Methods for determining accurate pore sizes and pore size distributions of hydrogels are typically involved, therefore we here use the electrophoretic mobility of the microgel particles as a qualitative indicator of the microgel pore size. Finally, we present some preliminary experiments on the uptake of lysozyme by the microgels.

## **2.2 Material and Methods**

### ***Materials***

Native potato starch was kindly provided by AVEBE, the Netherlands. The oxidation catalyst 2,2,6,6-tetramethyl-1-piperidinyloxy (TEMPO) was purchased from Merck, Germany. The cross-linker Sodium trimetaphosphate (STMP) and the globular protein lysozyme (from chicken egg white, Mw=14.4 KD) were supplied by Sigma-Aldrich. All other chemicals used were of analytical grade. Purified Milli-Q water was used throughout.

### ***Microgel synthesis***

Starch polymer was selectively oxidized at the 6-position to obtain a polyglucuronate with >95% selectivity at complete conversion of the primary alcohol groups[29], by TEMPO-mediated oxidation. In this way, starch polymers of 30%, 50%, 70% and 100% degree of oxidation (DO) were prepared, following the procedure developed at TNO Zeist[30], The Netherlands. The DO was controlled by the amount of sodium hypochlorite added during oxidation. The oxidation is performed at constant pH (pH 10.0) using 2.0 M NaOH in a pH-stat set up, the amount of NaOH needed to keep the pH constant is used to calculate the DO.

Microgels were prepared by cross-linking the oxidized starch polymer with STMP at pH 10.0. According to literature, STMP reacts with two alcohol groups belonging to two different polymer chains [31], thus forming an intermolecular linkage. First, 20 gram of oxidized starch polymer was dissolved in 95 mL distilled water at room temperature, which took around 30 minutes. Then, the cross-linker STMP and sodium hydroxide were added to the polymer

solution and the mixture was heated to 40 °C, and kept at that temperature for 10 minutes without stirring, which leads to a gel formation. The weight ratio of cross-linker to sodium hydroxide was 3:1. The weight ratio of cross-linker to polymer ( $R_{\text{cross-linker/polymer}}$ ) were 0.10, 0.15, 0.20, 0.30 and 0.40. After the gel was formed, the gel was put into an oven at 40 °C for one hour to allow the cross-linking reaction to take place. Then the gel was kept overnight in a cold room at 0 °C. The whole piece of gel was grinded through a sieve (1 mm) covered with a nylon cloth of 200 mesh (mesh size 0.074 mm), in order to obtain reasonably uniform microgel particles. The gel particles were washed three times with distilled water using the nylon covered above a sieve again, in order to remove the salts. Thereafter the microgel particles were washed three times again in 100% ethanol in order to remove water, and three times in 100% acetone in order to remove ethanol and last traces of water. Finally, the microgel particles were dried in oven at 40 °C overnight. The dried microgel powder was again grinded to achieve small and homogenous particles, using a sieve of 20 mesh (mesh size 0.841 mm).

#### ***Size distribution of microgel particles***

The size distribution of microgel particles in suspension was determined using a Malvern MasterSizer 2000 (Malvern, UK). During the laser diffraction measurement, particles pass through a focused laser beam, and scatter light at an angle that is inversely proportional to their size. Dual wavelength detection system (blue light combined with red light) was used to enhance sizing performance and sensitivity. A software-controlled sample dispersion unit Hydro 2000 SM(A) was used. The size of swelled microgel particles in suspension was measured in water at 25 °C. The weight concentration of particles used in measurement is 0.05mg/mL. Prior to the measurements, suspensions were sonicated for 15 minutes, in order to attain finely dispersed gel particles.

#### ***Determination of charge density***

The charge density of the microgels was determined using potentiometric proton titration. Titrations were performed using an automated titration set up [32, 33]. The titration set-up consists of a titration cell with a combined pH electrode (glass–Ag/AgCl), motor driven burette and a Schott TR250 titration interface linked to the burettes and the electrodes. The titration cell was kept under Argon atmosphere at 25 °C. The base and acid solutions that were used in the acid-base titration or pH stat titration were 0.100 M KOH and 0.100 M HCL. Especially for the acid-base titration, 50 mL of microgel suspension at a concentration of 0.4



g/L was prepared. The ionic strength of the microgel suspension was adjusted with KCL to 0.01M and 0.1M. The pH of the suspension was adjusted to 3.0, and equilibrated for half an hour. Titrations were carried out from pH 3.0 to 11.0. The suspension was left at pH 11.0 for one hour, and then titrated back to pH 3.0 to check for reversibility (indicating proper equilibration at each pH value). The change of the charge of the microgels was calculated from the difference of the amount of acid-base added and the mass balance of protons in the suspension. In the calculations, the adapted Davies equation[34] was used to calculate the activity coefficients. The relative position of the titration curves at different electrolyte concentrations was determined by the change of pH measured after the addition of the electrolyte solution (KCL). Proton titration curves give relative charge densities rather than the absolute ones. Conversion to absolute charges is straightforward if a point of zero charge can be determined, but for the starch polymers this is at extremely low pH, where titrations are impossible. Therefore, to estimate the absolute charge density of our polymers and gels, we fit our data using a simple titration model, Henderson-Hasselbalch approximation. For detailed fitting procedure please see Appendix.

### ***Electrophoretic mobility measurements***

Electrophoretic mobilities were measured by laser Doppler Velocimetry (LDV) using a Malvern ZetaSizer HS2000 (Malvern, UK). The rate of change of the phase shift between the scattered light and a reference beam is correlated to the particle velocity and thus allows for evaluating the particular electrophoretic mobility. The equipment was working with a 10mW He-Ne laser of wavelength 633nm. The applied field strength was 80 Vcm<sup>-1</sup>. The concentration of the microgel particles used in the measurement is 10 g/L. The measurements were performed in 0.001M, 0.01M and 0.1 M KCL solutions at pH 7 and 25 °C. Prior to the measurements, suspensions were sonicated for 15 minutes, in order to get finely dispersed suspension.

### ***Free swelling capacity measurements***

A known weight of collapsed/dried microgel powder (around 0.01 gram) was wetted by a large excess of distilled water/buffer at room temperature. The swollen microgel was immersed in buffer for 24 hours to obtain equilibrium. Then the excess water was wiped off with paper until there were no visible water droplets. Gel swelling was quantified using the equilibrium volumetric swelling ratio  $SW_v$ , defined as the ratio of the volume of swollen gel : volume of dry gel. By knowing the density of water ( $\rho_{H_2O} = 1 \text{ g/cm}^3$ ,  $\rho_{polymer} = 1.5 \text{ g/cm}^3$  for all

oxidized starch polymer), and the equilibrium weight swelling ratio  $SW_w$  (the ratio of the weight of swollen gel : weight of dry gel) obtained from swelling experiment, the volumetric swelling ratio  $SW_v$  can be calculated as:  $SW_v = 1 + \rho_{polymer}/\rho_{H_2O} (SW_w - 1)$ .

### ***Lysozyme uptake capacity measurements***

Prior to the measurements, suspensions were sonicated for 15 minutes, in order to attain finely dispersed gel particles. The uptake of lysozyme into microgel particles was studied by mixing gel suspension with solutions of increasing lysozyme concentration in steps of 1 mL with 10 minutes delay time after each step. The absorption of lysozyme in the microgel will become saturated after a certain time. 1 mL lysozyme solution (6.67 g/L) was added into 10 mL microgel suspension (2 g/L) while stirring. After 10 minutes loading time, 1 mL of the mixture solution was sampled, and another 1mL lysozyme solution was added while continually stirring for 10 minutes. This was repeated for another 9 times. Finally, all the samples were centrifuged under 10,000 rpm for 5 minutes, and the concentration of lysozyme in the supernants was determined by absorbance at wavelength 280 nm measured with UV spectrophotometer (HITACHI, Japan). The uptake (mg lysozyme/mg of dry gel) of lysozyme in the microgel particles was calculated from material balance. At a gel concentration of 2 g/L, the volume of the swollen gel is less than 5% of the total volume. This volume fraction was neglected when calculating lysozyme uptake. The absorption isotherm was obtained by plotting the amount of the lysozyme absorbed by the microgel against the equilibrium lysozyme concentration in solution.

## **2.3 Results and Discussion**

### ***Size distribution of microgel particles***

As shown in figure 2.1, our starch polymer microgels have relatively wide size distribution, ranging between 4 and 100 micrometers, although most sizes are distributed between 10 and 20 micrometers. By way of example, figure 2.2 presents an optical microscopic picture of DO30% microgel, to show the morphology of the microgels. Obviously, they have irregular shapes. Since the microgel particles swell in water, they have a transparent appearance.

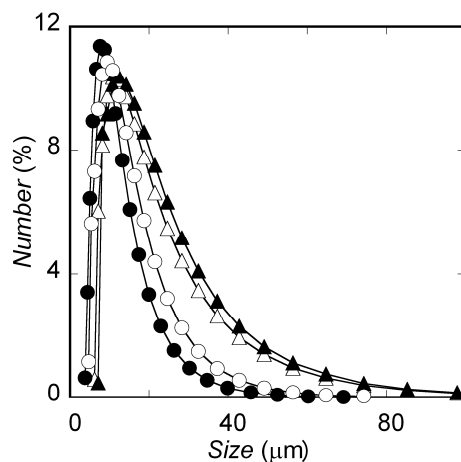


Figure 2.1 Size distribution curves: Numbers of starch polymer microgel particles in water vs their size (volume weighted mean diameter in  $\mu\text{m}$ ), for various values of the degree of oxidation (DO%). ( $\Delta$ ) DO30%, ( $\blacktriangle$ ) DO50%, ( $\bullet$ ) DO70%, ( $\circ$ ) DO100%; All gels have a weight ratio cross-linker/polymer of 0.20 (4 gram STMP per 20 gram of oxidized polymer).



Figure 2.2 Optical microscopic image of microgel particles dispersed in water (same DO30% microgel sample indicated in figure 2.1), scale bar shown in graph is 20  $\mu\text{m}$ .

### ***Charge densities from proton titration***

We first determined the charge density  $Q$  (C/g) of the polymers before cross-linking, as a function of pH at 0.1M KCL and 20 °C; results are shown in figure 2.3 A. The dissociation reaches a plateau value at pH around 5. The maximum charge density  $Q_{\text{max}}$  (C/g) obtained from the plateau is proportional to the degree of oxidation.

Since proton titration only probes changes in the charge of a sample, we used the slope positioning method in order to obtain the absolute charge density. Figure 2.4 shows an example of the slope-positioning that we use to fit the data [35] (see Appendix). The fitting procedure leads to values of  $Q_{\text{max}}$  and  $\text{p}K_{\text{a,eff}}$  for each titration curve.

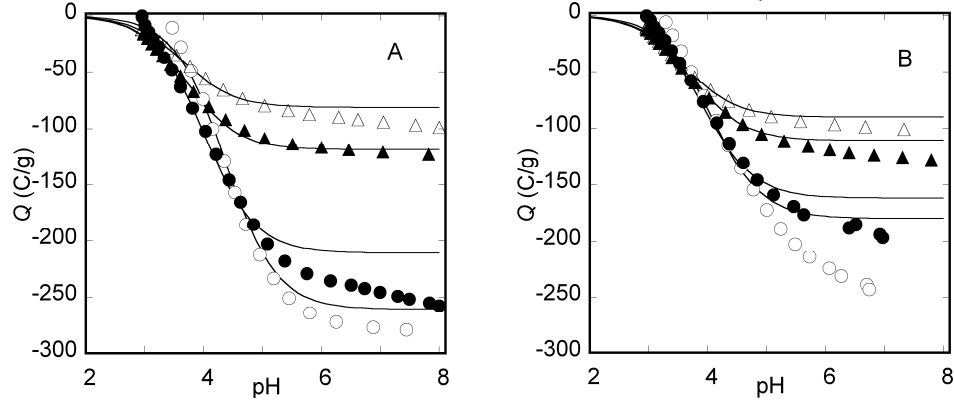


Figure 2.3 Titration curves: charge density  $Q$  (C/g) of uncross-linked and cross-linked starch polymers as a function of pH, for various values of the degree of oxidation (DO%). The absolute position of the curves has been determined using slope positioning, as explained in the text. (A) oxidized starch polymers of different degree of oxidation ( $\Delta$ ) DO30%, ( $\blacktriangle$ ) DO50%, ( $\bullet$ ) DO70%, ( $\circ$ ) DO100%; (B) oxidized starch polymer microgels of different degree of oxidation ( $\Delta$ ) DO30%, ( $\blacktriangle$ ) DO50%, ( $\bullet$ ) DO70%, ( $\circ$ ) DO100%. All gels have a weight ratio cross-linker/polymer of 0.15 (3 gram STMP per 20 gram of oxidized polymer). Solid lines are fits to the Henderson-Hasselbalch equation that are also used in the slope positioning.

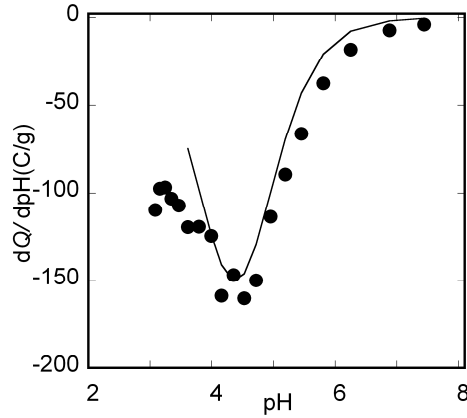


Figure 2.4 Example of slope positioning using the Henderson-Hasselbalch model. The slope  $dQ/dpH$  (C/g) is plotted versus pH. The experimental data ( $\bullet$ ) is for a DO100% starch polymer, the solid line is the model fit.

As shown in figure 2.5A, the maximum charge density  $Q_{\max}$  of various oxidized polymers increases more or less linearly with increasing DO, but for the gels of higher DO, the charge density is somewhat lower than that of the corresponding polymers. The  $pK_{a,\text{eff}}$  is shown on Fig.2.5B. It increases with increasing DO for both polymers and gels. The simple titration model fits the experimental data reasonably well and the value of  $Q_{\max}$  reaches 60-70% of the theoretical maximum charge density of carboxylic groups on one gram starch polymer. The fact that  $Q_{\max}$  of the polymer gel is lower than that of the polymers at higher DO

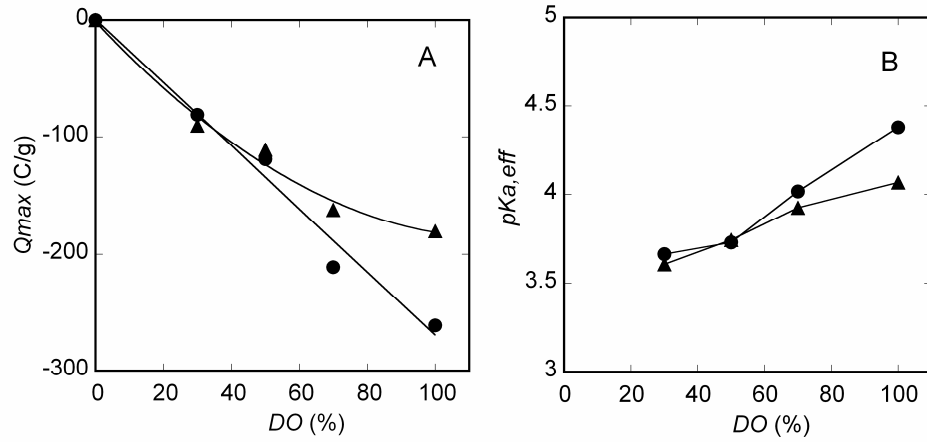


Figure 2.5 Parameters values resulting from fitting titration data to the Henderson-Hasselbalch model, for uncross-linked (●) and cross-linked (▲) oxidized starch polymer. Weight ratio cross-linker/polymer is 0.15 (3 gram of STMP per 20 gram of oxidized polymer). (A) Maximum charge density  $Q_{\max}$  versus degree of oxidation (DO %). (B)  $pK_{a,eff}$  versus degree of oxidation (DO %).

is mostly likely due to the fact that cross-linking the polymer makes polyelectrolyte effect stronger by bringing the chain close together. The dissociation of COOH groups is restricted by dissociation of neighboring COOH groups, which gives low  $Q_{\max}$  of cross-linked highly charged polymers. The trend of  $pK_{a,eff}$  of both polymer and gel are the same, and are as expected: for increasing DO, dissociation becomes progressively more difficult. Data for the DO100% gel was hard to fit using the simple model (see Fig.2.3B), this may have caused some deviation.

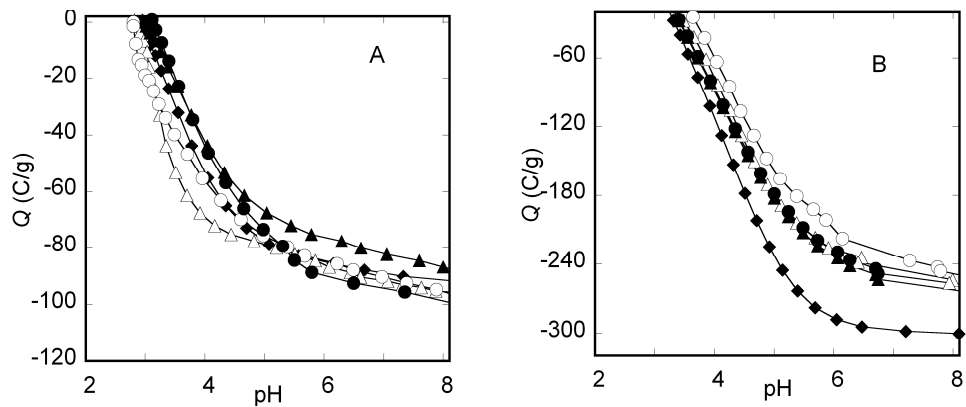


Figure 2.6 Effect of cross-link density on charge density  $Q$  (C/g) versus pH, for DO30% and DO100% oxidized starch polymers. (A) DO30% polymer (♦) and DO30% polymers cross-linked with 2 (Δ), 3 (▲), 4 (○), and 8 (●) gram of STMP per 20 g of oxidized polymer. (B) DO100% polymer (♦) and DO100% polymers cross-linked with 2 (Δ), 3 (▲), 4 (○), and 8 (●) gram of STMP per 20 g of oxidized polymer. The weight ratio cross-linker/polymer is 0.10, 0.15, 0.20, and 0.40 respectively.

The effect of electrolyte on proton titration is not significant (results not shown). The results of pH stat salt titration for polymers and microgels show that the charge density in 0.01M KCL solution is only few coulombs/gram higher than that in 0.1M KCL.

Charge densities of the microgel are hardly influenced by amount of cross-linker. The difference between charge densities of DO30% polymer and DO30% microgel is insignificant (Fig. 2.6A). Only the DO100% polymer shows a bit higher charge density than polymer microgel (Fig. 2.6B), again most likely due to the polyelectrolyte effect, that the  $pK_{a,eff}$  of cross-linked polymer is shifted from  $pK_a$  of uncross-linked polymer, which gives different behavior between cross-linked and uncross-linked polymers on dissociation of COOH groups.

### ***Swelling capacity***

Swelling capacities of microgels were measured as a function of DO and weight ratio of cross-linker STMP to oxidized starch polymer ( $R_{\text{cross-linker/polymer}}$ ) in the buffer of pH 7.0, ionic strength 0.05M, at room temperature. As shown in figure 2.7, the swelling capacity of microgels decreases with increasing weight ratio of STMP to polymer, and reaches a constant minimum value beyond 0.20 of  $R_{\text{cross-linker/polymer}}$ . Lack et al. [36] also found a critical cross-linker concentration above which rheological properties and swelling of the gel do not change anymore.

Somewhat unexpectedly, at low  $R_{\text{cross-linker/polymer}}$ , the dependence of swelling on the DO is opposite of what might be expected: the DO100% gels swell much less than the gels with lower charge densities. Since cross-linking is performed after oxidation, cross-linking efficiency may not be the same for gels with different degrees of oxidation. Indeed,  $^{31}\text{P}$ phosphate NMR spectrometry (data not shown) shows that the DO100% microgel only has one single cross-linked phosphate peak, but DO30% microgel has an extra phosphate peak around 5 ppm. This peak is supposed to be the peak of the side reaction in which only one polymer chain is connected to the di/tripolyphosphate [37]. Hence it seems that the DO100% polymer indeed cross-links more efficiently with STMP than the DO30% polymer. A possible reason could be that the chains of highly charged DO100% polymers are more stretched than those of the DO30% polymers during cross-linking. This would increase the accessibility for cross-linker leading to more efficient formation of a gel. It is also possible that the DO30% polymer tends to form intra-molecular cross-links rather than inter-molecular cross-links. In this case, cross-links contribute less effectively to the network formation. This is also consistent with the clear appearance of the DO100% gel before grinding, indicating a

homogenous gel structure, whereas the fact that DO30% gels are more turbid before grinding, may indicate a more inhomogeneous structure.

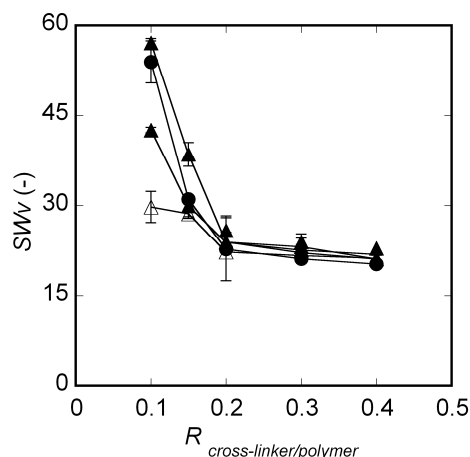


Figure 2.7 Volumetric swelling ratio  $SW_v$  (-) as a function of weight ratio of STMP to oxidized polymer  $R_{\text{cross-linker/polymer}}$  for starch polymers with different degree of oxidation: DO30% ( $\Delta$ ), DO50% ( $\blacktriangle$ ), DO70% ( $\bullet$ ) and DO100% ( $\circ$ ). Buffer conditions: 0.02M, pH 7.0 Citric acid-phosphate buffer, ionic strength 0.05M.

The pH dependence of the microgel swelling is shown in Figure 2.8. Swelling increases with increasing pH (Fig.2.8 A), and remains constant from pH 5 to 8, as expected since at these pH values the dissociation of carboxylic groups is complete and the repulsion between the polyelectrolyte chains is maximal. The effect of salt concentration on microgel swelling behavior has also been investigated. Swelling decreases with increasing salt concentration (Fig.2.8 B), and reaches a plateau value at 0.2 M salt concentration. This is due to screening of electric charges of microgel by presence of salt. Apparently, nearly all charges are screened at 0.2M salt. This is also consistent with the salt effect on the hydrodynamic radius of free polymers in solution, as observed by dynamic light scattering. As shown in figure 2.8C, the hydrodynamic radius of the DO30% polymer does not change any more as soon as the salt concentration is beyond 0.2M. Similar results of swelling as a function of pH and salt are also found for other polyelectrolyte microgels [38].

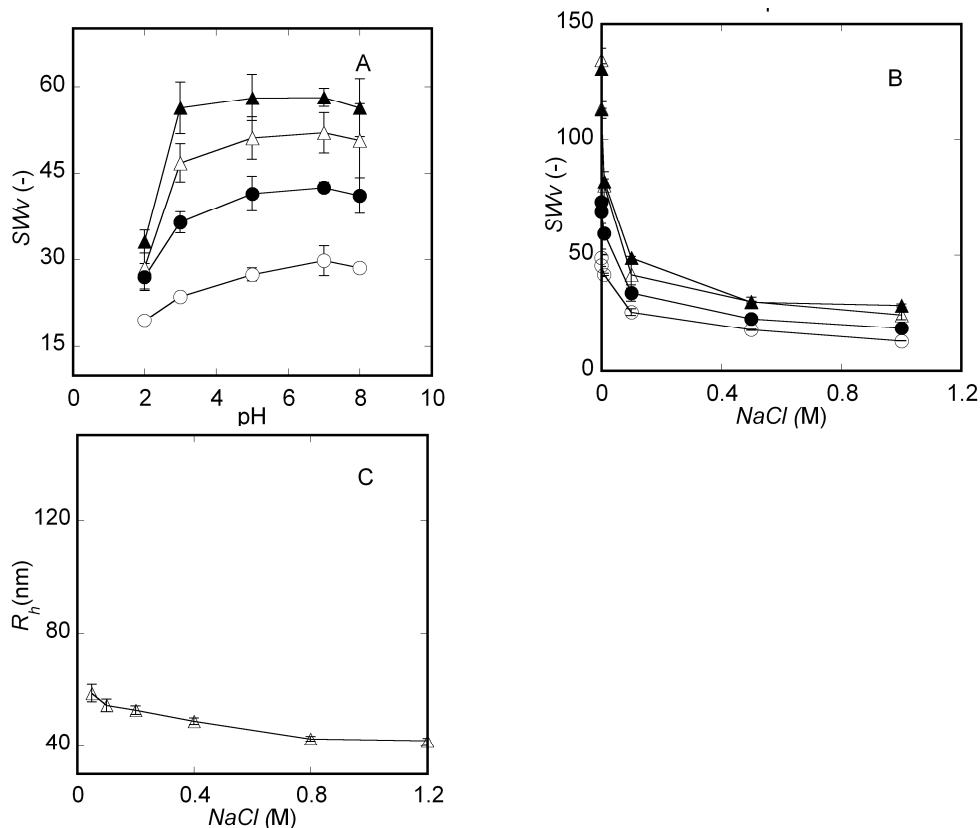


Figure 2.8 Influence of salt and pH of swelling of oxidized starch microgels. (A) Volumetric swelling ratio  $SW_v$  (-) as a function of pH for microgels of varying degree of oxidation: DO30% ( $\Delta$ ), DO50% ( $\blacktriangle$ ), DO70% ( $\bullet$ ) and DO100% ( $\circ$ ).  $R_{\text{cross-linker/polymer}}$  is 0.10 (2 gram of STMP per 20g of oxidized starch polymer). Buffer conditions: 0.02M Citric acid-phosphate buffer (pH 2-8), ionic strength 0.05M; (B) Volumetric swelling ratio  $SW_v$  as a function of NaCl concentration (M) for same series of microgels at pH 7.0; (C) Hydrodynamic radius  $R_h$  (nm) of uncross-linked DO30% starch polymer as obtained from Dynamic Light Scattering (DLS), as a function of NaCl concentration (M).

### Electrophoretic mobility

Direct measurement of the pore size of microgel particles does not yield unambiguous results, in part due to the irregular shape and broad size distribution of the particles. Swelling data suggested that at small ratios of cross-linker to polymer, the DO100% gels have smaller pore sizes than the more weakly charged gels. Here we test this hypothesis by using electrophoretic mobility as a qualitative indicator of pore size. The high salt electrophoretic mobility of microgel particles is related to the microgel pore size as we explain below.

According to Oshima [39], the electrophoretic mobility (electrophoretic velocity per unit field strength) of charged soft particles can be divided into two parts. The first part involves a weighted average of potentials over the surface charge layer, which is sensitive to ionic



strength. The second contribution involves the fixed charge density  $\rho_{\text{fix}}$  ( $\text{C}/\text{m}^3$ ) and softness  $\lambda^{-1}$  (nm) or penetrability of the microgel pores for the solvent. At high electrolyte concentration the first term vanishes due to screening, and only the second, ionic-strength independent term, remains:

$$\mu \approx \frac{\rho_{\text{fix}}}{\eta \lambda^2} \quad \text{for } \kappa \gg \lambda \quad (2.1)$$

Where  $\kappa$  ( $\text{nm}^{-1}$ ) is the reciprocal Debye length,  $\rho_{\text{fix}}$  ( $\text{C}/\text{m}^3$ ) is the fixed charge density and

$$\lambda^{-1} = \left( \frac{\eta}{\gamma} \right)^{1/2} \quad (2.2)$$

where  $\eta$  is the viscosity of solvent (Pa.s) and  $\gamma$  is an effective friction coefficient ( $\text{Nm}^{-4}\text{s}$ ) for the solvent in the microgel.

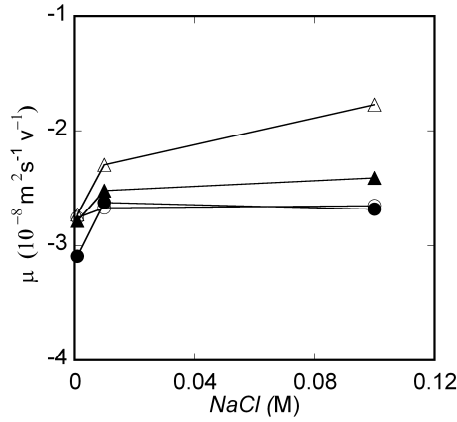


Figure 2.9 Electrophoretic mobility ( $10^{-8} \text{m}^2 \text{s}^{-1} \text{V}^{-1}$ ) of microgel particles as a function of NaCl concentration (M), for varying degree of oxidation: DO30% ( $\Delta$ ), DO50% ( $\blacktriangle$ ), DO70% ( $\bullet$ ), and DO100% ( $\circ$ ).  $R_{\text{cross-linker/polymer}}$  is 0.20 (4 gram STMP per 20 g of oxidized starch polymer).

As is clear from Figure 2.9, our microgel particles indeed show a typical soft particle behavior with a plateau for the electrophoretic mobilities at high salt, with the possible exception of the DO30% microgel for which the mobility keeps increasing slightly.

We can derive values for the softness parameter  $\lambda^{-1}$  from our mobility data by combining it with the swelling data and proton titration data. For the calculations, we use a viscosity of solvent  $\eta$  ( $\eta_{\text{H}_2\text{O}}$ : 0.001 Pa.s), the plateau mobility value  $\mu$  from figure 2.9, the volume charge density  $\rho_{\text{fix}}$  (which was calculated by the electric charge density from proton titration (Fig.2.3), and the swelling capacity (Fig.2.7)). Table 2.1 shows the values of the softness parameter  $\lambda^{-1}$  of different microgels derived from Eq. (2.1). Larger softness implies that the

fluid velocity profile penetrates more easily onto the microgel structure, implying larger pores.

Table 2.1 shows that the softness  $\lambda^{-1}$  (nm) of microgel particles decreases with increasing degree of oxidation (DO) and increasing weight ratio cross-linker to polymer ( $R_{\text{cross-linker/polymer}}$ ). This is in agreement with the dependency of the swelling capacity on DO and  $R_{\text{cross-linker/polymer}}$  (Fig.2.7). If we assume that the microgel has a homogenous structure (i.e. the structure of outer layer is similar as that of central part), we find that highly oxidized and highly cross-linked polymer microgels indeed have a smaller pore size, supporting our earlier hypothesis that highly oxidized polymers are cross-linked more efficiently with STMP than the polymer with a lower degree of oxidation.

Table 2.1 Calculation of softness parameter  $\lambda^{-1}$  (nm) using Oshima's theory, Eq.(2.1) and maximum internal salt concentration  $C_{\text{int, max}}$  (M) for microgels of varying degree of oxidized (DO30%, 50%, 70%, 100%) polymers and weight ratio of cross-linker STMP to polymer  $R_{\text{cross-linker/polymer}}$  of 0.1 and 0.2. Other entries are Volumetric swelling ratio  $SW_v$ , fixed volume charge density  $\rho_{\text{fix}}$  ( $10^6 \text{Cm}^{-3}$ ), electrophoretic mobility  $\mu$  ( $10^{-8} \text{m}^2 \text{s}^{-1} \text{V}^{-1}$ ).

DO (%)	$R_{\text{cross-linker/polymer}}$	$SW_v$	$\rho_{\text{fix}}$ ( $10^6 \text{Cm}^{-3}$ )	$\mu$ ( $10^{-8} \text{m}^2 \text{s}^{-1} \text{V}^{-1}$ )	$\lambda^{-1}$ (nm)	$C_{\text{int, max}}$ (M)
30	0.1	53.9	-3.3	-1.8	10.8	0.035
	0.2	22.7	-9.8	-1.6	3.3	0.102
50	0.1	57.1	-5.3	-2.2	8.4	0.055
	0.2	23.9	-15.5	-2.5	3.2	0.160
70	0.1	42.5	-9.8	-2.6	5.3	0.086
	0.2	25.9	-19.3	-2.6	2.7	0.201
100	0.1	29.8	-19.9	-3.0	3.0	0.208
	0.2	22.3	-30.2	-2.7	1.8	0.315

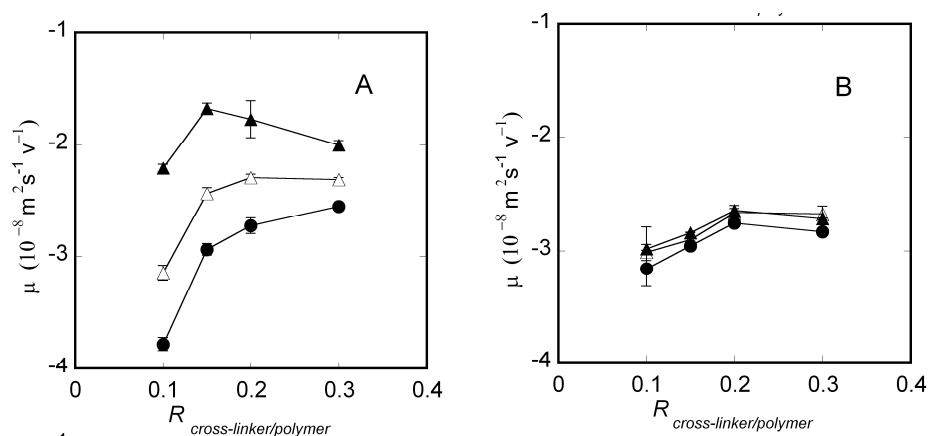


Figure 2.10 Electrophoretic mobility ( $10^{-8} \text{ m}^2 \text{ s}^{-1} \text{ V}^{-1}$ ) of microgels as a function of weight ratio of cross-linker STMP to starch polymer  $R_{\text{cross-linker/polymer}}$ , for increasing concentration of potassium chloride ((●)=0.001M; (Δ)=0.01M; (▲)=0.1M). (A) DO30% polymer microgels; (B) DO100% polymer microgels

Next, consider the dependence of the electrophoretic mobility on the weight ratio cross-linker to polymer ( $R_{\text{cross-linker/polymer}}$ ) in somewhat more detail. Figure 2.10 shows that the DO30% and DO100% polymer microgel particles exhibit distinctly different electrophoresis behavior. The mobility of the DO100% polymer microgel particles is hardly influenced by added salt (Fig.2.10B), but the DO30% polymer microgel particles are clearly salt dependent, and move faster at low salt concentration and low  $R_{\text{cross-linker/polymer}}$  (Fig.2.10A). The mobility increases with decreasing salt concentration and decreasing  $R_{\text{cross-linker/polymer}}$ . This trend was also observed for other types of microgel particles [40].

The independence to salt of the DO100% electrophoretic mobility may be related to the high internal salt concentration of highly charged microgels. We have calculated the internal salt concentration by assuming that all carboxylic groups in the microgel contribute one counterion. The maximum number of  $\text{COO}^-$  groups can be calculated from electric charge density (Fig.2.3) and swelling capacity (Fig.2.7). As can be seen in Table 2.1, the highly charged microgels have significantly higher internal salt concentrations than the more weakly charged ones. Only when the added salt concentration significantly exceeds the internal one, one may expect an influence of added salt.

### Lysozyme Uptake Capacity

Finally we present some preliminary data on lysozyme uptake capacity by our microgels, at varying degree of oxidation (DO%), and weight ratio cross-linker to polymer ( $R_{\text{cross-linker/polymer}}$ ).

#### Dependence on degree of oxidation (DO%)

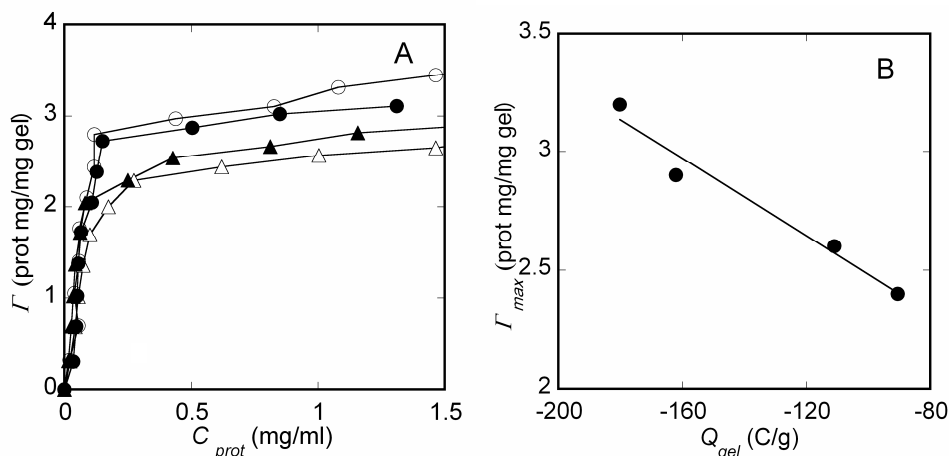


Figure 2.11 (A).Lysozyme uptake  $\Gamma$ (prot mg/mg gel) as a function of equilibrium lysozyme concentration in solution  $C_{prot}$  (mg/mL) at pH 7.0 Citric acid-phosphate buffer, ionic strength 0.05M for microgels of varying degree of oxidation (( $\Delta$ )=DO30%;( $\blacktriangle$ )=DO50%;( $\bullet$ )=DO70%;( $\circ$ )=DO100%) and  $R_{cross-linker/polymer}$  of 0.15 (3 gram STMP/20 gram polymer);(B) Linear relationship of maximum absorbed amount of lysozyme  $\Gamma_{max}$  (prot mg/mg gel) ( $\bullet$ ) as a function of charge density  $Q_{gel}$  (C/g) on microgels.

As shown in figure 2.11A, the initial part of the curve for  $\Gamma(C)$  (absorption  $\Gamma$  in mg lysozyme per mg dry gel versus solution concentration  $C_{prot}$  of lysozyme) rises steeply which indicates that lysozyme absorbs with high affinity at low protein concentration. The uptake increases and almost reaches a plateau value when the lysozyme concentration is above a threshold concentration of 0.1-0.2 mg/mL. The uptake capacity, i.e. the amount of lysozyme absorbed per gram dry gel, increases with increasing DO that is with increasing negative charge density in the gel. Hence it increases the strength of interaction between microgel and lysozyme. The uptake experiments are done at pH 7.0 (below the isoelectric point of lysozyme (pH=11.0)). Microgel and lysozyme carry opposite charges leading to electrostatic attraction, and complexation. Figure 2.11B shows that the maximum lysozyme uptake  $\Gamma_{max}$  (the plateau value in Fig.2.11A) increases linearly with the total amount of charges  $Q_{gel}$  on each microgel.

#### Dependence on weight ratio cross-linker to polymer

For a microgel of a given charge density (e.g. DO50%), the uptake capacity of the microgel decreases with increasing weight ratios of cross-linker to polymer ( $R_{cross-linker/polymer}$ ) (Fig.2.12). At  $R_{cross-linker/polymer}$  above 0.20, the cross-linking starts to negatively affect the absorption capacity, which is consistent with the swelling data. Lysozyme uptake does not vary a lot when the ratio is below 0.20. Probably, at low  $R_{cross-linker/polymer}$ , the pore sizes are

much larger than the size of the lysozyme molecules. For ratios  $> 0.20$  we are entering the regime where pore sizes become comparable to the size of lysozyme, which ultimately reduces lysozyme absorption.

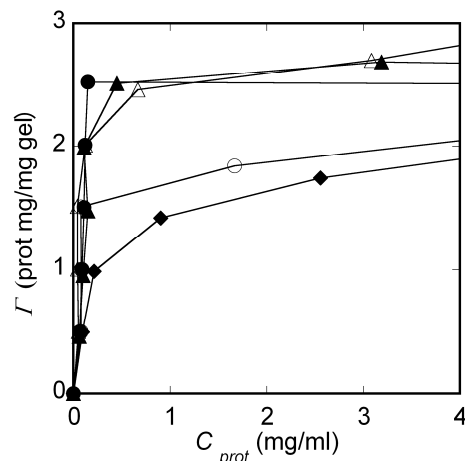


Figure 2.12 Lysozyme uptake  $\Gamma$  (prot mg/mg gel) as a function of equilibrium lysozyme concentration in solution  $C_{prot}$  (mg/mL) at pH 7.0 Citric acid-phosphate buffer, ionic strength 0.05M for DO50% microgels of varying  $R_{cross-linker/polymer}$  ((▲)=0.10;(△)=0.15;(●)=0.20;(○)=0.30g;(◆)=0.40)

## 2.4 Concluding remarks

In this chapter, we have characterized the physical-chemical properties of novel biodegradable starch microgel particles, and their interaction with lysozyme. The system was developed for use in controlled-uptake-release of protein, as in antimicrobial packaging. Our results indicate that we have good chemical control over the charge density of the microgels, which is directly reflected in the lysozyme uptake capacity. The cross-linking efficiency was found to depend on the degree of oxidation of the polymers, with highly charged polymers leading to more densely cross-linked microgels. Intermediate degrees of cross-linking for microgels seem to be optimal for the uptake of lysozyme: at high weight ratio cross-linker/polymer the pore sizes become too small, whereas at very low weight ratio cross-linker/polymer, the microgels may swell enormously, which is undesirable for packaging application.

## References

- [1] J.K. Oh, R. Drumright, D.J. Siegwart, K. Matyjaszewski, The development of microgels/nanogels for drug delivery applications, *Progress in Polymer Science*, 33 (2008) 448-477.
- [2] M. Das, S. Mardyani, W.C.W. Chan, E. Kumacheva, Biofunctionalized pH-responsive microgels for cancer cell targeting: Rational design, *Advanced Materials*, 18 (2006) 80-83.
- [3] H. Ichikawa, Y. Fukumori, Design of nanohydrogel-incorporated microcapsules for appropriate controlled-release of peptide drugs, *Yakugaku Zasshi-Journal of the Pharmaceutical Society of Japan*, 127 (2007) 813-823.
- [4] K. Iwai, Y. Matsumura, S. Uchiyama, A.P. de Silva, Development of fluorescent microgel thermometers based on thermo responsive polymers and their modulation of sensitivity range, *Journal of Materials Chemistry*, 15 (2005) 2796-2800.
- [5] G.B. Sukhorukov, D.V. Volodkin, A.M. Gunther, A.I. Petrov, D.B. Shenoy, H. Mohwald, Porous calcium carbonate microparticles as templates for encapsulation of bioactive compounds, *Journal of Materials Chemistry*, 14 (2004) 2073-2081.
- [6] M. Ballauff, Y. Lu, "Smart" nanoparticles: Preparation, characterization and applications, *Polymer*, 48 (2007) 1815-1823.
- [7] I. Berndt, J.S. Pedersen, W. Richtering, Temperature-sensitive core-shell microgel particles with dense shell, *Angewandte Chemie-International Edition*, 45 (2006) 1737-1741.
- [8] M.J. Garcia-Salinas, M.S. Romero-Cano, F.J. de las Nieves, Colloidal stability of a temperature-sensitive Poly(N- isopropylacrylamide/2-acrylamido-2-methylpropanesulphonic acid) microgel, *Journal of Colloid and Interface Science*, 248 (2002) 54-61.
- [9] B.H. Tan, K.C. Tam, Review on the dynamics and micro-structure of pH-responsive nano-colloidal systems, *Advances in Colloid and Interface Science*, 136 (2008) 25-44.
- [10] T. Takahashi, H. Watanabe, N. Miyagawa, S. Takahara, T. Yamaoka, Application of photopolymer to core-hair type microgels with various hair length, *Polymers for Advanced Technologies*, 13 (2002) 33-39.
- [11] B. Zhao, J.S. Moore, Fast pH- and ionic strength-responsive hydrogels in microchannels, *Langmuir*, 17 (2001) 4758-4763.
- [12] T. Hoare, R. Pelton, Charge-switching, amphoteric glucose-responsive microgels with physiological swelling activity, *Biomacromolecules*, 9 (2008) 733-740.
- [13] H. Shinohara, M. Aizawa, Control of polymer gel morphology by small potential electric-stimulation with a conducting polymer electrode, *Kobunshi Ronbunshu*, 46 (1989) 703-708.
- [14] M. Zrinyi, Intelligent polymer gels controlled by magnetic fields, in, 2000, pp. 98-103.
- [15] R. Pelton, Temperature-sensitive aqueous microgels, *Advances in colloid and interface science*, 85 (2000) 1-33.
- [16] G.M. Eichenbaum, Alkali earth metal binding properties of ionic microgels, *Macromolecules*, 33 (2000) 4087-4093.
- [17] V. Boyko, Thermo-sensitive poly(N-vinylcaprolactam-co-acetoacetoxyethyl methacrylate) microgels: 1 - Synthesis and characterization, *Polymer*, 44 (2003) 7821-7827.
- [18] J.I. Amalvy, Synthesis and characterization of novel pH-responsive microgels based on tertiary amine methacrylates, *Langmuir*, 20 (2004) 8992-8999.
- [19] L. Bromberg, Dually responsive microgels from polyether-modified poly(acrylic acid): Swelling and drug loading, *Langmuir*, 18 (2002) 4944-4952.

- 
- [20] T.G. Van Thienen, Protein release from biodegradable dextran nanogels, *Langmuir*, 23 (2007) 9794-9801.
- [21] G. Fundueanu, M. Constantin, P. Ascenzi, Preparation and characterization of pH- and temperature-sensitive pullulan microspheres for controlled release of drugs, *Biomaterials*, 29 (2008) 2767-2775.
- [22] C.A. Farrugia, Gelatin behaviour in dilute aqueous solution: Designing a nanoparticulate formulation, *Journal of Pharmacy and Pharmacology*, 51 (1999) 643-649.
- [23] S.A. Agnihotri, N.N. Mallikarjuna, T.M. Aminabhavi, Recent advances on chitosan-based micro- and nanoparticles in drug delivery, *Journal of Controlled Release*, 100 (2004) 5-28.
- [24] D.B. Shenoy, G.B. Sukhorukov, Microgel-based engineered nanostructures and their applicability with template-directed layer-by-layer polyelectrolyte assembly in protein encapsulation, *Macromolecular Bioscience*, 5 (2005) 451-458.
- [25] H.M.W.M. Thijssen, R. C. ;Timmermans, J. W. ;Van Veen, J. J. F. , Inducible release vehicles. Eur.Patent EP1628529, 2006.
- [26] R. de Vries, F. Weinbreck, C.G. de Kruif, Theory of polyelectrolyte adsorption on heterogeneously charged surfaces applied to soluble protein-polyelectrolyte complexes, *Journal of Chemical Physics*, 118 (2003) 4649-4659.
- [27] V.A. Kabanov, V.B. Skobeleva, V.B. Rogacheva, A.B. Zezin, Sorption of proteins by slightly cross-linked polyelectrolyte hydrogels: Kinetics and mechanism, *Journal of Physical Chemistry B*, 108 (2004) 1485-1490.
- [28] J.W.M. Timmermans, R. C. ;Thijssen,H. M. W. M. , Antimicrobial Envelopes. Patent WO03101196, 2003.
- [29] A.E.J. De Nooy, A.C. Besemer, H. vanBekkum, Highly selective nitroxyl radical-mediated oxidation of primary alcohol groups in water-soluble glucans *Carbohydrate Research*, 269 (1995) 89-98.
- [30] A.E.J. De Nooy, Selective Oxidation of Primary Alcohol Groups in Polysaccharides, in, Technical University of Delft, Delft, The Netherlands, 1997.
- [31] S. Lack, V. Dulong, D. Le Cerf, L. Picton, J.F. Argillier, G. Muller, Hydrogels based on pullulan crosslinked with sodium trimetaphosphate (STMP): Rheological study, *Polymer Bulletin*, 52 (2004) 429-436.
- [32] R. Vermeer, Interactions between humic acids and hematite and effects on metal ion speciation, in, Wageningen University and Research Center, Wageningen, The Netherlands, 1996, pp. 167.
- [33] W.F. Tan, L.K. Koopal, L.P. Weng, W.H. van Riemsdijk, W. Norde, Humic acid protein complexation, *Geochimica Et Cosmochimica Acta*, 72 (2008) 2090-2099.
- [34] C.W. Davies, *Ion Interactions*, Butterfly, London, 1962.
- [35] M. Borkovec, G.J.M. Koper, C. Piguet, Ion binding to polyelectrolytes, *Current Opinion in Colloid & Interface Science*, 11 (2006) 280-289.
- [36] S. Lack, Hydrogels based on pullulan crosslinked with sodium trimetaphosphate (STMP): Rheological study, *Polymer bulletin*, 52 (2004) 429-436.
- [37] M.C. Silva, E.C. Ibezim, T.A.A. Ribeiro, C.W.P. Carvalho, C.T. Andrade, Reactive processing and mechanical properties of cross-linked maize starch, *Industrial Crops and Products*, 24 (2006) 46-51.
- [38] E. Seyrek, P.L. Dubin, C. Tribet, E.A. Gamble, Ionic strength dependence of protein-polyelectrolyte interactions, *Biomacromolecules*, 4 (2003) 273-282.
- [39] H. Ohshima, T. Kondo, On the electrophoretic mobility of biological cells, *Biophysical Chemistry*, 39 (1991) 191-198.

- [40] M. Rasmusson, B. Vincent, N. Marston, The electrophoresis of poly(N-isopropylacrylamide) microgel particles, *Colloid and Polymer Science*, 278 (2000) 253-258.



## Appendix

Titration curve positioning using the Henderson-Hasselbalch approximation.

For fitting the titration data, we assume a simple Henderson-Hasselbalch titration curve, in terms of an effective  $pK_{a,\text{eff}}$  that determines the degree of dissociation of the COOH groups. This gives a pH dependent charge density  $Q$  (C/g) of the polymer:

$$Q = \frac{Q_{\text{max}}}{1 + 10^{pK_{a,\text{eff}} - pH}} \quad (\text{A2.1})$$

Where  $Q_{\text{max}}$  (C/g) is the charge density at full dissociation. The value of  $pK_{a,\text{eff}}$  may deviate from the intrinsic  $pK_a$  value of the COOH groups if dissociation of the COOH groups is influenced by the dissociation of neighboring COOH groups<sup>35</sup>. The predicted slope of the titration curve is

$$\frac{dQ}{dpH} = \frac{Q_{\text{max}}}{(1 + 10^{pK_{a,\text{eff}} - pH})^2} \cdot \ln 10 \cdot 10^{pK_{a,\text{eff}} - pH} \quad (\text{A2.2})$$

which has a maximum at  $pH = pK_{a,\text{eff}}$ , that is proportional to  $Q_{\text{max}}$ . We analyze the experimental titration data by numerically differentiating, and fitting to Eq. (A2.2). Titration data at both low and high pH has large errors, so we fit to the central part of the titration curve, in the vicinity of  $pK_a$ .



---

# Chapter 3

## Lysozyme uptake by oxidized starch polymer microgels

---

### *Abstract*

With the aim of determining suitable conditions for uptake and release of globular proteins on microgels, we studied the interaction between phosphated, highly cross-linked, negatively charged oxidized potato starch polymer (OPSP) microgel particles and lysozyme from hen's egg. Our microgel shows a typical protein-induced de-swelling behavior for charged microgels. The protein distributes rather homogenously through the microgel. We found that at low salt concentration the saturation protein uptake  $\Gamma_{\text{sat}}$  increases with increasing pH. This is because the binding capacity is mainly determined by charge compensation: with increasing pH the (positive) charge on the lysozyme molecules decreases, while the (negative) charge of the microgel particles increases. Therefore, more protein molecules are needed to compensate for the charge on the gel and the binding capacity increases. The protein binding affinity, however, decreases sharply with increasing pH, presumably because this affinity is mainly sensitive to the lysozyme charge density. At high pH the binding affinity is relatively low, and by adding salt the protein can easily be released from the gel. This leads to a maximum in the curves of  $\Gamma_{\text{sat}}$  versus pH, and this maximum shifts to lower pH values with increasing ionic strength. We conclude that for protein uptake and release applications, the present system works best around pH 5 due to a sufficiently high binding affinity and a sufficiently high binding capacity.

### 3.1 Introduction

The number of protein and polypeptide drugs is increasing rapidly, and this has stimulated interest in the development of protein/peptide drug delivery systems. Polymer microgels have received a lot of attention as potential carrier system. In view of their biodegradability and biocompatibility, microgels from natural polymers are particularly interesting. An example of such microgels are systems of phosphated cross-linked amylose starch and these have been widely investigated for controlled drug release [1-4]. However, a disadvantage of these systems is that it is difficult to control the charge density on the polysaccharides and therefore the electrostatic binding of proteins and peptides. Previously, we have introduced a system based on phosphated cross-linked oxidized potato starch polymer (OPSP) [5], which offers full control over the polysaccharide charge density.

Complex formation of polysaccharides with oppositely charged proteins has been studied over decades [6-8]. The main driving force for this process is the gain in entropy as a result of the release of counterions into the solution. Depending on conditions, soluble protein-polyelectrolyte complexes may be formed, or there may be macroscopic phase separation of the gas-liquid type in which a dilute colloidal phase coexists with a very concentrated colloidal phase [9].

As compared to complex formation in solution, protein uptake by cross-linked polyelectrolytes (i.e., gels) involves additional aspects: the swelling and de-swelling of the network, changes in excluded volume interaction, osmotic pressure, etcetera. For a slightly cross-linked hydrogel system, Kabanov et al. [10] concluded that the driving force for protein uptake is similar to that for a linear polyelectrolyte: it is the increase in entropy of released counterions that drives formation of the cross-linked protein-polyelectrolyte complex. However, the combination with phase separation and gel elasticity may give rise to complicated effects: at intermediate stages of complex formation these authors found a morphology consisting of an outer weakly swollen complex shell and a highly swollen hydrogel core [10]. For slightly cross-linked poly(acrylic acid) microgels (60-80  $\mu\text{m}$ ), such a "core-shell" formation was also found by Johansson et al. [11, 12]. They discovered that the uptake process could be divided into two steps, firstly the shell formation combined with de-swelling of the outer part of the microgel and with no lysozyme diffusing into the core. In the second phase, microgel de-swelling is negligible and lysozyme diffuses into the microgel core. Byssell and Malmsten [13] studied the uptake of poly-L-lysine by poly(acrylic acid) (PAA) microgels (50-150  $\mu\text{m}$ ) as a function of pH, ionic strength, size of the peptides and

peptide concentration. Like Johansson et al., they found a peptide induced de-swelling during absorption.

Compared to slightly cross-linked microgels, the knowledge on higher cross-linked microgels is still very limited. Eichenbaum et al. [14] reported that protein loading on poly(methacrylic acid-co-acrylic acid) microgels (4-10  $\mu\text{m}$ ) strongly depends on the cross-link density and the pore size of the microgel. Using neutron scattering Rubio-Retama et al. [15] investigated the microstructure of poly(magnesium acrylate) microgels (40  $\mu\text{m}$ ), before and after loading with glucose oxidase. They found an increase of the network mesh size after encapsulation of enzyme. The effect of the cross-link density on the enzymatic activity of the encapsulated glucose oxidase was also studied. They concluded that a higher porosity of the polymer matrix facilitates the diffusion of the substrate towards the catalytic center of the enzyme.

Since proteins and weak polyelectrolytes can adapt their charge to the local electric potential, another aspect that may play a role in protein uptake by polyelectrolyte gels is charge regulation [16-18]. Charge regulation was found to be important, for example, in the uptake of bovine serum albumin into poly(acrylic acid) brushes: the protein was found to strongly adjust its charge due to the highly negative electrostatic potential in the brush[19].

As mentioned, we have previously reported on the synthesis and characterization of oxidized potato starch polymer (OPSP) microgels [5]. From preliminary experiments on lysozyme uptake we concluded that the most highly charged microgels (degree of oxidation 100%, denoted as DO100%, prepared with a cross-linker to polymer ratio of 0.20 w/w; see materials and methods section) have the highest protein uptake capacity, and therefore may be suitable for uptake and delivery applications. The present chapter reports on further studies with this type of microgel, focusing on the conditions that are optimal with respect to protein uptake and release.

As a function of solution conditions (pH and ionic strength), we systematically measured binding affinity, saturation protein uptake and protein release using UV spectrophotometry. Microgel de-swelling due to protein uptake is determined using optical microscopy. The distribution of absorbed fluorescently labeled lysozyme throughout the microgel particles is determined using confocal laser scanning microscopy (CLSM). Finally, we also determined the extent to which charge regulation plays a role in protein uptake by the polyelectrolyte microgels by performing pH-STAT titrations.

The combined results allow us to provide a coherent picture of the factors that influence protein uptake and release by these highly charged, highly cross-linked potato starch polymer microgels.

### 3.2 Material and Methods

#### *Materials*

Native starch was kindly provided by AVEBE, The Netherlands. The oxidation catalyst 2,2,6,6-tetramethyl-1-piperidinyloxy (TEMPO) and ethanol (100%) were purchased from Merck, Germany. The cross-linker sodium trimetaphosphate (STMP), poly-DL-lysine hydrobromide and the globular protein lysozyme (from chicken egg white,  $M_w = 14,400$  g/mole) were supplied by Sigma-Aldrich. Coomassie brilliant blue R250 was purchased from Bio-rad, UK. Acetic acid (96%) was obtained from Acros Organics, Belgium.

Polymer gels were synthesized by chemically cross-linking the TEMPO-oxidized potato starch polymers by sodium trimetaphosphate (STMP). Microscopic gel particles were made from the macroscopic gel. The particles bear irregular shapes after washing and drying steps; The details of oxidation of starch polymer and preparation of microgel particles are presented in Chapter 2. Unless indicated otherwise, we used gel particles of 5 to 40  $\mu\text{m}$  in diameter with a degree of oxidation (DO) of 100% and prepared with a weight ratio of cross-linker/polymer of 0.20. Purified Milli-Q water was used throughout for preparing solutions. To control the pH, buffer solutions (0.02 M) of citric acid-phosphate buffer were used for the pH range 3 - 8. Sodium chloride was added to obtain the appropriate ionic strength. In the pH-STAT experiments, no buffer was used, but 0.01 M solutions of HCl and NaOH to adjust the pH. Table 3.1 shows the volumetric swelling characteristics of the DO100% microgel that is used in this Chapter.

Table 3.1 Volumetric swelling (%) of the DO100% microgel particles. Data from Li et al.[5]).

pH (in buffer of ionic strength 0.05M)	Volumetric swelling	Ionic strength (M) (in water)	Volumetric swelling
2	13	0	48.9
3	16	0.001	45.5
5	18.6	0.01	41.6
7	20.2	0.1	25.4
8	18	0.5	17.6

### ***Binding affinity measurements***

Adsorbed amount [mg/mg] of lysozyme per dry weight of polysaccharide microgel were measured using a UV spectrophotometer UV 2010 (Hitachi, Japan) and a flow cell. In our set-up a beaker on a stirrer was filled with a microgel dispersion; a lysozyme solution (6.67 mg/mL) was added in steps (50  $\mu$ L each time). The solution in the beaker is pumped via a 650 nm syringe filter (only allows the protein solution pass) to the flow-cell (a curvet with in and out openings) in the UV spectrometer, and then is returned into the beaker. By using this circulating system, we continuously measured the concentration  $C_{prot}$  [mg/mL] of protein in solution. After each addition the absorbance at 280 nm (from which one can calculate  $C_{prot}$ ) was recorded until it remained constant, indicating that a steady state of saturation was reached.

The amount of protein left in solution,  $m_{left}$  [mg], can be calculated as

$$m_{left} = C_{prot} \times V_{mixture} \quad (3.1)$$

In which  $V_{mixture}$  is the total volume of the microgel dispersion and the protein solution added. The amount of protein absorbed in the microgel,  $m_{abs}$  [mg], can be calculated from the total protein added,  $m_{add}$  [mg], and  $m_{left}$ ,

$$m_{abs} = m_{add} - m_{left} \quad (3.2)$$

The absorbed amount per gram dry gel mass  $\Gamma$  [mg/mg], is given by

$$\Gamma = m_{abs} / m_{dry\ gel} \quad (3.3)$$

The binding affinity is just the initial slope of the isotherm, defined as  $K_{aff}$  [mL/mg]:

$$K_{aff} = \frac{d\Gamma}{dC_{prot}} \quad (3.4)$$

***Saturation protein uptake capacity***

We suspended 3 mg of the dry gel particles in 7 mL buffer at various pH values, added 3 mL of 6.67 mg/mL protein solution and gently stirred for 4 hours (enough time to reach saturation [5]). Subsequently, the samples were centrifuged at 10,000 rpm for 5 minutes and the concentration of lysozyme in the supernatant was determined by UV spectrophotometry. The total protein adsorption at saturation level  $\Gamma_{\text{sat}}$  (mg protein/mg dry gel) in the microgel particles was calculated from mass balance.

***Protein release under dilution***

Samples of microgel-protein mixtures of different pH values were prepared in the same way as described above, stirred for 4 hours and centrifuged at 10,000 rpm for 5 minutes. The sediments (protein-gel complexes) were diluted with 10 mL fresh buffer, and mildly stirred for another 4 hours. After a second centrifugation, the absorbance in the supernatants was measured. The percentage of protein released  $P_{\text{release}}$  is calculated from the measured protein concentration  $C_{\text{prot}}$  as

$$P_{\text{release}} = \frac{C_{\text{prot}} \times 10\text{mL}}{\Gamma_{\text{sat}} \times m_{\text{dry gel}}} \times 100\% \quad (3.5)$$

It is noted here that the released amount depends on the equilibration time (4 hours may not be entirely sufficient to reach equilibrium) and the volume of buffer added to the centrifuged protein gel-complexes, so it is a somewhat arbitrary quantity. However, by using the above described standard procedure, we can compare the protein release from the gel under different conditions.

***De-swelling ratio of single microgel particles after protein uptake***

The negatively charged microgel was fixed on a glass surface that had been modified using poly-DL-lysine to give it a positive charge. This was done by first cleaning the glass with water and methanol three times. After drying, the glass surface was wetted with a drop of 0.01% poly-lysine and allowed to dry overnight in air. The dried slide was washed with water and methanol again for three times, to remove any unattached poly-lysine. A drop of 1% microgel dispersion was put on the glass surface and after 1 hour the slide was washed with water and methanol, to remove unattached gel particles.



To measure the de-swelling as a result of protein uptake we observed various single gel particles on the prepared slides by optical microscopy. We first added 50  $\mu\text{L}$  buffer on top of the glass slide and measured the particle size, that is the length of an arbitrarily chosen cross-section of the fixed particles. Subsequently, we added 50  $\mu\text{L}$  lysozyme solution (20 mg/mL) and measured the particle size as a function of time. Evaporation of water was negligible during our short observation time, which was confirmed by the low weight loss of water during experiments (less than 5%). For each measurement two different gel particles were selected.

We assume that the particles de-swell homogeneously, so that the degree of de-swelling defined as  $v/v_0$  can be calculated as

$$\frac{v}{v_0} = \left( \frac{L}{L_0} \right)^3 \quad (3.6)$$

with  $v$  and  $v_0$  the volume of the gel particle before and after adding protein solution, and  $L$  and  $L_0$  the length of the corresponding cross-sections.

#### ***Calculation of the average mesh size of the swollen microgel***

To estimate average mesh sizes, we used Flory and Rehner theory[20]. The effective cross-link density  $\nu_e$  [mol/cm<sup>3</sup>] is given by [21]:

$$\nu_e = \frac{-[\ln(1-V_2) + V_2 + \chi V_2^2]}{(V_2^{1/3} - 0.5V_2)V_1} \quad (3.7)$$

where  $V_1$  is the molar volume of the solvent [cm<sup>3</sup>/mol],  $V_2$  is the volume fraction of polymer in the swollen gel, and  $\chi$  is the polymer-solvent Flory-Huggins interaction parameter (here we use  $\chi = 0.2$  as an estimation for the  $\chi$  value for charged dextran and water). It should be noted that the average crosslink density calculated in this way is not better than a first approximation, because the Flory-Rehner model is much idealized, even for simple systems. However, the calculations can provide some indication on how the mesh size of the polymer network changes as a result of protein absorption at different pH values and we will use this later (Figure 3.9).

Following Huglin et al.[22], the effective cross-link density is related to the density of the dry polymer  $\rho_p$  (1.50 g/cm<sup>3</sup>) and the average molecular weight between cross-links  $M_c$  [g/mol] by

$$v_e = \frac{\rho_p}{M_c} \quad (3.8)$$

Finally,  $M_c$  was used to estimate the mesh size using[23]

$$\xi_{empty} = 0.071 V_2^{-1/3} M_c^{-1/2} \quad (3.9)$$

where  $\xi_{empty}$  is the mesh size [nm] for the empty gel. The mesh size of the microgel after protein uptake  $\xi_{filled}$  was estimated using the measured de-swelling ratios  $v/v_0$  :

$$\xi_{filled} = \xi_{empty} \times \left( \frac{v}{v_0} \right)^{1/3} \quad (3.10)$$

### ***Protein distribution in the microgel particles***

Coomassie blue is a fluorescent dye that can only bind to the protein, not to the starch microgels. The protein-gel complexes were stained with coomassie blue. As a control, the same staining procedure was applied to empty microgel particles.

The staining solution consisted of 0.03 g coomassie blue dissolved in 15 mL ethanol, 15 mL water and 3 mL acetic acid (96%). To remove all unbound coomassie blue we used a de-staining solution consisting of 5 mL acetic acid (96%) and 25 mL ethanol. An amount of 0.06 g complex sediment (DO100% microgel with lysozyme at pH 7.0 and ionic strength 0.05 M) was suspended in 5 mL staining solution and mixed for 30 minutes. After centrifuging at 10,000 rpm for 5 minutes, the supernatant was removed and the sediment was washed two times with water. The final sediment was washed three times with the de-staining solution by dispersing it in 5 mL of this solution and stirring for 1 hour. The stained protein-microgel complexes were observed with confocal microscopy (Carl Zeiss Axiovert 200 microscope, Zeiss, Germany, equipped with a LSM 5 Exciter configuration and a 40x10.6 NA objective). The coomassie blue was excited by a He-Ne laser (633 nm).

### ***Determination of charge regulation by pH-STAT titrations***

pH-STAT titrations were carried out with a Schott titration set-up [24]. First 0.01 g of the microgel particles was dispersed in 50 mL KCl solutions with ionic strengths of 0.05 M, 0.10 M and 0.20 M. The titrant was a 6.67 mg/mL solution of lysozyme. Both the dispersion of gel particles and the protein solution were adjusted to the desired pH using 0.01 M HCl or KOH. Immediately after adding 0.5 mL of protein solution to the microgel dispersion, the pH was observed to increase, indicating that the complex formation is accompanied by proton uptake. To adjust the pH value to its original value, 0.001 M HCl was added automatically. After 20 minutes the pH did not change anymore and it was assumed that equilibrium had been reached. Then another 0.5 mL of the lysozyme solution was added. This was repeated in total five times, until finally the pH did not change anymore after protein addition. The uptake of protons as a consequence of adding the protein is equal to the amount of added HCl to keep the pH at the set fixed value. The experiments were done at pH 3.0, 4.0, 5.0 and 8.0.

## **3.3 Results and Discussion**

### ***Binding affinity of lysozyme to the microgel***

The binding affinity, the saturation protein uptake and protein release under dilution as a function of pH and ionic strength are crucial for determining the optimal conditions of protein uptake and release of the microgel particles. Figure 3.1 shows an example of an absorption isotherm at pH 3.0 and at ionic strengths of 0.05 M and 0.10 M. The affinity can be determined from the initial slope  $dI/dC_{prot}$  of the curve (Eq. 3.4). However, at low ionic strength it is difficult to determine the initial slope, since in that case at low protein concentration practically all protein is bound to the microgel. At higher ionic strengths the initial slope can be easily determined, since binding is not too strong. Figure 3.2 shows, by way of example,  $\Gamma(C_{prot})$  data from which the affinity of lysozyme for microgels of different degrees of oxidation at pH 3 and a ionic strength of 0.2 M can be obtained by single linear regression.

Figure 3.3 summaries the binding affinities for DO30%, DO50% and DO100% microgels as a function of pH, at a ionic strength of 0.20 M. The binding affinity for all microgels decreases with increasing pH and this effect is most pronounced for the DO100% microgel. These results indicate that the affinity is mainly determined by the (positive) charge

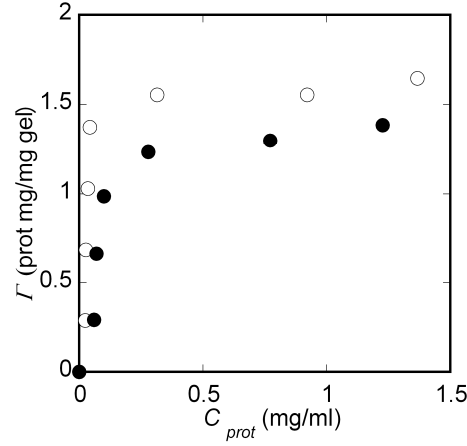


Figure 3.1 Lysozyme uptake  $\Gamma$  as a function of equilibrium lysozyme concentration in solution  $C_{prot}$ , for a DO100% microgel, at pH 3.0 for ionic strengths 0.05 M (○) and 0.10 M (●).

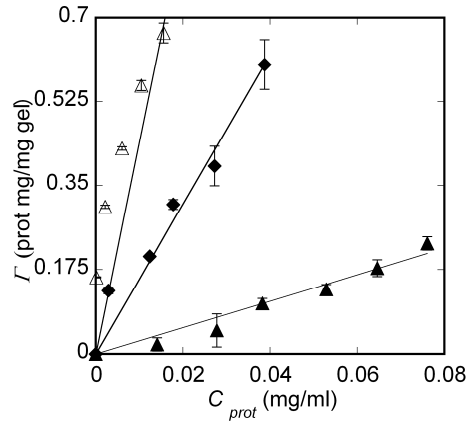


Figure 3.2 Lysozyme uptake  $\Gamma$  as a function of equilibrium lysozyme concentration in solution  $C_{prot}$  at low protein concentration, at pH 3.0 and ionic strength 0.20 M, for microgels of different degrees of oxidation: DO30% (▲), DO50% (◆), DO100% (Δ) microgels. The solid lines are linear fits of the data, the slopes give the affinities of the protein for the microgels.

on the protein, since this decreases with increasing pH, whereas the (negative) charge on the microgel increases with increasing pH. However, it may seem somewhat unexpected that the affinity drops so fast with increasing pH over the pH range 3-5, because the charge of free protein decreases only modestly over this range [25], namely by 3 or 4 charges per protein molecule ( $Z_p$ ). The charge of the protein in the complex may be different, though, because part of its carboxylates take up protons. This strongly adds to the electrostatic binding energy. We will return to this point later (see Figure 3.11 and discussion).

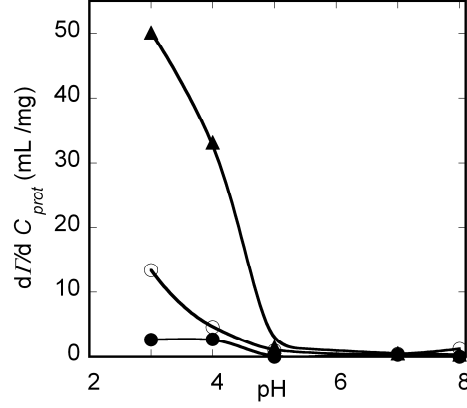


Figure 3.3 Absorption affinity as a function of pH for DO30% (●), DO50% (○) and DO100% (▲) microgels. Ionic strength 0.20 M. Lines are only meant as a guide to the eye.

Figure 3.4 shows the effect of the ionic strength on the affinity between lysozyme and the DO100% microgel at pH 8.0. As expected, the affinity decreases with increasing salt concentration due to the screening of attractive electrostatic interactions. We find a linear relationship between  $\log(dI/dC_{prot})$  and  $\log C_{salt}$ , which is in line with the findings of other researchers for complex formation between proteins and flexible polyelectrolytes[26]. For the competitive binding of monovalent salt cations and  $z$ -valent cations to DNA, Record et al.[27] have derived:

$$\frac{\partial \log K_{obs}}{\partial \log C_{salt}} = -z \quad (3.11)$$

where  $K_{obs}$  is the observed binding constant of the  $z$ -valent cations. However, Dubin et al.[26] have shown that this relation does not simply apply to the case of protein-polyelectrolyte interactions. For the lysozyme-microgel system, we find  $\partial \log(dI/dC_{prot})/\partial \log C_{salt} = -2.6$  which indeed is an appreciably smaller number than the total charge on free protein (e.g., at pH 8.0 and an ionic strength of 0.1 M,  $Z_p = 7$ , *i.e.*, the protein molecule carries an excess of 7 positive charges).

In view of applications, we also studied the release of the protein from the microgels. In order to find out how the binding affinity influences the protein release, protein-gel complexes were diluted with buffer solutions of various pH values (3 - 8) and ionic strengths (0.05 M - 0.2 M) as described in the materials and methods section. Figure 3.5 shows that the degree of protein release from the complexes increases with increasing pH and ionic strength.

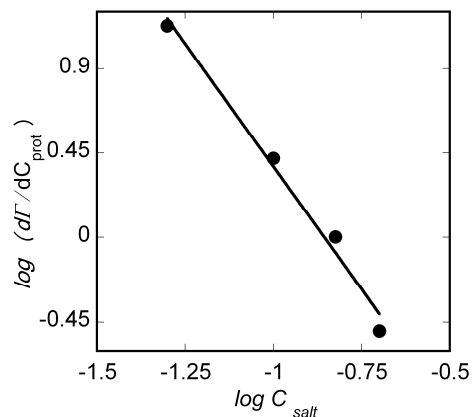


Figure 3.4  $\log (d\Gamma/dC_{prot})$  as a function of  $\log C_{salt}$  (i.e., the total ionic strength of buffer and added salt, in M) for the DO100% microgel at pH 8.0. The line is the linear fit:  $y=-2.6x-2.2$  (correlation coefficient  $R=0.99$ ).

The release curves in Figure 3.5 look like a mirror images of the absorption affinity curves in Figure 3.3: the protein binds with low affinity at high pH and high salt concentration and is under these conditions easily released by dilution. In contrast, at low pH and low salt concentration the protein binds so strongly that dilution does hardly result in any protein release. A complete release occurs for 0.2 M salt by increasing the pH from 4 to 8.

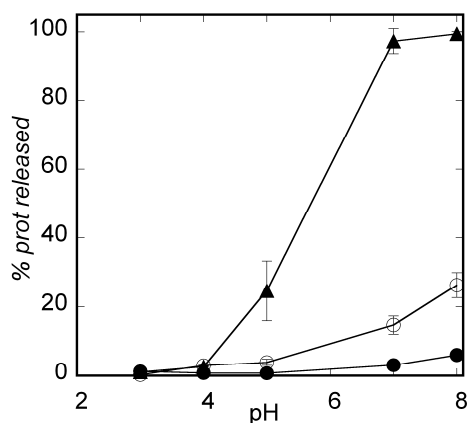


Figure 3.5 Percentage of lysozyme released from DO100% microgel by dilution with buffer as a function of pH, at ionic strengths of 0.05 M (●), 0.10 M (○) and 0.20 M (▲) (i.e., the same conditions as used to determine the affinity curves in Figure 3.3).

The above results indicate that our microgels may be used in biomedical or food applications: e.g., protein or peptide drugs (with charge properties comparable to lysozyme) encapsulated by the microgel can be protected in the stomach where the pH is low, and

released in the intestine, where the pH is high. At suitable ionic strengths ( $\approx 0.2$  M) the release can be almost quantitative.

### ***Protein distribution in the microgel particles***

For weakly cross-linked microgels it has been found that absorbed proteins/polypeptides do not always distribute homogeneously [11, 13]. As mentioned before, a “core-shell” morphology consisting of an outer protein-microgel complex shell and a highly swollen microgel core has been reported by Johansson et al. [11, 12]. They found that there is more protein present in the shell than in the core. To determine whether in our case of a highly cross-linked microgel, the protein molecules distribute homogeneously or not, we stained “empty” and protein-loaded DO100% microgel particles with fluorescent coomassie blue, at pH 7 and a low ionic strength of 0.05 M, and examined them using confocal scanning laser microscopy. As expected, we find no signal for the empty microgel particles. A strong signal was observed only for stained protein-microgel complexes, indicating that the signal is exclusively due to stained protein. In contrast to Johansson et al., we found that the protein distributes rather homogeneously through the microgel (Figure 3.6A). Figure 3.6B shows a SEM micrograph of a gel particle, showing the surface morphology; it indicates the porous structure of the microgel.

The microgel used by Johansson et al. is synthesized from poly-acrylic acid, which also contains COOH- groups. They used lysozyme as a model protein as well. Although their gel differs from our gel with respect to charge density and cross-link density, it is still a similar and simple system to compare with. Johansson et al. found that protein diffusion to the core is a limiting step. However, in our case protein diffusion is not a rate-determining step. The observation by Johansson et al. is probably due to the core-shell formation occurring during protein absorption in their microgel. Our confocal microscopy experiments never showed core-shell formation. This difference in behavior may be related to differences in surface structure and internal homogeneity.

The internal structure (the average mesh size as well as the heterogeneity) may play an important role in the protein distribution and uptake and release kinetics. This will be presented in detail in a further chapters.

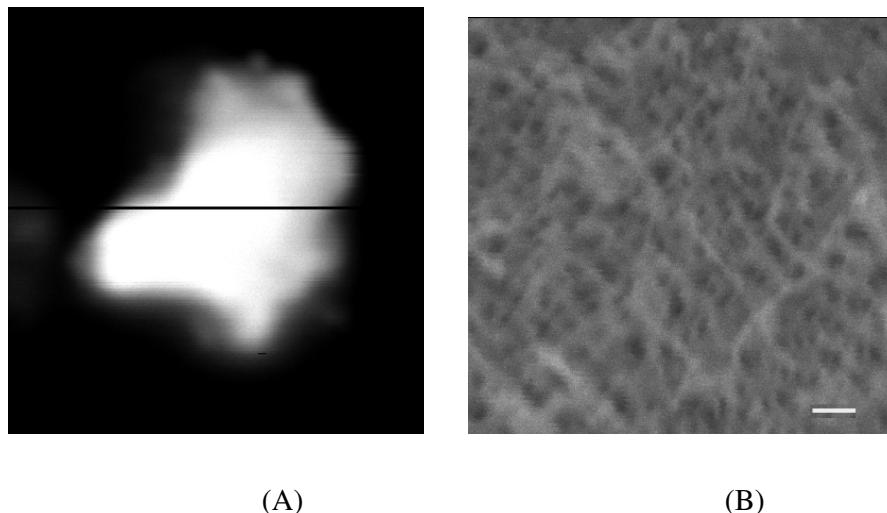


Figure 3.6(A). Fluorescence signal from a coomassie blue stained lysozyme-gel complex. Ionic strength 0.05 M, pH 7. The picture is a cross section at half the height of the DO100% microgel particle. The scan direction was parallel to the black line, which is 7  $\mu\text{m}$  in length (from the left edge to right edge of the particle). (B) Scanning electron microscopic photo of the surface of a DO100% particle in the dry state. Scale bar = 50 nm.

### ***Saturation protein uptake capacity of the microgels***

The binding affinity is the result of the direct interaction between polysaccharide chains and protein molecules. The saturation protein uptake, however, is also affected by protein-protein and polysaccharide-polysaccharide interactions, as well as the gel elasticity. Hence, it is a much more complex quantity. In order to determine the relation between affinity and saturation protein uptake,  $\Gamma_{sat}$  was measured as a function of pH and at various ionic strengths.

Figure 3.7 shows that for intermediate ionic strengths (0.10 and 0.20 M)  $\Gamma_{sat}$  has a maximum at a certain pH, denoted as  $\text{pH}_{opt}$ . For high (0.5 M) and low (0.05 M) ionic strengths the curves are monotonic. Their shapes suggest that there may still be a maximum for 0.5 M and 0.05 M, but that it is outside the pH range studied; the  $\text{pH}_{opt}$  shifts to lower pH with increasing ionic strength. The saturation protein uptake at each pH decreases with increasing ionic strength, except around pH 3.

The monotonous increase of the uptake capacity at low ionic strength can be understood on the basis of charge stoichiometry. If we assume that at low salt concentration protein binding is dominated by charge compensation, the total number of protein molecules that can bind to the gel ( $N_b$ ) is approximately given by the total charge on the gel ( $Q_{gel}$ ) divided by the



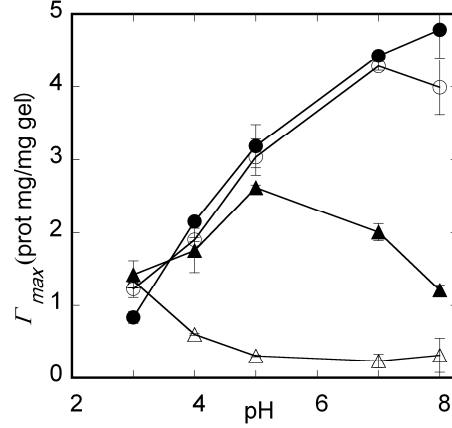


Figure 3.7 Saturation lysozyme uptake capacity  $\Gamma_{sat}$  for the DO100% microgel at various ionic strengths as a function of pH, at ionic strengths of 0.05 M (●), 0.10 M (○), 0.20 M (▲) and 0.50 M (△).

total charge of the bound protein ( $Q_{prot}$ ). It is simple to see that  $N_b$  increases with increasing pH. However, with increasing salt concentration, due to the screening effect, charge compensation becomes less important, and this leads to a decrease in protein uptake capacity  $\Gamma_{sat}$ . This effect is strong for pH values higher than  $pH_{opt}$ . This can be explained from the finding that at high pH the binding affinity is relatively low, so adding salt can easily release the protein from the gel. Strikingly, the saturation protein uptake at low pH is almost independent of ionic strength, suggesting that screening plays no role in this pH range.

We calculated the charge ratio  $R$  between bound protein molecules and gel at protein saturation conditions, based on the charge of the protein [25, 28] and the gel [5], obtained from proton titrations:  $R = Q_{LSZ} \times \Gamma_{sat} : Q_{gel}$ , in which  $Q_{LSZ}$  and  $Q_{gel}$  are the net charge densities (C/g) of the protein and the gel (free in solution), respectively. The results are presented in Table 3.2. Indeed we found for the ionic strengths of 0.10 M and 0.20 M that the charge ratio is 1:1 at the pH value at which the protein uptake capacity  $\Gamma_{sat}$  has a maximum. For 0.05 M the maximum in  $\Gamma_{sat}$  seems to be outside the pH range studied: in this case the 1:1 charge ratio would appear at  $pH > 8.0$ ; for 0.5 M the maximum may be located at the other end ( $pH \approx 3$ ). It should be noted that the large values for  $R$  at pH 3 are mainly due to the fact that we used the charge densities of the protein and gel free in solution; due to their interaction their actual charge densities in the protein-gel complex are different. We will come back to this later.

Table 3.2 Total charge ratio  $R$  of lysozyme to microgel at various ionic strengths and pH values, for the DO100% microgel.  $R = Q_{\text{LSZ}} \times \Gamma_{\text{sat}} : Q_{\text{Gel}}$ .  $\Gamma_{\text{sat}}$  is the saturation protein uptake in units of mg protein/mg gel.  $Q_{\text{LSZ}}$  and  $Q_{\text{Gel}}$  are the net charge densities (C/g) from proton titration experiments, so any charge regulation is not taken into account. The conditions at which a maximum in protein uptake capacity occurs are indicated by a circle.

pH	$R (Q_{\text{LSZ}} \times \Gamma_{\text{max}} : Q_{\text{Gel}})$ at varying ionic strength		
	0.05M	0.10M	0.20M
3	6.8	4.6	7.2
4	2.2	1.1	1.3
5	1.2	0.9	1.0
7	1.1	1.0	0.6
8	1.1	0.9	0.3

### *De-swelling of the microgel as a result of complex formation*

De-swelling was monitored by observing the change in the size of microgel particles after adding a protein solution (pH 3, 5, and 8; 0.2 M ionic strength) using optical microscopy. The concentration of the protein solution (20 mg/mL) was chosen in such a way that the saturation protein uptake by the microgel was achieved. Since the particles are of irregular shape, we take the length of an (arbitrarily chosen) cross-section  $L$  of the fixed particles as a measure of their size. We define the relative shrinkage as  $1 - v/v_0$  (see Eq. 3.6).

Figure 3.8A shows that the particles obtain an equilibrium size within 10 - 20 minutes after adding lysozyme solution. The shrinkage is 10% for pH 8, 30% for pH 5 and 44% for pH 3. As an example Figures 3.8B and 3.8C show a microgel particle before and after adding protein solution (pH 3.0).

The lysozyme-induced microgel de-swelling is in agreement with the finding by Johansson et al. [11, 12] for poly(acrylic acid) microgels. Bysell et al. [13] also found microgel de-swelling induced by poly-L-lysine uptake. It is noted here that, microgel swelling after protein incorporation has also been reported by various authors [15, 29, 30].

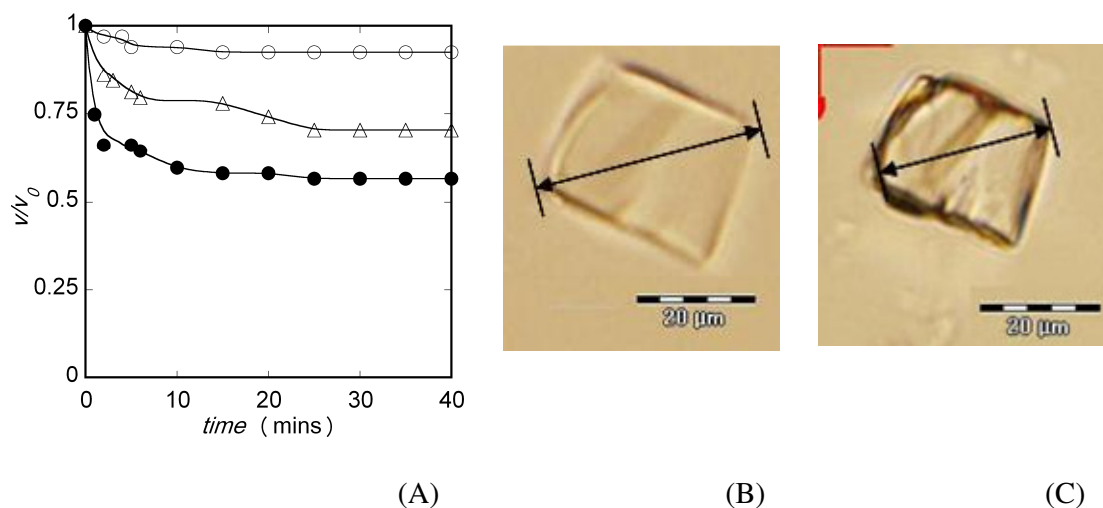


Figure 3.8 (A) De-swelling of DO100% microgel particles after protein uptake as a function of time. Protein concentration 20 mg/mL, ionic strength 0.2 M; pH 3.0 ( $\bullet$ ), pH 5.0 ( $\Delta$ ), pH 8.0 ( $\circ$ ). (B) DO100% microgel particle in the equilibrium swollen state at pH 3.0 before protein addition. (C) The same particle in the equilibrium shrunk state after adding protein.

In order to compare the mesh size before and after protein uptake, we first calculated the mesh size of the empty gel  $\zeta_{empty}$  [nm] according to the Flory-Rehner theory [20] (Eqs.3.7-3.9). Based on the experimental volumetric swelling capacity [5] (also see materials and methods), we then calculated the cross-link density, the volume fraction of polymer in the swollen gel, and the average molecular weight between cross-links, and finally we obtained the mesh size in nanometers. The mesh size of the microgel after protein uptake  $\zeta_{filled}$  was estimated as the mesh size of the empty particles  $\zeta_{empty}$  multiplied by the  $(v/v_0)^{1/3}$  (Eq. 3.10). Table 3.3 lists the results of the calculations. We stress that these results are just estimations because of the approximate nature of the Flory-Rehner model.

To summarize the data that we obtained in the previous sections, Figure 3.9 shows a schematic representation of the fully saturated microgel at pH 3, 5 and 8 and a ionic strength of 0.2 M, as compared with the empty gel. The shrinkage of the gel network after protein uptake increases with decreasing pH.

The electric charge density on the gel increases over the pH range 3 - 5, while the average mesh size is only slightly dependent on pH. It indicates that the repulsion among charged polymers in the network contributes little to the swelling of the gel.

The shrinkage of the gel network upon protein uptake increases with decreasing pH. It is caused by the electrostatic attraction between the protein and the gel. Our results suggest that the binding strength depends more on the charge of protein rather than on that of the gel.

Lysozyme carries more charges at low pH and therefore the binding is the strongest and the gel shrinks most.

Table 3.3 Calculated parameters related to the volumetric swelling capacity of the empty gel according to Flory-Rehner theory:  $SW_v$  is the volumetric swelling capacity,  $v_e$  is the effective cross-link density (mol/cm<sup>3</sup>) (Eq. 3.7),  $V_2$  is the volume fraction of polymer in the swollen gel,  $M_c$  is the average molecular weight between cross-links (Eq. 3.8),  $\xi_{empty}$  (Eq.3.9) is the mesh size of the empty gel. The mesh size of the microgel after protein uptake  $\xi_{filled}$  (Eq. 3.10) was estimated as  $\xi_{empty} * (v/v_0)^{1/3}$ . For all cases the ionic strength was 0.2 M.

pH	$SW_v$	$V_2$	$v_e$	$M_c$	$\xi_{empty}$	$\xi_{filled}$
			mol/cm <sup>3</sup>	g/mol	nm	nm
3	10.5	0.066	0.0037	402.1	9.0	7.4
5	10.7	0.064	0.0036	416.4	9.3	8.3
8	11.0	0.063	0.0034	438.3	9.7	9.5

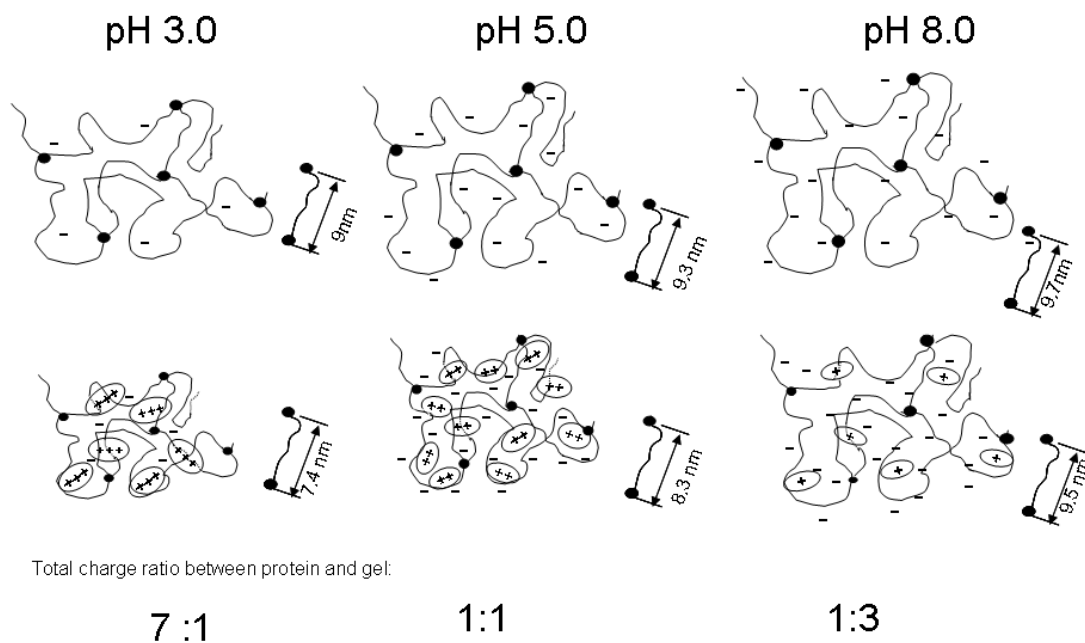


Figure 3.9 Schematic representation of the DO100% microgel before and after absorbing lysozyme at pH 3.0, 5.0 and 8.0, and a ionic strength of 0.20 M. Indicated is the average distance between two cross-links (the mesh size), and the total charge ratio between the bound protein and the gel. The mesh size of the microgel was calculated by Flory-Rehner theory, for details see Table 3.3. The amount of protein molecules schematically represents the saturation protein uptake  $\Gamma_{sat}$ ; +++ indicates a high charge density on the protein molecules, + a low charge density. For clarity, the counterions are not included in this sketch.

Figure 3.10 shows a picture of various microgel dispersions, which was made after protein saturation (pH 3, 5, 7 and 8 and at an ionic strength of 0.2 M). It is clearly visible that at pH 5 the solution is the most turbid. In addition, we observed that at pH 5 the complexes sediment faster than at pH 3, 7 and 8. The empty gel particles (range from 1 - 40  $\mu\text{m}$ ) can be dispersed in water because of the charges on their surface, and their density is similar to water. When protein is absorbed, the charges on the gel are neutralized and the particle density increases. Table 3.2 shows that the charge ratio between protein and gel is 1:1 at pH 5 and 0.20 M, so under these conditions full charge compensation occurs and the gel particles aggregate and settle down.

The faster sedimentation speed of the complexes at a pH where the complexes are charged-balanced is in agreement with observations of others [6, 31, 32].

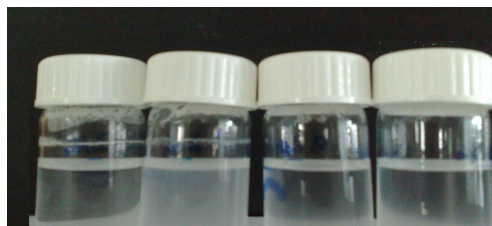


Figure 3.10 Photograph of protein-DO100% microgel mixtures (at saturation protein uptake and ionic strength 0.20 M, equilibrated for 4 h). From left to right: pH 3.0, 5.0, 7.0 and 8.0.

### ***Charge regulation during absorption***

Charge regulation is the adjustment of the charge density of one or more species resulting from their mutual interaction. This process usually involves species that contain weak acid or weak base groups. Charge regulation commonly occurs when proteins interact with charged polyelectrolytes immobilized on a surface [16-18], e.g. a polymer brush [19]. It is to be expected that in our case of interaction between proteins and charged microgel particles, charge regulation may take place as well. We checked this by adding concentrated protein solution to a microgel solution of exactly the same pH and ionic strength in a so-called pH-STAT titration. Any pH change upon addition of the protein solution is caused by protons uptake by protein molecules or dissociation of protons from the gel particles. Thus, the amount of protons required to keep the pH constant is a measure for the overall charge adjustment that takes place upon complex formation.

Figures 3.11A and 3.11B give the total number of protons taken up during complex formation (expressed per protein molecule) for a range of ionic strengths (0.05 - 0.20 M) at pH 5.0, and for a range of pH values (pH 4, 5, and 8) at a ionic strength of 0.05 M,

respectively. Figure 3.11A shows that the charge regulation decreases with increasing ionic strength. Figure 3.11B shows that there is a maximum in the degree of charge regulation as a function of pH: at pH 5 it is larger than at pH 4 and 8.

These results indicate that under the influence of the negative electric potential of the microgels, the protein molecules take up protons from solution in order to increase their charge density, facilitating their binding to the microgel. The charge regulation occurs most prominently in the initial steps of the titration, and therefore largely affects the affinity. As more protein molecules bind to the microgel, the negative charges of the microgel become neutralized, so the electric potential in the gel approaches to zero and the tendency of the protein molecules to pick up more protons diminishes. The decrease in charge regulation with increasing ionic strength is due to screening of the electric potential in the gel.

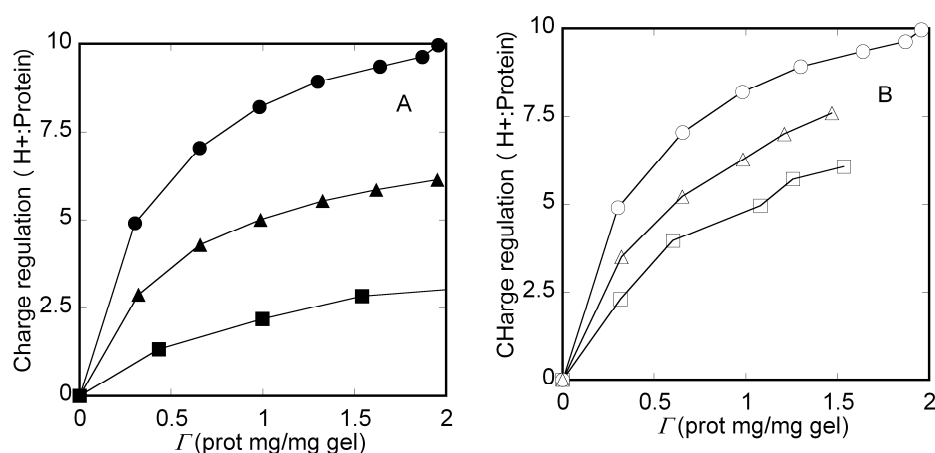


Figure 3.11 Number of protons taken up per protein molecule during complex formation with the DO100 % microgel as a function of the protein uptake  $\Gamma$ . (A) at pH 5.0, for ionic strengths 0.05 M (●) 0.10 M (▲), and 0.2 M (■). (B) for a ionic strength of 0.05 M, at various pH values: pH 4.0 (□), pH 5.0 (○), pH 8.0 (Δ).

To further clarify the effect of the pH on the degree of charge regulation, we measured the amount of protons taken up or released for a protein uptake  $\Gamma$  of 0.30 mg/mg gel, as a function of the pH at an ionic strength of 0.05 M. The results are shown in Figure 3.12. Clearly, there is a maximum in the charge regulation at pH 5.0. The value at pH 3.0 (an approximate value, see materials and methods section) is negative, indicating that in this case the weakly charged microgel particles charge up more strongly when they interact with the highly positively charged proteins. It is a general phenomenon in charge regulation that for interaction between two charged species or surfaces that can adapt their charge densities, it is the one with the lowest electric potential (positive or negative) with respect to the bulk solution (hence, the highest susceptibility), that adjusts its charge density [33, 34]. At low pH,

this is the microgel, but with increasing pH the electric potential in the gel becomes more negative and the charge on the protein less positive, so charge regulation happens increasingly by proton uptake by the protein. The decrease in the degree of charge regulation between pH 5 and 8 is because in this pH range the proton charge of the lysozyme is nearly invariant [25].

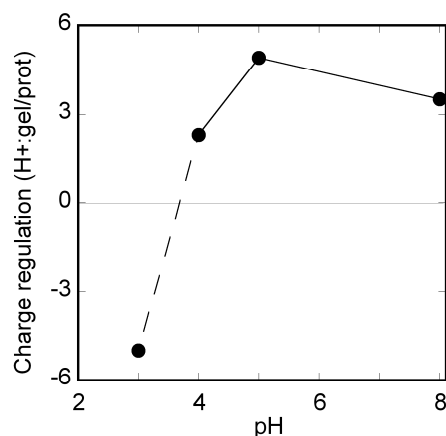


Figure 3.12 Number of protons taken up or released during complex formation, expressed per protein molecule, as a function of pH. The protein uptake  $\Gamma$  at all pH values is 0.30 mg protein /mg gel and the ionic strength is 0.05 M. A positive value indicates that protons are taken up by the protein, a negative value means that protons are release from the gel.

### 3.4 Concluding remarks

The results on the interaction between oxidized potato starch polymer (OPSP) microgel and the protein lysozyme presented in this chapter, provide insight in the factors that control the uptake and release properties of this system. For application in practice protein uptake capacity should be high and one should be able to control the binding affinity. For our system the protein uptake capacity at low salt concentration is mainly determined by the charge ratio between protein and microgel and increases with increasing pH. For higher salt concentrations an optimum pH for protein uptake is observed, which shifts to lower pH values with increasing salt concentration. The binding affinity, on the other hand, seems to be dominated by the charge density on the protein and decreases with increasing pH. As a result, the protein binds with low affinity at high pH and high salt concentration and is under these conditions easily released by dilution. In contrast, at low pH and low salt concentration the protein binds so strongly that dilution does hardly result in any protein release. Therefore, at intermediate pH (around pH 5) there is an optimal balance between protein uptake capacity and binding affinity. Protein release can be triggered by increasing the pH and/or ionic strength.

In the complex formation between protein and gel, charge regulation plays a moderate role at low salt concentration: at low pH the gel adapts its charge density under influence of the highly positively charged protein molecules, while at higher pH values (pH > 3 to 4) the protein molecules charge up because of the negative electric potential in the gel.

We further established that the microgel particles de-swell upon protein uptake, mainly caused by electrostatic attraction. The protein distributes rather homogenously through the microgel.



## References

- [1] B.S.F. Cury, A.D. Castro, S.I. Klein, R.C. Evangelista, Modeling a system of phosphated cross-linked high amylose for controlled drug release. Part 2: Physical parameters, cross-linking degrees and drug delivery relationships, *Int. J. Pharm.*, 371 (2009) 8-15.
- [2] V. Lenaerts, I. Moussa, Y. Dumoulin, F. Mebsout, F. Chouinard, P. Szabo, M.A. Mateescu, L. Cartilier, R. Marchessault, Cross-linked high amylose starch for controlled release of drugs: recent advances, *J. Control. Release*, 53 (1998) 225-234.
- [3] J. Mulhbachter, P. Ispas-Szabo, V. Lenaerts, M.A. Mateescu, Cross-linked high amylose starch derivatives as matrices for controlled release of high drug loadings, *J. Control. Release*, 76 (2001) 51-58.
- [4] M. Rahmouni, F. Chouinard, F. Nekka, V. Lenaerts, J.C. Leroux, Enzymatic degradation of cross-linked high amylose starch tablets and its effect on in vitro release of sodium diclofenac, *Eur. J. Pharm. Biopharm.*, 51 (2001) 191-198.
- [5] Y. Li, R. De Vries, T. Slaghek, J. Timmermans, M.A. Cohen Stuart, W. Norde, Preparation and characterization of oxidized starch polymer microgels for encapsulation and controlled release of functional ingredients, *Biomacromolecules*, 10 (2009) 1931-1938.
- [6] C. Schmitt, C. Sanchez, S. Desobry-Banon, J. Hardy, Structure and technofunctional properties of protein-polysaccharide complexes: A review, *Critical Reviews in Food Science and Nutrition*, 38 (1998) 689-753.
- [7] C.G. de Kruif, F. Weinbreck, R. de Vries, Complex coacervation of proteins and anionic polysaccharides, *Curr. Opin. Colloid Interface Sci.*, 9 (2004) 340-349.
- [8] S.L. Turgeon, C. Schmitt, C. Sanchez, Protein-polysaccharide complexes and coacervates, *Curr. Opin. Colloid Interface Sci.*, 12 (2007) 166-178.
- [9] C.L. Cooper, P.L. Dubin, A.B. Kayitmazer, S. Turksen, Polyelectrolyte-protein complexes, *Curr. Opin. Colloid Interface Sci.*, 10 (2005) 52-78.
- [10] V.A. Kabanov, V.B. Skobeleva, V.B. Rogacheva, A.B. Zezin, Sorption of proteins by slightly cross-linked polyelectrolyte hydrogels: Kinetics and mechanism, *Journal of Physical Chemistry B*, 108 (2004) 1485-1490.
- [11] C. Johansson, P. Hansson, M. Malmsten, Interaction between lysozyme and poly(acrylic acid) microgels, *Journal of Colloid and Interface Science*, 316 (2007) 350-359.
- [12] C. Johansson, P. Hansson, M. Malmsten, Mechanism of lysozyme uptake in poly(acrylic acid) microgels, *Journal of Physical Chemistry B*, 113 (2009) 6183-6193.
- [13] H. Bysell, M. Malmsten, Visualizing the interaction between poly-L-lysine and poly(acrylic acid) microgels using microscopy techniques: Effect of electrostatics and peptide size, *Langmuir*, 22 (2006) 5476-5484.
- [14] G.M. Eichenbaum, P.F. Kiser, A.V. Dobrynin, S.A. Simon, D. Needham, Investigation of the swelling response and loading of ionic microgels with drugs and proteins: the dependence on cross-link density, *Macromolecules*, 32 (1999) 4867-4878.
- [15] J. Rubio-Retama, F.M. Tamimi, M. Heinrich, E. López-Cabarcos, Synthesis and characterization of poly(magnesium acrylate) microgels, *Langmuir*, 23 (2007) 8538-8543.
- [16] P.M. Biesheuvel, A. Wittemann, A modified box model including charge regulation for protein adsorption in a spherical polyelectrolyte brush, *Journal of Physical Chemistry B*, 109 (2005) 4209-4214.
- [17] F.A.M. Leermakers, M. Ballauff, O.V. Borisov, On the mechanism of uptake of globular proteins by polyelectrolyte brushes: A two-gradient self-consistent field analysis, *Langmuir*, 23 (2007) 3937-3946.

- [18] A. Wittemann, M. Ballauff, Interaction of proteins with linear polyelectrolytes and spherical polyelectrolyte brushes in aqueous solution, *Physical Chemistry Chemical Physics*, 8 (2006) 5269-5275.
- [19] W.M. De Vos, P.M. Biesheuvel, A. De Keizer, J.M. Kleijn, M.A.C. Stuart, Adsorption of the protein bovine serum albumin in a planar poly(acrylic acid) brush layer as measured by optical reflectometry, *Langmuir*, 24 (2008) 6575-6584.
- [20] P.J. Flory, J. Rehner Jr, Statistical mechanics of cross-linked polymer networks II. Swelling, *The Journal of Chemical Physics*, 11 (1943) 521-526.
- [21] J. Rigney, M.D. Little, D.C. Martin, Swelling studies of cross-linked poly(p-phenylene terephthalamide) copolymers in sulfuric-acid, *Journal of Polymer Science Part B-Polymer Physics*, 32 (1994) 1017-1021.
- [22] M.B. Huglin, M. Rehab, M.B. Zakaria, Thermodynamic interactions in copolymeric hydrogel *Macromolecules*, 19 (1986) 2986-2991.
- [23] R.J.H. Stenekes, S.C. De Smedt, J. Demeester, G.Z. Sun, Z.B. Zhang, W.E. Hennink, Pore sizes in hydrated dextran microspheres, *Biomacromolecules*, 1 (2000) 696-703.
- [24] P.M. Biesheuvel, M. Van Der Veen, W. Norde, A modified Poisson-Boltzmann model including charge regulation for the adsorption of ionizable polyelectrolytes to charged interfaces, applied to lysozyme adsorption on silica, *Journal of Physical Chemistry B*, 109 (2005) 4172-4180.
- [25] W. Norde, F.G. Gonzalez, C.A. Haynes, Protein adsorption on polystyrene latex-particles, *Polymers for Advanced Technologies*, 6 (1995) 518-525.
- [26] R.K. Hallberg, P.L. Dubin, Effect of pH on the binding of beta-lactoglobulin to sodium polystyrenesulfonate, *Journal of Physical Chemistry B*, 102 (1998) 8629-8633.
- [27] T.M. Lohman, P.L. Dehaseth, M.T. Record, Pentylsine-deoxyribonucleic acid interactions-a mode for the general effects of ion concentrations on the interactions of proteins with nucleic-acids, *Biochemistry*, 19 (1980) 3522-3530.
- [28] C.A. Haynes, E. Sliwinsky, W. Norde, Structural and electrostatic properties of globular protein at a polystyrene water interface *Journal of Colloid and Interface Science*, 164 (1994) 394-409.
- [29] E. Fernández, D. López, E. López-Cabarcos, C. Mijangos, Viscoelastic and swelling properties of glucose oxidase loaded polyacrylamide hydrogels and the evaluation of their properties as glucose sensors, *Polymer*, 46 (2005) 2211-2217.
- [30] A.P. Sassi, A.J. Shaw, H. Sang Min, H.W. Blanch, J.M. Prausnitz, Partitioning of proteins and small biomolecules in temperature- and pH-sensitive hydrogels, *Polymer*, 37 (1996) 2151-2164.
- [31] F. Weinbreck, R.H. Tromp, C.G. de Kruif, Composition and structure of whey protein/gum arabic coacervates, *Biomacromolecules*, 5 (2004) 1437-1445.
- [32] C. Sanchez, G. Mekhloufi, C. Schmitt, D. Renard, P. Robert, C.M. Lehr, A. Lamprecht, J. Hardy, Self-assembly of beta-lactoglobulin and acacia gum in aqueous solvent: Structure and phase-ordering kinetics, *Langmuir*, 18 (2002) 10323-10333.
- [33] Parsegia.Va, D. Gingell, Electrostatic interaction across a salt solution between two bodies bearing unequal charges, *Biophysical Journal*, 12 (1972) 1192-1204.
- [34] D.T. Atkins, R.M. Pashley, Surface forces between zns and mica in aqueous-electrolytes, *Langmuir*, 9 (1993) 2232-2236.

---

# Chapter 4

## Mobility of lysozyme inside oxidized starch microgels

---

### *Abstract*

The aim of this chapter is to determine the mobility of protein molecules inside oxidized potato starch polymer (OPSP) microgel particles (spherical, 10-20  $\mu\text{m}$  in diameter). This provides relevant information for controlled uptake and release applications of such systems. The mobility of Alexa-488 labelled lysozyme inside the microgel is measured by fluorescence recovery after photo bleaching (FRAP) in combination with confocal laser scanning microscopy (CLSM). CLSM images show that the protein molecules distribute quite homogeneously over the microgel particles. By fitting the FRAP data with a model based on exchange between bleached and unbleached protein molecules inside the gel, we identified several protein fractions of different mobility. Increasing the salt concentration (NaCl) or the pH causes a shift in the distribution towards the more mobile fractions. This is consistent with earlier uptake and release measurements, which showed that the binding affinity decreases with increasing salt concentration and pH. At low protein concentrations, at which the microgel is not saturated with protein, the mobility of the bound protein molecules is more restricted than at protein concentrations where the uptake is complete. This is attributed to binding of the protein molecules to multiple binding sites. The model explains reasonably the mechanism of protein mobility inside the microgel, indicating that embedded ingredients with charge properties comparable to those of lysozyme can be protected at low salt concentration and low pH. Increasing the salt concentration or the pH triggers the release.

## 4.1 Introduction

The Controlled uptake and release of functional compounds like peptides and proteins from microgel carriers have been studied extensively [1-4]. Due to the stimulus-responsive features of such carriers, the release of ingredients may be triggered by changes in temperature [5], pH [1, 6, 7], ionic strength [8, 9], solvent [5, 10, 11], or by applying an electric [12] or magnetic field [13]. Most of these studies focus on uptake and release characteristics. The mobility of proteins and peptides inside the microgel has received less attention. Yet this may be highly important for controlled uptake and release applications. The mobility of protein inside the polymer network reflects its binding strength to the polymer network, and this, in turn, is important for triggering its release. In addition, the mobility of macromolecules through polymer gels is essential for macromolecule-based therapies [14, 15].

In Chapter 2 and 3 [16, 17] we described the physical-chemical properties of oxidized potato starch polymer (OPSP) microgel particles and their uptake and release of lysozyme under different conditions. Our study presented here focuses on the mobility of positively charged lysozyme molecules entrapped and bound in these negatively charged oxidized microgel particles, as determined by fluorescence confocal laser scanning microscopy (CLSM) and fluorescence recovery after photo bleaching (FRAP).

CLSM is a useful tool to study the interaction between microgels and oppositely charged proteins or peptides as shown by recent studies [17-23].

FRAP is a widely used method to measure the mobility of fluorescently labelled molecules inside a certain matrix or in solution. The technique has been used, for example, to study the mobility of macromolecules in heterogeneous biomaterials [24], cell monolayers [25] and gels [26, 27]. A high intensity laser is used to photo bleach the fluorescent labels at a defined spot in the system. The recovery of fluorescence after this photo bleaching, due to the neighbouring fluorescent probes diffusing into the bleached area, is measured as a function of time. The exchange rate of bleached with unbleached protein molecules is the measure for the mobility.

Partitioning and transport of charged protein molecules in charged hydrogels has been studied before to some extent in order to establish the influence of electrostatic interactions on the diffusion process. For instance, Johnson et al. [28] found by FRAP and gel chromatography, that the effective diffusion coefficients,  $D_{eff}$ , of negatively charged proteins in like-charged sulphated agarose gels are 2-2.5 times smaller compared to their diffusion coefficients in solution,  $D_0$ . This was explained on the basis of a model describing the

diffusivity of spherical molecules within a random fibre matrix, taking into account the effective volumes of the fibres and the molecules (including repulsive double layer interactions). According to literature, the FRAP curve of polyelectrolyte capsules loaded with protein, indicates that deposited proteins are strongly bound to the polyelectrolyte [29].

Van Tomme et al. [30] investigated a system of lysozyme incorporated into a gel consisting of oppositely charged dextran microspheres by bulk release measurements and FRAP. They found that possibly two fractions of protein molecules are present in the gel. One fraction of protein has a high mobility and represents the protein existing in the pores between the microspheres, another fraction of protein showed restricted mobility, due to binding to the dextran.

Alternatively, the occurrence of different mobile fractions may be related to different affinities between the protein and the binding sites in the gel. Wang et al. [31] reported two kinds of binding sites (low and high affinity) for binding of caffeine to methacrylic acid microgel spheres. Vaughan et al. [32] found a number of binding sites for ethyladenine-9-acetate of varying affinity in their poly(MAA-co-EGDMA) microgel. In this Chapter we introduce a simple model to analyse our FRAP data. It is based on the exchange between bleached protein and unbleached protein at sites with different binding strengths.

The microgel particles that we used in Chapter 2 and 3 [16, 17] were irregularly shaped with a wide size distribution due to the preparation method, involving grinding, sieving and drying. For investigating the mobility of the protein inside the gel particles and the uptake and release kinetics, however, it is important to have spherical microgel particles with a narrow size distribution (10-20  $\mu\text{m}$  in diameter). For this reason we adopted inverse-emulsion polymerization as the preparation method. The resulting spherical microgel particles have the same physical-chemical properties as the previous used particles.

The partition coefficient of FITC-labelled dextran of different molecular weights in the hydrogel particles was used to estimate the pore size distribution of the gel [33]. This method is based on the phenomenon that diffusion is strongly restricted when the size of the dextran molecules is larger than the pore size of the gel [34]. Using CLSM we measured for single microgel particles the relative affinity of fluorescently labelled lysozyme as a function of pH and ionic strength and the distribution of the protein molecules over the particles. The mobility of the protein molecules inside the microgel was determined by FRAP.

## 4.2 Material and Methods

### *Materials*

Native starch was kindly provided by AVEBE, The Netherlands. The oxidation catalyst 2, 2, 6, 6-tetramethyl-1-piperidinyloxy (TEMPO) and ethanol (100%) were purchased from Merck, Germany. The cross-linker sodium trimetaphosphate (STMP), poly-DL-lysine hydrobromide, FITC-dextran (4-2000 kDa) and lysozyme (from chicken egg white,  $M_w$ = 14,400 g/mole) were supplied by Sigma-Aldrich. The fluorescent dye, Alexa Fluor 488 carboxylic acid succinimidyl ester (mixed with isomers) was purchased from Invitrogen. Span 80 and n-hexane were purchased from Sigma-Aldrich. Solutions were prepared using millipore water with a resistance = 18.3 M $\Omega$ /cm. All experiments were performed at room temperature.

### *Microgel preparation*

For details on the oxidation of starch polymers we refer to Chapter 2 [16]. Spherical microgel particles of cross-linked oxidized starch polymer were synthesized by inverse suspension polymerization, see below. For polymers with a degree of oxidation of 30% (DO30%) we obtained a high yield of stable gel particles, but the preparation method was not successful for DO100%.

Hexane was used as the continuous phase and Span 80 as the surfactant. Firstly, 25 mg Span 80 was dissolved in 10 mL hexane while stirring under nitrogen. A reaction mixture of 1 mL DO30% polymer (200 mg/mL), 0.5 mL cross-linker sodium trimetaphosphate (STMP) (100 mg/mL) and 0.3 mL NaOH (1 M) was stirred, also under nitrogen. The next step was pre-emulsification: 1.8 mL reaction mixture was added to 10 mL Span 80 containing hexane solution and stirred for 10 minutes at room temperature. After pre-emulsification, the mixture was passed 10 times through a 10  $\mu$ m (pore diameter) filter membrane in order to obtain a homogeneous size distribution around 10  $\mu$ m. Thereafter, the starch in the emulsion droplets was cross-linked to make microgel particles by heating to 40 °C while mildly stirring for 40 minutes. Finally, the microgel particles were washed with methanol three times by dispersion and centrifugation (3000 rpm, 3 minutes), followed by decantation of methanol and equilibration in excess water. The gel particles were stored in 2 mL water. Spherical 10-20  $\mu$ m sized microgel particles were obtained as confirmed by light microscopy. The yield, determined by freeze-drying, was 36.6%.

***Alexa Fluor 488 labeling of lysozyme***

A 400  $\mu\text{L}$  solution of 4 g/L lysozyme was prepared in 50 mM  $\text{K}_2\text{HPO}_4/\text{KH}_2\text{PO}_4$  buffer at pH 7.8. Alexa Fluor 488 was dissolved in DMSO (dimethyl sulfoxide) (1 mg/100  $\mu\text{L}$ ) and 40  $\mu\text{L}$  of this solution was added to the lysozyme solution. The reaction mixture was left in the dark for one hour. Then, the mixture was centrifuged for one minute at 13000 rpm and an orange precipitate separated from the yellow solution. The supernatant was eluted over a Bio-Gel P6DG (Bio-Rad) column and concentrated using a 10000 kDa spin filter. Then the precipitate was dissolved by adding 150  $\mu\text{L}$  7 M GuHCL in  $\text{K}_2\text{HPO}_4/\text{KH}_2\text{PO}_4$  buffer at pH 6 and centrifuged again. The supernatant of this mixture and the previous concentrated supernatant fraction were purified by gel filtration using a Superdex 75 HR column.

The precipitates, which are rich in labelled lysozyme, were pooled and concentrated using a 10000 kDa spin filter. Then all the labelled protein from supernatants as well as precipitates was collected and stored in 20% glycerol. The average number of labels per lysozyme molecule was determined to be 3. The lysozyme concentration was 70  $\mu\text{g} / \text{mL}$ .

***Fluorescence confocal laser scanning microscopy***

A confocal microscope (Carl Zeiss Axiovert 200 microscope, Zeiss, Germany) equipped with a LSM 5 Exciter configuration and a 63 $\times$ /0.75 objective and an Argon laser set at 488 nm was used. The standard settings were: pinhole 1.8  $\mu\text{m}$ ; gain 755; transmission 1.39%. For analysis the software “Zen 2008” was used.

As flow cell (channel) under the microscope  $\mu$ -Slides I Luer0.2 (50  $\mu\text{L}$ ; Ibidi, Germany) were used. Z-stack scanning was used to make 3D images of microgel particles loaded with fluorescent labelled protein.

***Pore size distribution***

According to Russel et al [33]., the relative uptake of dextran of various molar masses can be used to determine the pore size of a hydrogel. FITC-dextran powders of molar masses 4, 70, 150, 250, 500 and 2000 kDa were dissolved in phosphate/citric acid buffer pH 7 to make a concentration of 0.1%. The gel particle suspension was 100 $\times$  diluted using the same buffer and 1 mL of this diluted suspension was mixed with 1 mL of the various FITC-dextran solutions. The test tubes containing these mixtures were sealed using parafilm and kept in a box covered with aluminium foil in order to prevent exposure to light. After 2 weeks of equilibration, the dextran-loaded microgels were examined by confocal microscopy. The

evaporation of water was less than 10 wt% and was neglected, since it would hardly influence the uptake of the dextran in the microgel.

### ***Exchange reaction between labeled and unlabeled protein***

This experiment is to determine how fast protein in the bulk solution can exchange with protein bound to the gel. The gel particles were fixed at the flow cell surface in order to be able to observe one and the same particle during the whole process. The bottom surface of the flow cell was coated with poly-DL-lysine by adsorption from a 0.1% poly-DL-lysine solution for two hours. Then, unabsorbed poly-lysine was flushed away and a diluted dispersion of microgel particles in water was added for one hour. Subsequently, unattached gel particles were rinsed off, and 3 mg/mL unlabelled lysozyme solution was supplied into the cell for 30 minutes. This high lysozyme concentration was to guarantee reaching the uptake saturation. The unabsorbed protein was rinsed away with water. Then 1.4  $\mu\text{g/mL}$  Alexa Fluor 488 labelled lysozyme was added into the cell to exchange with the unlabelled protein absorbed inside the gel particles. Time series of fluorescence scanning pictures were taken continuously. (The time series button was already clicked on before adding labelled protein, in order to observe the exchange reaction from the beginning.)

### ***Fluorescence recovery after photo bleaching (FRAP)***

Diluted gel dispersions were mixed with Alexa Fluor 488 lysozyme solutions (of different protein concentrations, pH values and salt concentrations). Equilibration was allowed for 2 hours and after that individual gel particles were selected under the fluorescence microscope. Confocal scans (512×512 pixel images) were made in the xy plane of the sample at a fixed z-position (through the centre of the particle). First 5 pre-bleach scanned images at low laser intensity (1.39%) were monitored (0.5 s each), then a selected area was bleached with 100 iterations (about 50 s in total) at 100% laser intensity, followed by detection of the fluorescence recovery again at low intensity. Scans were collected for each sample until full recovery was reached.

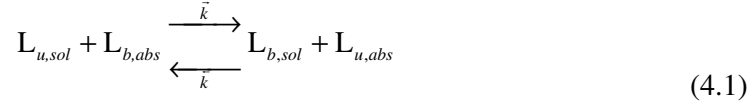
### ***Theoretical analysis of FRAP data***

The FRAP experiment implies an exchange process between bleached protein and unbleached protein. After bleaching the selected area in the gel, the bleached protein may be replaced by unbleached protein. At pH 11, at which the protein bears no net charge ( $pI = 11$ ), we found that diffusion of lysozyme to the centre of the gel particles only takes 1 - 2 seconds.



This is in line with expectation, since at this pH the protein does not bind to the gel [17] and the effective diffusion coefficient of the protein in the gel network is of the same order of magnitude as the one in solution [28] ( $D_0 = 1.1 \times 10^{-10} \text{ m}^2/\text{s}$ ) [35].

Since diffusion of unbleached protein into the pores is fast, for pH values at which the protein does bind to the gel, the fluorescence recovery rate of the bound protein is determined by the rate of the exchange reaction:



Here, L represents lysozyme, the subscripts u and b refer to unbleached and bleached, respectively, and sol and abs for free in solution and bound (absorbed) to the gel. When there is enough protein supply (from solution) full recovery of fluorescence can be reached. The time required for full recovery depends on the strength of the binding of the protein to the gel. The kinetics of fluorescence recovery can be written as:

$$\frac{d\theta_u}{dt} = \bar{k}C_{p,u}\theta_b - \bar{k}C_{p,b}\theta_u \quad (4.2)$$

where  $\theta_u$  and  $\theta_b$  are the fractions of unbleached and bleached bound protein, and  $C_{p,b}$  and  $C_{p,u}$  are the bleached and unbleached protein concentrations in solution, respectively. Experimentally,  $\theta_u$  is calculated by

$$\theta_u(t) = \frac{I(t) - I_b}{I_0 - I_b} \quad (4.3)$$

where  $I(t)$  is the fluorescence intensity of the bleached spot at time  $t$ ;  $I_b$  is the fluorescence intensity of the bleached spot immediately after bleaching ( $t = 0$ ) and  $I_0$  is the fluorescence intensity of the spot prior to bleaching.

Because the bleached protein free in solution (in the pores) is very quickly replaced by unbleached protein,  $C_{p,b}$  is extremely low so that  $C_{p,u} \approx C_p$  and the reverse reaction can be neglected. Now  $\bar{k}$  is denoted as  $k$ . Hence, Equation (4.2) simplifies to

$$\frac{d\theta_u}{dt} = kC_p\theta_b \quad (4.4)$$

Because  $\theta_b + \theta_u = 1$ ,

$$\frac{d\theta_u}{1 - \theta_u} = kC_p dt \quad (4.5)$$

Integration of this equation gives:

$$\theta_u = 1 - \exp(-kC_p t) \quad (4.6)$$

In practice, the protein molecules in the gel may not all be bound with the same strength and, hence, show different exchange kinetics. Assume that the total amount of bound protein consists of  $n$  fractions with different binding strengths:  $\theta_1, \theta_2, \theta_3 \dots \theta_n$ . During fluorescence recovery each of these fractions contains bleached as well as unbleached protein molecules:

$$\theta_n = \theta_{n,u} + \theta_{n,b}$$

For each fraction an equation similar to Equation (4.5) can be written, e.g. for the fluorescence recovery of fraction 1:

$$\frac{d\theta_{1,u}}{1 - \theta_{1,u} - \theta_2 - \theta_3 - \dots - \theta_n} = \frac{d\theta_{1,u}}{\theta_1 - \theta_{1,u}} = k_1 C_p dt \quad (4.7)$$

with  $k_1$  the exchange rate constant for this fraction.

The result of integration is:

$$\theta_{1,u} = \theta_1 [1 - \exp(-k_1 C_p t)] \quad (4.8)$$

The total fraction of unbleached bound protein is then simply given by:

$$\theta_u = 1 - \sum_n \theta_n \exp(-k_n C_p t) \quad (4.9)$$

## 4.3 Results and discussion

### *Pore size distribution within the gel particles*

After incubation of the gel particles with FITC-dextran for two weeks, the partition coefficients (ratio between the fluorescence intensities inside and outside the gel) were determined and the ratio between these values is plotted in Figure 4.1 as a function of the molar mass of the dextran. Based on the approximate Stokes' radii of the FITC-dextran molecules of different molar masses, it is inferred that the sizes (radii) of most of the pores range between 4 and 25 nm. This size range is well beyond the dimensions of Alex-488 labelled lysozyme (dimensions 4.6×3.0×3.0 nm) [36], so that the protein can diffuse into all parts of the gel network. It is worth to mention that the partition coefficient for 4 kDa dextran is 0.6. This may indicate that there are still some pores < 4 nm, and that some regions are inaccessible to lysozyme.

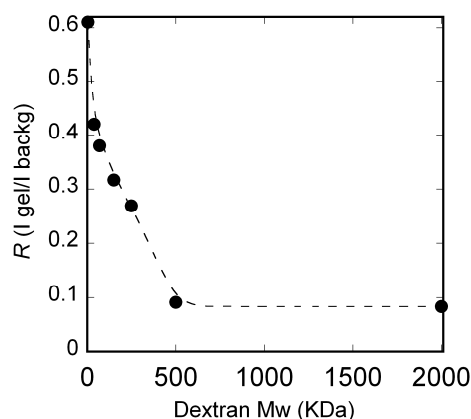


Fig. 4.1 The ratio between the fluorescence intensities inside the microgel and in solution as a function of the molecular weight (in kDa) of FITC-dextran incorporated. The gel particles were mixed with FITC dextran of different sizes in water and equilibrated for two weeks.

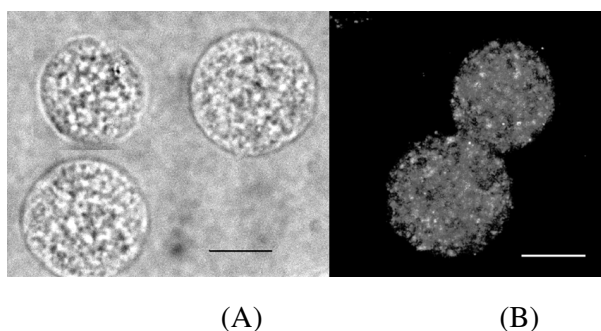


Fig. 4.2 (A) 2D image of empty microgel particles in water by optical microscopy. (B) 3D image of microgel particles loaded with Alexa Fluor 488 labelled lysozyme by fluorescence CLSM. The protein absorption was done in water with a protein concentration of 2.74  $\mu\text{g/mL}$ , pH 7. Equilibration was allowed for 2 hours. The scale bars in both figures represent 10  $\mu\text{m}$ .

### ***Protein distribution within the gel particles***

A homogeneous distribution of protein in the microgel is important for controlled release applications. Information on this distribution can be obtained by fluorescence confocal laser scanning microscopy (CLSM).

Figure 4.2A shows the appearance of the optimized microgel particles dispersed in water. They are spherical and transparent. The 3D image obtained by z-stack scanning fluorescence CLSM (Figure 4.2B) shows microgel particles loaded with Alexa-488 labeled lysozyme in water. Figure 4.3 gives the intensity profile along a line through the center of a particle loaded with protein. This profile indicates that the protein is distributed rather homogeneously over the microgel; the slight fluctuations may be due to variations in the density (i.e., the density of

protein binding sites) of the gel and the presence of small pores (see above). This confirms the conclusion from the pore size determination that the protein can diffuse into practically all parts of the microgel particles.

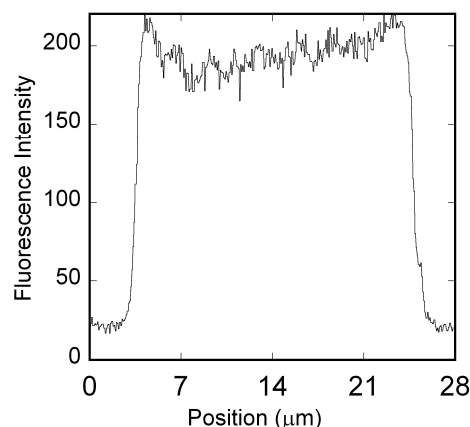


Fig. 4.3 Fluorescence intensity profile (arbitrary units) along a line through the center of a microgel particle (same conditions as in Fig. 4.2B). The position from left to right: 0-3  $\mu\text{m}$  outside the microgel; 4-25  $\mu\text{m}$  inside the microgel; 26-28  $\mu\text{m}$  outside the microgel. The curve demonstrates that the protein distributes fairly homogeneously throughout the microgel.

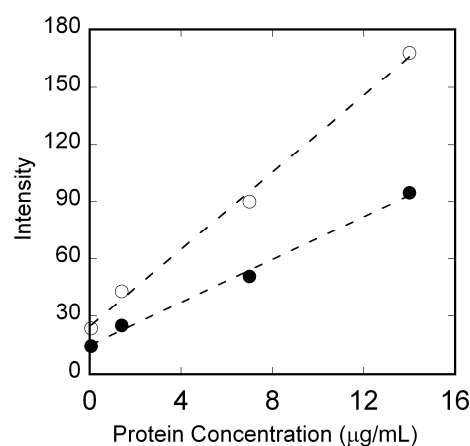


Fig. 4.4 The fluorescence intensity (arbitrary units) of Alexa Fluor 488 labelled lysozyme solution (in water) as a function of the protein concentration ( $\mu\text{g/mL}$ ). (○) Transmission 2.55%; (●) Transmission 1.39%.

This result differs from the finding of Johansson et al. [21] that lysozyme distributes nonuniformly within poly(acrylic acid) microgels, forming a lysozyme/microgel shell in the outer parts of the microgel. The authors associate this with lysozyme induced deswelling of the gel network, leading to effective pore sizes in the shell smaller than the size of the protein

molecule. The reasons that we do not observe this phenomenon are most probably that our microgel has much larger pore sizes and lysozyme induced deswelling of our starch polymer gel is much less pronounced [17].

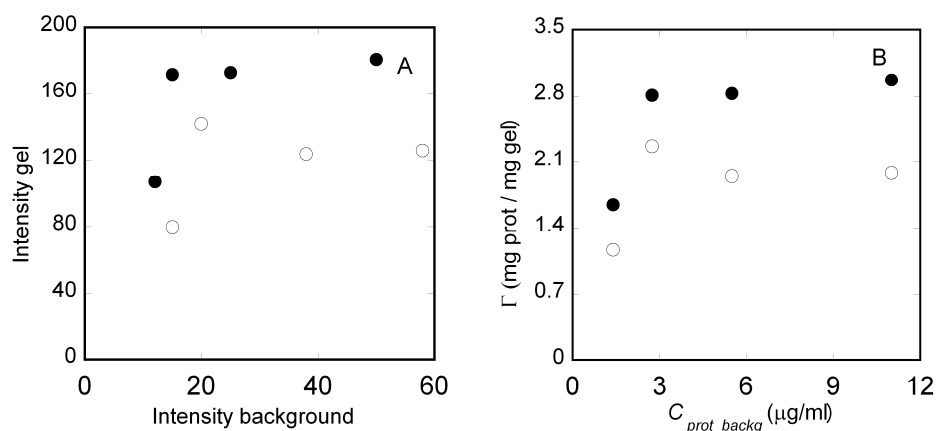


Fig. 4.5 (A) Fluorescence intensity (arbitrary units) of the gel particles as a function of the intensity of the protein solution in the background. With increasing Alexa-488 labelled lysozyme concentration, the microgel becomes more loaded with this protein until saturation is reached. The points from left to right represent the following protein concentrations: 1.4, 2.74, 5.5, and 11  $\mu\text{g/mL}$ ; pH 7. (●) 0 M NaCl; (○) 0.005 M NaCl. (B). Absorption isotherm obtained by calculating the protein concentrations and uptake from the intensities in Fig. 4.5A using the calibration line in Fig. 4.4 and the density of the gel.

### ***Binding affinity of protein to microgel***

In order to obtain more quantitative results by fluorescence confocal laser scanning microscopy, a calibration curve for the fluorescence intensity as function of protein concentration was determined. The fluorescence label Alexa Fluor 488 is a very stable dye and not very sensitive to quenchers such as dissolved oxygen. Figure 4.4 shows that the fluorescence intensity from an Alexa-488 labelled lysozyme solution varies linearly with protein concentration, up to at least 16  $\mu\text{g/mL}$ . Hence, quantitative results can be obtained if the protein concentration is within this range.

Figure 4.5A shows that the fluorescence intensity from a protein loaded gel particle reaches a plateau value above a certain protein concentration in solution. Before each measurement equilibration was allowed for 2 hours. The concentration at which protein uptake reaches saturation amounts to about 2.74  $\mu\text{g/mL}$ , both in water without added salt and in 0.005 M NaCl. At this protein concentration the fluorescence contrast between particles and solution ( $I_{\text{gel}} - I_{\text{sol}}$ ) has a maximum value and therefore we used this protein concentration

in most of our experiments described here. As it is known that the density of polymer in a single swollen gel particle is approximately 0.01 mg/ml (calculated on the basis of swelling data [16]), the absorbed amounts can be roughly calculated from the intensity data in Fig. 4.5A using the calibration curve in Fig. 4.4. The results are presented in Fig. 4.5B. For pH 7 and no salt added, the saturation protein uptake is 2.8 mg/mg gel, which is comparable to our earlier results on protein uptake by bulk measurements[16]: 2.4 mg/mg gel for DO30% particles at pH 7 and an ionic strength of 0.05 M. This plateau in uptake was reached at a protein concentration of 0.3 mg/mL. The affinity here is much higher, since the plateau is reached already at a very low protein concentration. This is also consistent with previous results that show that the affinity strongly increases with decreasing ionic strength[17].

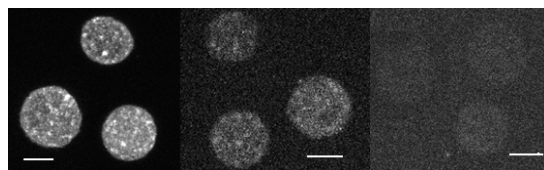


Fig. 4.6 2D image of microgel particles loaded with Alexa Fluor 488 labelled lysozyme by fluorescence CLSM at pH 3, 4 and 8 (from left to right). The ionic strength (buffer) is 0.05 M. The scale bar indicated is 10  $\mu\text{m}$ . Equilibration time is 2 hours.

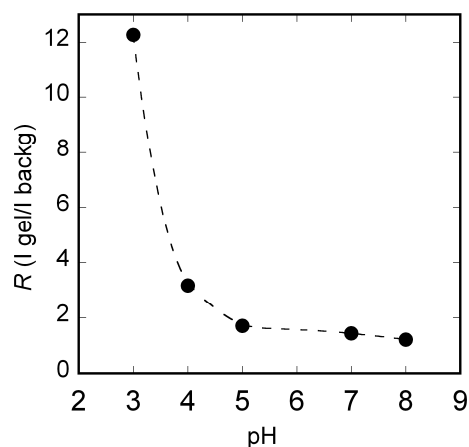


Fig. 4.7 The ratio of fluorescence intensities inside and outside the microgel as a function of pH. The ionic strength (buffer) is 0.05 M. Equilibration time is 2 hours.

### *pH effect on binding affinity of protein to microgel*

The binding affinity is an important parameter for controlled release, as protein release is only possible from sites where the binding affinity is not too high. The partition coefficient, describing the distribution of protein between gel and solution, can be considered as a measure of the binding affinity. Figure 4.6 shows CLSM images of microgel particles loaded with Alexa-488 labeled lysozyme at different pH values and an ionic strength of 0.05 M. The contrast between the gel and the background decreases with increasing pH. The ratio between the intensities inside and outside the gel particles is plotted in Figure 4.7. It shows that the binding strength decreases with increasing pH, which is in line with the pH dependency of the affinity for lysozyme in DO100% microgels as reported in Chapter 3 [17], which was obtained from the initial slopes of binding isotherms. In Chapter 3 we concluded that the binding is mainly determined by electrostatic interactions; the observed trend results from the decrease of the (positive) charge on the protein with increasing pH.

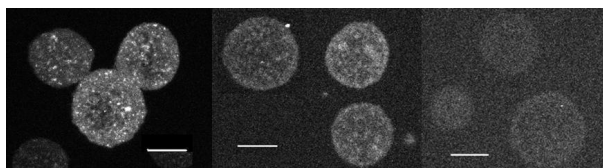


Fig. 4.8 2D image of microgel particles loaded with Alexa Fluor 488 labelled lysozyme by fluorescence CLSM for increasing NaCl concentration; from left to right: 0 M; 0.005 M; 0.01 M. The scale bar indicated is 10  $\mu\text{m}$ . Equilibration time is 2 hours.

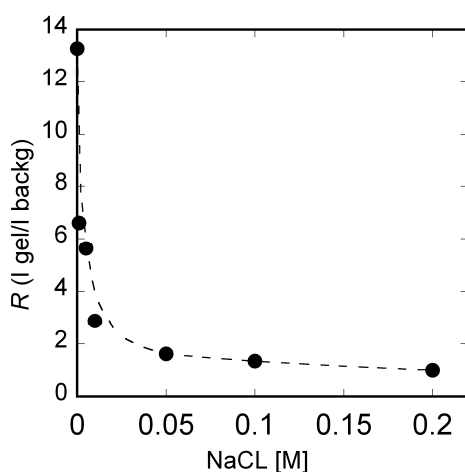


Fig. 4.9 The ratio of intensities inside and outside the microgel as a function of increasing NaCl concentration at pH 7. Equilibration time is 2 hours.

### *Salt effect on binding affinity of protein to microgel*

CLSM images of lysozyme loaded microgel particles at different NaCl concentrations at pH 7 are shown in Figure 4.8. The solutions contained no buffer; pH variation upon protein absorption from the solution into the gel was found to be less than 0.3 units. (As can be seen from Fig. 4.7 such slight shifts in pH around pH 7 do not significantly affect the protein binding.) As it is shown in Fig.4.8, the intensity contrast decreases with increasing salt concentration. In Figure 4.9, the variation of the ratio of intensity inside/intensity outside gel as a function of NaCl concentration is given. As expected, and in line with results in Chapter 3 [17], the affinity decreases with increasing salt concentration due to the screening of attractive electrostatic interactions.

It is worth mentioning that the “light spots” in Figs 4.6 and 4.8 probably represent somewhat denser parts of the microgel particles, leading to a higher concentration of bound proteins. It is not very likely that these spots reflect protein aggregates, since aggregation of lysozyme in solution does not occur under the experimental conditions used. Lysozyme only forms large aggregates at pH > 10, while it may self-associate into dimers, trimers and tetramers between pH 4 and 10, but only at higher salt concentrations than applied in our experiments[17, 21].

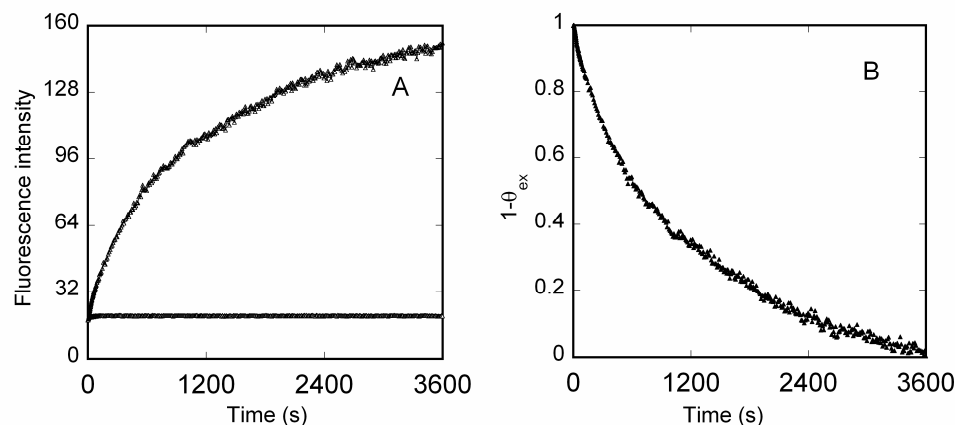


Fig. 4.10 (A) Change in fluorescence intensity (arbitrary units) inside the microgel after exchange of the solution of unlabelled lysozyme by a solution of Alexa-488 labelled lysozyme.  $C_p = 1.4 \mu\text{g/mL}$ , pH 7, no salt added. The fluorescence intensity from the solution is also indicated and is constant ( $I = 20$  arbitrary units). (B) Fraction of not yet exchanged bound protein ( $1 - \theta_{ex}$ ) calculated using  $\theta_{ex} = (I(t) - I_{backg}) / (I_{final} - I_{backg})$ .

### *Exchange of unlabeled protein with labeled protein*

In order to investigate the mobility of the protein molecules inside the gel, the gel particles were saturated with unlabeled lysozyme in water. Subsequently, we induced



exchange by changing the unlabeled protein solution by a solution containing labeled protein ( $C_p = 1.4 \mu\text{g/mL}$ , pH 7, no salt added). This exchange process was monitored by following in time the average fluorescence intensity for the whole section of the gel particle in the focal plane. During the process fluorescence images were recorded continuously. The shape of the radial intensity profile was found to be rather flat (as in Figure 4.3) at all times, indicating that the exchange rate is invariant with the position in the gel. Figure 4.10A shows that already at very short times (practically instantaneously) the fluorescence intensity in the gel equals that in the background solution ( $I = 20$  arb. units). This proves that diffusion of protein into the pores is indeed very fast compared to the exchange of protein molecules bound to the gel. The fraction of non-exchanged bound protein molecules,  $1 - \theta_{ex}$ , vs. time can be nicely fitted with an exponential function (Fig. 4.10B). The overall rate constant ( $kC_p$ ) obtained from a single exponential fit (Fig. 4.10B) is  $0.001 \text{ s}^{-1}$ . The reason that the process is relatively slow is probably that detachment of the unlabeled protein from the binding sites is the rate determining step. Only after this step labeled protein from the solution can adsorb onto the binding sites.

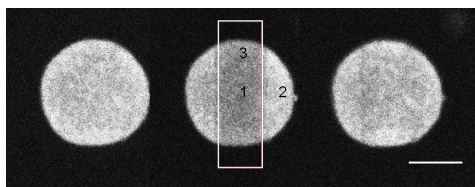


Fig. 4.11 Left: Fluorescence CLSM image of a protein loaded microgel particle before bleaching. Middle: image immediately after photo bleaching. (Only the part indicated by the rectangle was bleached). Right: image after fluorescence recovery (full recovery takes about 5 minutes). The Alexa Fluor 488 lysozyme concentration in solution was  $7 \mu\text{g/mL}$ , at pH 3 and ionic strength 0.05 M. The scale bar indicated is  $10 \mu\text{m}$ .

### ***Fluorescence recovery after photo bleaching (FRAP)***

Figure 4.10 shows the exchange reaction between unlabeled protein absorbed in the gel and labeled protein dissolved in the surrounding bulk solution. We used fluorescence recovery after photo bleaching (FRAP) in combination with confocal laser scanning microscopy (CLSM) to study the mobility of the protein inside the gel and the exchange kinetics in more detail and at various pH values and ionic strengths. The gel network was loaded with fluorescent labeled protein molecules and a high intensity laser was used to photo bleach them within a defined area (usually covering the whole surface area in the center position of the gel

particle). The recovery of fluorescence after photo bleaching was measured as a function of time.

Figure 4.11 shows that the area in the middle of the microgel particle turns black upon bleaching and recovers fully after about 5 minutes. The intensities of the bleached region (noted as “1” in Figure 4.11) and the unbleached region (“2” in Fig 4.11) were monitored and are given in Figure 4.12A. The intensity of the bleached region increases, while that of the unbleached region remains fairly constant; the slight decrease in intensity is due to gradual photo bleaching as a result of laser illumination during the measurements. This was checked by monitoring the fluorescence intensity of a gel particle loaded with protein without bleaching. Although there is an exchange of protein from the unbleached region to bleached region, there is always immediate protein supply from the solution in the pores, and therefore the intensity in region “2” is virtually unchanged.

In Figure 4.12B the fraction of bound bleached protein that has been replaced by unbleached protein ( $\theta_u$ , calculated according to Equation 4.3) is given. The data show that the recovery rate for the edge position (“3” in Figure 4.11) is the same as for the center position (“1”). This indicates that the FRAP results are invariant with the position in the gel.

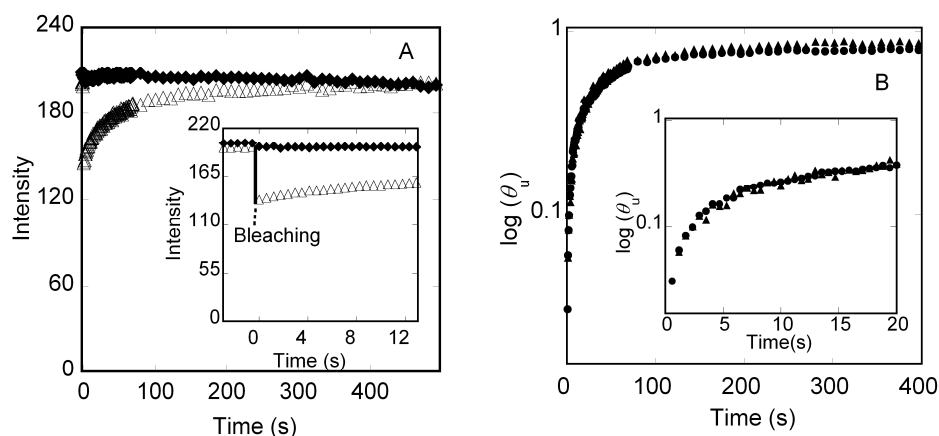


Fig. 4.12 (A) The time course of the intensity of the photo bleached region (noted as “1” in Figure 4.11) ( $\Delta$ ) and the unbleached region (“2” in Figure 4.11) ( $\diamond$ ). The insert gives the fluorescence recovery curves for the initial 12 seconds (full recovery took about 5 minutes). (B) Log value of the recovered fraction  $\theta_u$  (the fraction of bound proteins that has been replaced by unbleached protein molecules; see Equation 4.3) near the outside of the gel particle (noted as “3” in Figure 4.11) ( $\bullet$ ) and for the center position (“1” in Figure 4.11) ( $\blacktriangle$ ) in the bleached area. The insert gives the same data for the initial 20 seconds.

### *Influence of ionic strength on FRAP*

We examined the fluorescence recovery in more detail at various concentrations NaCl. Figure 4.13A shows the increase of the unbleached fraction  $\theta_u$  after photobleaching for NaCl concentrations of 0, 0.005, 0.01 and 0.05 M, at a protein concentration in solution of 7  $\mu\text{g/mL}$  and pH 7. The recovery rate increases with increasing salt concentration. Since the binding of the protein molecules is mainly determined by electrostatic interactions, this is in line with expectation: the screening effect of the salt enhances the rate of the exchange of bleached with unbleached molecules.

Figure 4.13B shows exponential fits of the data plotted as  $1 - \theta_u$  versus time, which according to Equations (6) and (9) should reveal a one- or multi-exponential behavior. This is made visible in the insert of this figure, which gives the same data on a log-linear scale. At low NaCl concentration (0 and 0.005 M) the data can be fitted assuming three regions of different exchange rate; at the higher salt concentrations (0.01 and 0.05 M) two of such regions are visible. The corresponding exchange rate constants are given in Table 4.1 and Figure 4.14.

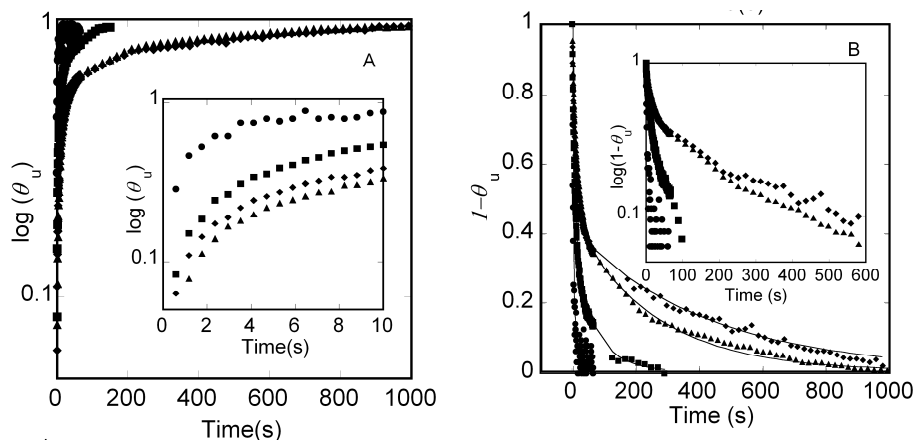


Fig. 4.13 (A) Log value of the recovered fraction  $\theta_u$  for NaCl concentrations of 0 M (▲), 0.005 M (◆), 0.01 M (■) and 0.05 M (●). The insert gives the same curves for the initial 20 seconds after photo bleaching. Alexa Fluor 488 lysozyme concentration in solution was 7  $\mu\text{g/mL}$ , at pH 7. (B) The same data as in (A) now plotted as  $1 - \theta_u$  versus time. The lines are multi-exponential fits for each salt concentration. The insert figure shows  $\log(1 - \theta_u)$  as a function of time.

Binding of the protein to the starch restricts the mobility because the molecules have to detach from the binding sites before they can be replaced by unbleached molecules. As the binding is of electrostatic nature, the affinity decreases with increasing salt concentration and, consequently, FRAP occurs faster. As shown in Table 4.1, the fractions of bound protein  $\theta_n$

and exchange rates  $kC_p$  increase with increasing ionic strength. The slowest fraction  $\theta_3$  disappears at 0.01 and 0.05 M NaCl. The slowest exchange process involves the protein molecules with the lowest mobility.

Table 4.1. Fractions of protein bound to the gel of different mobility ( $\theta_1$ ,  $\theta_2$ ,  $\theta_3$ ) and their exchange rates ( $kC_p$  in  $s^{-1}$ ) at various NaCl concentrations. The protein concentration in solution  $C_p = 7 \mu\text{g/mL}$  and  $\text{pH} = 7$ .

[NaCl] (M)	$\theta_1$	$\theta_2$	$\theta_3$	$k_1 C_p (s^{-1})$	$k_2 C_p (s^{-1})$	$k_3 C_p (s^{-1})$
0	0.16	0.44	0.4	0.33	0.05	0.003
0.005	0.14	0.45	0.4	0.52	0.07	0.002
0.01	0.65	0.35	-	0.13	0.01	-
0.05	0.77	0.23	-	0.61	0.06	-

Binding of the protein to the starch restricts the mobility because the molecules have to detach from the binding sites before they can be replaced by unbleached molecules. As the binding is of electrostatic nature, the affinity decreases with increasing salt concentration and, consequently, FRAP occurs faster. As shown in Table 4.1, the fractions of bound protein  $\theta_n$  and exchange rates  $kC_p$  increase with increasing ionic strength. The slowest fraction  $\theta_3$  disappears at 0.01 and 0.05 M NaCl. The slowest exchange process involves the protein molecules with the lowest mobility.

It should be noted that, although our model fits the data well, the dynamics of the proteins in the gel might be more complex. For example, in pores comparable to or smaller than the dimensions of the protein, the mobility will be strongly reduced and crowding may

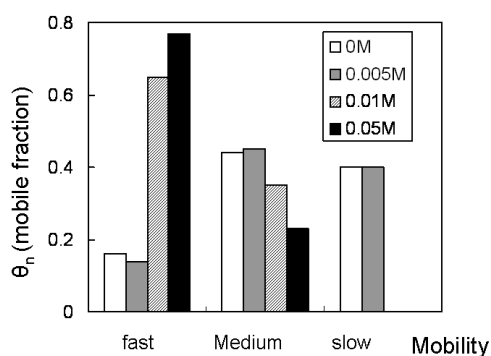


Fig. 4.14 Fractions of bound protein in the gel with different mobilities obtained by fitting the recovery data with a multi-exponential function (two-exponential for 0.01 and 0.05 M NaCl; three-exponential for 0 and 0.005 M NaCl).  $C_p = 7 \mu\text{g/mL}$ ,  $\text{pH} = 7$ . The low, medium, and high mobility fractions are defined by the order of magnitude of the exchange rate  $kC_p$  (respectively  $0.001 s^{-1}$ ,  $0.01 s^{-1}$  and  $0.1 s^{-1}$ ). The results show that the fraction with low mobility has disappeared at high NaCl concentration.

occur. We anticipate, however, that this is a minor effect, since most pores are relatively large and because of the pronounced effect of the salt concentration on the binding characteristics.

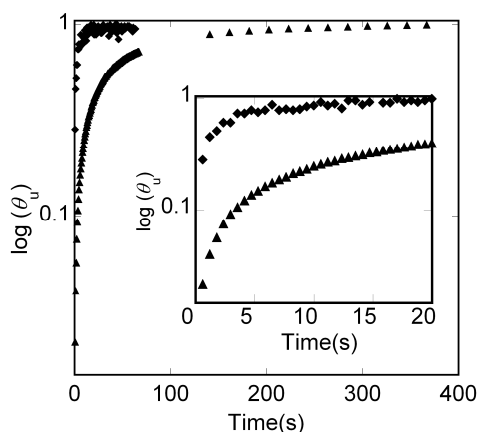


Fig. 4.15 Log value of the recovered fraction  $\theta_u$  (fraction bleached protein that has been replaced by unbleached protein) as a function of time for pH 3 (▲) and pH 7 (◆). The inserted figure gives the same curves in the initial 20 seconds after photo bleaching. The Alexa-488 lysozyme concentration is  $7\mu\text{g/mL}$ , the NaCl concentration is 0.05 M.

It is further noted that the rate of the slowest recovery process in the FRAP experiments is of the same order of magnitude (i.e.,  $0.001\text{ s}^{-1}$ ) as that of the exchange reaction between labeled and unlabeled protein, presented in Fig. 4.10. In that case  $C_p$  was about 5 times lower, and no salt was added to the solution; at this low  $C_p$  saturation uptake is not yet achieved (see Fig. 4.5). Apparently, under those conditions almost all protein molecules are bound to the highest affinity sites or, alternatively, occupied multiple binding sites in the gel.

### ***Influence of pH on FRAP***

In Figure 4.15 FRAP data collected at pH 3 and pH 7, at 0.05 M NaCl, are shown. Using the same model analysis, we found for pH 3 two fractions of different mobilities: one with an exchange rate of  $0.06\text{ s}^{-1}$  ( $\theta = 0.42$ ), the other with an exchange rate of  $0.01\text{ s}^{-1}$  ( $\theta = 0.58$ ). It is noted that the fast exchange process observed at pH 7 (see data in Table 4.1) has disappeared at pH 3. As was already clear from the data presented in Figs. 4.6 and 4.7, below pH 5 the binding strength strongly increases with decreasing pH; this agrees with the more restricted mobility at pH 3.

Bysell et al. [37] also found that increasing the pH facilitates detachment and diffusion of peptides in a poly (acrylic acid) microgel. They state that this may be caused by swelling of

the gel, which implies larger pores. Our microgel also swells upon increasing the pH, but this effect is relatively small. Moreover, diffusion of lysozyme through the pores does not seem to be a limiting factor for the exchange of bound protein. Therefore, we attribute the disappearance of the fast exchanging fraction in our microgel at low pH completely to an increased binding strength to the starch, and not to a decrease in pore volume.

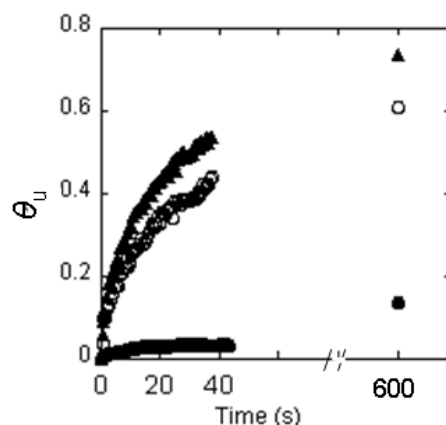


Fig. 4.16 The recovered fraction  $\theta_u$  (fraction bleached protein that has been replaced by unbleached protein) as a function of time for pH 7 at different ionic strengths 0M ( $\bullet$ ), 0.005M ( $\circ$ ), 0.01M ( $\blacktriangle$ ). Alexa-488 lysozyme concentration is 0.7 $\mu$ g/mL.

#### **FRAP at low protein concentration**

When the protein concentration is very low, the amount of protein molecules bound to the gel particles also decreases and their mobility is strongly restricted. This is illustrated by the results presented in Fig. 4.16 for a protein concentration of 0.7  $\mu$ g/mL (pH 7). Complete recovery did not occur on the time scale of our experiments. The estimated recovery rates (overall value for  $kC_p$ ) from the data in Fig. 4.16 are  $2 \times 10^{-4} \text{ s}^{-1}$  for 0 M NaCl,  $0.001 \text{ s}^{-1}$  for 0.005 M NaCl and  $0.003 \text{ s}^{-1}$  for 0.01 M NaCl. Comparison with the values in Table 4.1 (obtained for a 10 times higher protein concentration) shows that, indeed, the fraction of bound protein molecules with the lowest mobility must be larger for the low protein concentration.

## **4.4 Concluding remarks**

To study the mobility of lysozyme in oxidized potato starch polymer (OPSP) microgels, we successfully prepared well-defined spherical gel particles with a narrow size distribution (10 - 20  $\mu$ m diameter). The size of most of the pores are in the range of 4 to 25 nm and CLSM

images and intensity profiles show that the protein distributes rather homogeneously inside the microgel.

The mobility of the protein in the gel was studied by following the exchange of unlabeled lysozyme by fluorescently labeled lysozyme, and by FRAP measurements. The results of both types of measurement are consistent. The data show that diffusion of free protein in the pores of the gel network is not a limiting factor for the rate of exchange of the proteins bound to the gel fibers. We developed a simple model to analyze the data and this shows that there are several fractions of bound protein of different mobility in the microgel particles. Since it is not likely that the functional groups that provide binding sites in the gel (the charged carboxylic groups of the starch polymers) show themselves a broad distribution in binding strength, the mobility is most probably determined by the number of sites to which a protein molecule is bound. By way of the condition at pH 7, 50mM ionic strength ( $Q_{LSZ}^+ = 7$ ), where the charge ratio between protein bound and gel is 1:1, it indicates that in average one protein molecule can bind 7 carboxyl groups [17]. The distribution over the fractions is affected by the pH and the salt concentration. This is in line with our previous finding that binding of lysozyme in the gel particles is dominated by electrostatic interactions and that the charge of the protein is determining the binding affinity. A high salt concentration and high pH lead to larger populations in the more mobile fractions, because the electrostatic interactions are weaker here. It implies that the ingredients embedded in the gel can be protected when salt concentration and pH are kept low. They can be triggered to be released at high salt concentration and high pH.

At a low protein concentration in solution, at which the maximum uptake of protein by the gel is not yet reached, the exchange rate of the bound protein is severely limited, at low as well as higher salt concentrations (0 – 0.01 M), showing that it is largely present in the low mobility fraction, attached to multiple binding sites in the gel.

## References

- [1] S. Schachschal, A. Balaceanu, C. Melian, D.E. Demco, T. Eckert, W. Richtering, A. Pich, Polyampholyte Microgels with Anionic Core and Cationic Shell, *Macromolecules*, 43 (2010) 4331-4339.
- [2] R.K. Shah, J.W. Kim, D.A. Weitz, Monodisperse Stimuli-Responsive Colloidosomes by Self-Assembly of Microgels in Droplets, *Langmuir*, 26 (2010) 1561-1565.
- [3] B.R. Saunders, N. Laajam, E. Daly, S. Teow, X.H. Hu, R. Stepto, Microgels: From responsive polymer colloids to biomaterials, *Advances in Colloid and Interface Science*, 147-48 (2009) 251-262.
- [4] J.K. Oh, R. Drumright, D.J. Siegwart, K. Matyjaszewski, The development of microgels/nanogels for drug delivery applications, *Progress in Polymer Science*, 33 (2008) 448-477.
- [5] Q.F. Luo, P.X. Liu, Y. Guan, Y.J. Zhang, Thermally Induced Phase Transition of Glucose-Sensitive Core-Shell Microgels, *Acs Applied Materials & Interfaces*, 2 (2010) 760-767.
- [6] S. Fujii, S. Kameyama, S.P. Armes, D. Dupin, M. Suzuki, Y. Nakamura, pH-responsive liquid marbles stabilized with poly(2-vinylpyridine) particles, *Soft Matter*, 6 (2010) 635-640.
- [7] G.X. Sun, M.Z. Zhang, Y. Xu, Y.M. Lu, P.H. Ni, Synthesis and Properties of pH-Responsive Cationic Microgels, *Acta Chimica Sinica*, 67 (2009) 1685-1690.
- [8] W.J. Liu, Y. Zhou, H.Y. Chen, Y.M. Huang, H.L. Liu, Flocculation and aggregation Behavior of doubly responsive microgel, *Acta Chimica Sinica*, 66 (2008) 449-453.
- [9] Y.R. Ren, X.S. Jiang, J. Yin, Copolymer of poly(4-vinylpyridine)-g-poly(ethylene oxide) respond sharply to temperature, pH and ionic strength, *European Polymer Journal*, 44 (2008) 4108-4114.
- [10] V. Lapeyre, C. Ancla, B. Catargi, V. Ravaine, Glucose-responsive microgels with a core-shell structure, *Journal of Colloid and Interface Science*, 327 (2008) 316-323.
- [11] T. Hoare, R. Pelton, Charge-switching, amphoteric glucose-responsive microgels with physiological swelling activity, *Biomacromolecules*, 9 (2008) 733-740.
- [12] H. Li, R.M. Luo, K.Y. Lam, Multiphysics Modeling of Electrochemomechanically Smart Microgels Responsive to Coupled pH/Electric Stimuli, *Macromolecular Bioscience*, 9 (2009) 287-297.
- [13] S. Bhattacharya, F. Eckert, V. Boyko, A. Pich, Temperature-, pH-, and magnetic-field-sensitive hybrid microgels, *Small*, 3 (2007) 650-657.
- [14] R.K. Jain, Barriers to drug-delivery in solid tumors, *Scientific American*, 271 (1994) 58-65.
- [15] J.W. Baish, R.K. Jain, Cancer, angiogenesis and fractals, *Nature Medicine*, 4 (1998) 984-984.
- [16] Y. Li, R. de Vries, T. Slaghek, J. Timmermans, M.A.Cohen Stuart, W. Norde, Preparation and Characterization of Oxidized Starch Polymer Microgels for Encapsulation and Controlled Release of Functional Ingredients, *Biomacromolecules*, 10 (2009) 1931-1938.
- [17] Y. Li, R. de Vries, J.M.Kleijn, T. Slaghek, J. Timmermans, M.A.Cohen Stuart, W. Norde, Lysozyme Uptake by Oxidized Starch Polymer Microgels *Biomacromolecules*, 11 (2010) 1754-1762.
- [18] H. Bysell, P. Hansson, M. Malmsten, Effect of Charge Density on the Interaction between Cationic Peptides and Oppositely Charged Microgels, *Journal of Physical Chemistry B*, 114 (2010) 7207-7215.
- [19] H. Bysell, P. Hansson, M. Malmsten, Transport of poly-L-lysine into oppositely charged poly(acrylic acid) microgels and its effect on gel deswelling, *Journal of Colloid and Interface Science*, 323 (2008) 60-69.



- 
- [20] C. Johansson, P. Hansson, Distribution of cytochrome c in polyacrylate microgels, *Soft Matter*, 6 (2010) 3970-3978.
- [21] C. Johansson, P. Hansson, M. Malmsten, Interaction between lysozyme and poly(acrylic acid) microgels, *Journal of Colloid and Interface Science*, 316 (2007) 350-359.
- [22] C. Johansson, J. Gernandt, M. Bradley, B. Vincent, P. Hansson, Interaction between lysozyme and colloidal poly(NIPAM-co-acrylic acid) microgels, *Journal of Colloid and Interface Science*, 347 (2010) 241-251.
- [23] C. Johansson, P. Hansson, M. Malmsten, Mechanism of Lysozyme Uptake in Poly(acrylic acid) Microgels, *Journal of Physical Chemistry B*, 113 (2009) 6183-6193.
- [24] N. Loren, M. Nyden, A.M. Hermansson, Determination of local diffusion properties in heterogeneous biomaterials, *Advances in Colloid and Interface Science*, 150 (2009) 5-15.
- [25] N.J. Kavimandan, N.A. Peppas, Confocal microscopic analysis of transport mechanisms of insulin across the cell monolayer, *International Journal of Pharmaceutics*, 354 (2008) 143-148.
- [26] F. Brandl, F. Kastner, R.M. Gschwind, T. Blunk, J. Tessmar, A. Gopferich, Hydrogel-based drug delivery systems: Comparison of drug diffusivity and release kinetics, *Journal of Controlled Release*, 142 (2010) 221-228.
- [27] M.C. Branco, D.J. Pochan, N.J. Wagner, J.P. Schneider, Macromolecular diffusion and release from self-assembled beta-hairpin peptide hydrogels, *Biomaterials*, 30 (2009) 1339-1347.
- [28] E.M. Johnson, D.A. Berk, R.K. Jain, W.M. Deen, Diffusion and partitioning of proteins in charged agarose gels, *Biophysical Journal*, 68 (1995) 1561-1568.
- [29] X.D. Li, X.H. Li, J.X. Zhang, S.F. Zhao, J.C. Shen, A novel system for water soluble protein encapsulation with high efficiency: "Micelles enhanced" polyelectrolyte capsules, *Journal of Biomedical Materials Research Part A*, 85A (2008) 768-776.
- [30] S.R. Van Tomme, B.G. De Geest, K. Braeckmans, S.C. De Smedt, F. Siepmann, J. Siepmann, C.F. van Nostrum, W.E. Hennink, Mobility of model proteins in hydrogels composed of oppositely charged dextran microspheres studied by protein release and fluorescence recovery after photobleaching, *Journal of Controlled Release*, 110 (2005) 67-78.
- [31] D.X. Wang, S.P. Hong, G.L. Yang, K.H. Row, Caffeine molecular imprinted microgel spheres by precipitation polymerization, *Korean Journal of Chemical Engineering*, 20 (2003) 1073-1076.
- [32] A.D. Vaughan, S.P. Sizemore, M.E. Byrne, Enhancing molecularly imprinted polymer binding properties via controlled/living radical polymerization and reaction analysis, *Polymer*, 48 (2007) 74-81.
- [33] S.M. Russell, G. Carta, Mesh size of charged polyacrylamide hydrogels from partitioning measurements, *Industrial & Engineering Chemistry Research*, 44 (2005) 8213-8217.
- [34] G.M. Eichenbaum, P.F. Kiser, A.V. Dobrynin, S.A. Simon, D. Needham, Investigation of the swelling response and loading of ionic microgels with drugs and proteins: The dependence on cross-link density (vol 32, pg 4867, 1999), *Macromolecules*, 34 (2001) 6526-6526.
- [35] D. Brune, S. Kim, Predicting protein diffusion-coefficients, *Proceedings of the National Academy of Sciences of the United States of America*, *Proceedings of the National Academy of Sciences of the United States of America*, 90 (1993) 3835-3839.
- [36] C.A. Haynes, E. Sliwinsky, W. Norde, Structural and electrostatic properties of globular-proteins at a polystyrene water interface, *Journal of Colloid and Interface Science*, 164 (1994) 394-409.
- [37] H. Bysell, A. Schmidtchen, M. Malmsten, Binding and Release of Consensus Peptides by Poly(acrylic acid) Microgels, *Biomacromolecules*, 10 (2009) 2162-2168.



---

# Chapter 5

## Uptake and release kinetics of lysozyme in and from an oxidized starch polymer microgel

---

### *Abstract*

The kinetics of uptake and release of fluorescently labeled lysozyme by/from spherical oxidized starch polymer microgel particles (diameter 10 - 20  $\mu\text{m}$ ) was investigated using confocal laser scanning microscopy. Both the protein and the microgel have a pH dependent charge; in the pH range 3 - 9, the protein ( $pI \approx 10$ ) is positive and the gel is negative. Uptake was monitored at different protein concentrations, pH values and ionic strengths. Lysozyme release was triggered by changing the pH and salt concentration and measured during enzymatic degradation of the gel by  $\alpha$ -amylase. To analyze the uptake and release kinetics we used a model based on diffusion, taking into account equilibrium exchange between protein bound to the gel matrix and free protein in the gel. For the uptake process the time-dependent evolution of the protein concentration profile in the gel phase and the medium was computed numerically. The calculated concentration profiles closely resemble the experimentally found profiles. The diffusion coefficient of free protein in the gel,  $D_{p,g}$ , was found to be on the order of  $10^{-11} \text{ m}^2\text{s}^{-1}$ , about one order of magnitude lower than the diffusion coefficient of lysozyme in bulk solution. The experimental release curves obtained at pH 7 yielded estimated values for the concentration ratio of bound and free protein in the gel and, related to this ratio, the effective diffusion coefficient of lysozyme in the gel,  $D_{\text{eff}}$ . These values are extremely dependent on the ionic strength, ranging from ca 1000 and  $10^{-14} \text{ m}^2\text{s}^{-1}$  at 0.025 M NaCl to 50 and  $2 \times 10^{-12} \text{ m}^2\text{s}^{-1}$  at 0.05 M, respectively.

Accepted for publication: Y. Li, Z. Zhang, H. P. van Leeuwen, M.A. Cohen Stuart, W. Norde, J.M. Kleijn, Uptake and release kinetics of lysozyme in and from an oxidized starch polymer microgel, soft matter, DOI: 10.1039/C1SM06072D.

## 5.1 Introduction

Nano- and micro-particles of hydrogels have received much attention in relation to encapsulation of functional ingredients, and the progress of scientific research in this field has been reviewed extensively [1-4]. Especially gels of biodegradable materials have long been recognized as suitable carriers for controlled uptake and release of active compounds (see, e.g., Refs [5-10]).

In previous Chapters [11-13] we have reported on a biodegradable and biocompatible microgel synthesized from a natural potato starch polymer. We have a good control of its charge density and cross-link density. The binding affinity and uptake capacity of the gel for lysozyme, an antimicrobial protein, have been studied.

Adsorption measurements and exchange experiments (between bleached and unbleached fluorescently labeled lysozyme) [13] showed that the affinity of lysozyme to the gel decreases sharply with increasing pH and salt concentration. From the exchange experiments at pH 7 we derived various fractions of bound protein with different exchange rates ('mobility'); the distribution over these fractions is highly dependent on ionic strength. These exchange rates, however, do not give direct clues with respect to the kinetics of uptake by initially empty gel particles and release from loaded gel particles.

In this Chapter, we focus on the kinetics of protein uptake and release, the latter triggered by increasing the pH and salt concentration. This is of relevance for controlled release applications, e.g., gastro-intestine delivery of functional ingredients or drugs. In addition, protein release as a result of enzymatic degradation (by  $\alpha$ -amylase) of the microgel has been monitored. This kind of release is important for antimicrobial applications, e.g. in food packaging.

Fluorescence confocal laser scanning microscopy (CLSM) is used to follow the uptake and release process of protein for individual spherical gel particles (diameter 10 - 20  $\mu\text{m}$ ). We model the kinetics of both processes starting from basic diffusion equations. For the diffusion rate in the gel particle, an effective diffusion coefficient  $D_{\text{eff}}$ , based upon the equilibrium exchange between protein bound to the gel matrix and free protein in the gel pores, is used. For the uptake experiments we take into account the evolution of a concentration profile in the solution around the gel particles and solve the equations numerically. Our analysis of the temporal release of protein from the gel to a flowing solution of zero protein concentration is based on Crank's theoretical approach, holding for the case where diffusion in the medium can be ignored [14].

## 5.2 Material and Methods

### *Materials*

Native starch was kindly provided by AVEBE (Veendam, The Netherlands). The oxidation catalyst 2, 2, 6, 6-tetramethyl-1-piperidinyloxy (TEMPO) and ethanol (100%) were purchased from Merck. The cross-linker sodium trimetaphosphate (STMP), poly-DL-lysine hydrobromide, lysozyme (from chicken egg white,  $M_w = 14,400$  g/mole), Span 80 and n-hexane were supplied by Sigma-Aldrich. The fluorescent dye, Alexa Fluor-488 carboxylic acid succinimidyl ester (mixed with isomers) was purchased from Invitrogen. Heat-stable  $\alpha$ -amylase (Termamyl® 120L, Type L, activity 120 KNU/g) was purchased from Novo Nordisk.

Solutions were prepared using millipore water with a specific resistance of 18.3 M $\Omega$ /cm. All experiments were performed at room temperature.

### *Microgel preparation*

The spherical microgel particles (diameter 10 - 20  $\mu$ m) of cross-linked oxidized starch polymer were synthesized by inverse emulsion polymerization. First the primary alcohol groups on the starch polymer were oxidized into carboxyl groups; the degree of oxidation was 30%. To form the gel a 0.20 cross-linker to polymer weight ratio was used. For more details on the oxidation of the starch polymers and preparation of the microgel particles we refer to Chapter 2 and 4 [11, 13].

### *Fluorescence confocal laser scanning microscopy*

A confocal microscope (Carl Zeiss Axiovert 200 microscope, Zeiss, Germany) equipped with an LSM 5 Exciter configuration, a 40 $\times$ /0.6 objective and an Argon laser set at 488 nm was used. The standard settings were: pinhole 1.8  $\mu$ m; gain 755; transmission 2.55 %. For analysis the software “Zen 2008” was used. The labeling of Alexa Fluor-488 to lysozyme has been described in Chapter 4 [13].

As flow cells under the microscope  $\mu$ -Slides I Luer 0.8 (200  $\mu$ L; Ibidi, Germany) were used. The kinetics of lysozyme uptake and release was measured by continuously taking fluorescence scanning pictures.

***Lysozyme uptake kinetics***

The gel particles were fixed at the flow cell surface to be able to observe one and the same particle during the whole process. For this the negatively charged cell surface was coated with positively charged poly-DL-lysine by absorption from a 0.1% poly-DL-lysine solution in water for two hours. Subsequently, unabsorbed polylysine was flushed away and a dispersion of negatively charged microgel particles in water was added for attachment to the surface. After one hour unattached gel particles were rinsed out of the cell. One attached gel particle was brought into focus. Then 100  $\mu\text{L}$  of an Alexa-488 labeled lysozyme solution (0.7 or 1.4  $\mu\text{g/mL}$ ) was added to the cell and the protein uptake was monitored. (Recording of fluorescence images, 0.5 s/image, was already started before adding the labeled protein to observe the kinetics from the start.) Uptake kinetics were determined at pH 3 and 7 (at 0.01 M ionic strength) and at different NaCl concentrations (at pH 7).

The fraction of protein uptake at time  $t$  is calculated from the fluorescence intensity of the gel particle by

$$\frac{M(t)}{M_{eq}} = \frac{I(t) - I_b}{I_{\infty} - I_b} \quad (5.1)$$

where  $M(t)$  is the protein uptake at time  $t$ , and  $M_{eq}$  is the amount of protein in the gel when equilibrium uptake is reached;  $I(t)$  is the fluorescence intensity of the protein loaded gel particle (averaged over the whole section in the focal plane) at time  $t$ ,  $I_{\infty}$  is the intensity at equilibrium protein uptake, and  $I_b$  is the fluorescence background intensity in solution.

The fluorescence label Alexa Fluor 488 is a stable dye and not sensitive to quenchers such as dissolved oxygen. The fluorescence intensity from an Alexa-488 labeled lysozyme solution varies linearly with protein concentration, up to at least 16  $\mu\text{g/mL}$  [13]. Hence, quantitative results can be obtained if the protein concentration is within this range. Therefore, the amount of protein absorbed as a function of time relative to the equilibrium protein uptake,  $M(t)/M_{eq}$ , as found from the fluorescence intensities is a good measure for the uptake kinetics.

***Lysozyme release kinetics***

For measuring the lysozyme release kinetics at different pH values and salt concentrations, the same experimental set-up was used as in the uptake experiments. In addition we made use

of a flow system to pump buffer solutions through the flow cell. Firstly, 100  $\mu\text{L}$  of a 0.7  $\mu\text{g/mL}$  Alexa-488 labeled lysozyme solution was brought into contact with the fixed gel particles for 2 hours (in water, no salt) to allow equilibrium uptake. Then the protein in solution was flushed out of the flow cell with water. Protein was not released from the gel by this rinsing with water (this was checked once by monitoring the fluorescent intensity from a gel particle for two hours after rinsing). After that the flow system with buffer was switched on and simultaneously the recording of CLSM fluorescence images was started. The fraction of protein released at time  $t$  is given by

$$\frac{M_{\text{rel}}(t)}{M_0} = 1 - \frac{I(t) - I_b}{I_0 - I_b} \quad (5.2)$$

where  $M_{\text{rel}}(t)$  is defined as the amount of protein released at time  $t$ ,  $M_0$  is the initial amount of protein in the gel (at  $t = 0$ ),  $I_0$  is the initial fluorescence intensity of the gel particle and  $I(t)$  the fluorescence intensity at time  $t$ ;  $I_b$  has the same meaning as in Eq. (5.1).

Release kinetics was measured at various salt concentrations, i.e., 0.025 M, 0.035 M and 0.05 M, at a fixed pH of 7. (For higher ionic strengths, release was found to occur too rapidly to follow by confocal microscopy.) In addition, measurements were performed at pH 3 and pH 8, at a fixed salt concentration of 0.01 M.

### ***Enzyme induced protein release***

In these experiments, performed in the same set-up as described before, the fixed gel particles were first saturated with protein in the same way as described above. Then 100  $\mu\text{L}$  of an amylase solution in water ( $10^5 \times$  dilutions of original 120 KNU/g enzyme activities) was added into the protein loaded gel particle. (1 KNU - kilo Novo Unit, is defined as the amount of enzyme which breaks down 5.26 g of starch in one hour). The degradation of the gel was followed by optical microscopy. Again, a time series of fluorescence images was used to monitor the protein release.

### ***Modeling of protein uptake and release***

To analyze the uptake and release kinetics we use a comprehensive diffusion model assuming instantaneous equilibrium between matrix-bound and freely dissolved protein.

### ***Modeling of protein uptake***

Under the conditions of our uptake experiments, the protein strongly binds to the gel network [12]. Local equilibrium between bound and free protein is established and effectively the protein is slowed down during its way of diffusing into the center. The consequence is that, after protein addition to the medium, a protein concentration gradient develops as depicted in Fig. 5.1 Initially, the solution near the gel particle is completely depleted from protein because of the strong binding and protein accumulates in the exterior of the gel particle; this gives rise to steep protein gradients near the gel/solution interface. As the gel network becomes saturated with protein, the concentration profiles level off again.

The exact formulation of the time-dependent protein concentration profiles can be derived from the pertaining basic diffusion equations:

$$0 \leq r \leq a: \quad \frac{\partial c_p}{\partial t} = \frac{D_{p,g}}{1+R} \nabla^2 c_p \quad (5.3)$$

$$r \geq a: \quad \frac{\partial c_p}{\partial t} = D_p \nabla^2 c_p \quad (5.4)$$

where  $r$  is the distance from the center of the gel particle and  $a$  is the particle radius.  $D_{p,g}$  is the diffusion coefficient of the free protein molecules inside the gel.  $R$  is the ratio between bound and free protein in the gel, i.e.,  $c_{\text{bound}}/c_{\text{free}}$ .  $D_p$  is the diffusion coefficient of the protein molecules in solution;  $c_p$  represents the total protein concentration ( $c_{\text{bound}} + c_{\text{free}}$ ).

Note that Eq. (5.4) ignores convection in the medium; for particle sizes in the micrometer regime this is generally justified [15].

The typical boundary conditions for our uptake experiments are the following.

At initial conditions:

$$t = 0; \quad 0 < r < a \quad c_p = 0 \quad \text{empty particles} \quad (5.5)$$

$$r > a \quad c_p = c^* \quad \text{bulk solution}$$

In a spherical symmetry there is no gradient at the particle center:

$$t > 0; \quad r = 0: \quad \frac{\partial c_p}{\partial r} = 0 \quad (5.6)$$



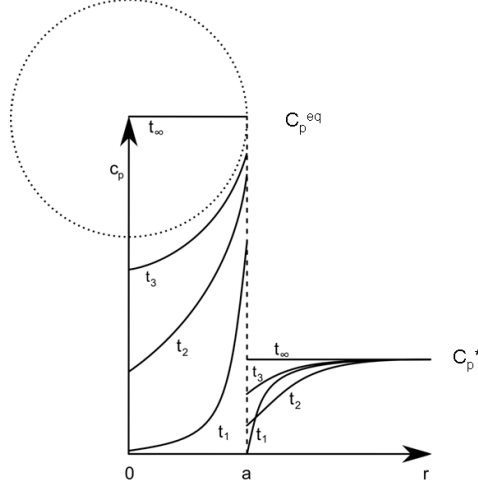


Figure 5.1. Development of protein concentration profiles in and around a gel particle (symbolized by the dotted circle) during protein uptake, after increasing the protein concentration in the bulk solution from 0 to  $c^*$  at  $t = 0$ . The total protein concentration  $c_p$  (the sum of the bound protein and freely dissolved protein concentrations) is depicted as a function of the position  $r$ ; the distance from the centre of the gel particle;  $a$  is the particle radius;  $t_1, t_2, t_3, \dots$  indicate increasing times. The final equilibrium state, in which the protein concentration in the particle  $c_p = c_p^{eq}$ , is given by the lines with  $t_{\infty}$ .

Accumulation of protein at the gel-solution interface does not occur and consequently there is continuity of the flux:

$$D_{p,g} \left( \frac{dc_p}{dr} \right)_{r \uparrow a} = D_p \left( \frac{dc_p}{dr} \right)_{r \downarrow a} \quad (5.7)$$

On the basis of the set of equations (5.3 – 5.7), the time-dependent evolution of the protein concentration profile can be computed numerically [16]. Typical results for profiles of  $c_p$  inside the gel particle are given in section 3.

For spherical geometry and a particle size in the micrometer regime, the steady state protein supply flux  $J_p$  from the medium to the particle is given by Crank [14]:

$$J_p = D_p c^* / a \quad (5.8)$$

The time necessary to establish such a steady state is related to  $a^2/D_p$ , the characteristic diffusion time  $\tau$  over a distance  $a$ . Typically, for a protein with  $D_p$  of the order of  $10^{-10} \text{ m}^2/\text{s}$  and a gel particle with radius  $a$  of  $10 \text{ }\mu\text{m}$ ,  $\tau$  would be of the order of 1 s. Thus, in case of strong binding to the gel network, within a few seconds the flux towards the particle is typically given by the limiting flux in the medium (Eq. 5.8). This situation completely invalidates treatments that ignore the diffusion in the supplying medium [17].

With the accumulation progressing in time, the concentration gradients in solution and inside the gel start to level off (see Fig. 5.1). Finally the protein concentration in the gel particle reaches an equilibrium value  $c_p^{eq}$ .

### ***Modeling of protein release***

Unlike the protein uptake experiments, in which at  $t = 0$  the protein concentration around an empty gel particle ( $r > a$ ) is increased from 0 to a chosen value, in the release experiments from  $t = 0$  a protein-loaded gel particle is flushed with buffer ( $c_p = 0$ ) in order to maintain a zero protein concentration in the medium. It is convenient to write the diffusion law for release of the protein from a sphere of radius  $a$  in polar coordinate form [14]:

$$\frac{\partial c_p}{\partial t} = D_{eff} \left[ \frac{\partial^2 c_p}{\partial r^2} + \frac{2}{r} \frac{\partial c_p}{\partial r} \right] \quad (5.9)$$

which is solved under the boundary conditions:

$$t = 0; \quad 0 < r < a: \quad c_p = c_p^* \quad (5.10)$$

$$r > a \quad c_p = 0$$

where  $c_p^*$  now is the initial total protein concentration inside the gel phase, and implying that diffusion in the medium is ignored.

$$t > 0; \quad r > a: \quad c_p = 0 \quad (5.11)$$

In Eq. (5.9)  $D_{eff}$  is the effective diffusion coefficient for the protein in the gel particle, counting both the free and the bound forms, which are supposed to be equilibrium with each other. The simplest case is that protein molecules are immobile when they are bound to the network (as was already tacitly assumed in Eq. 5.3). Then only free protein molecules contribute to the effective diffusion and  $D_{eff}$  is given by:

$$D_{eff} = \frac{D_{p,g} c_{free}}{c_{free} + c_{bound}} \quad (5.12)$$

The solution for Eq. (5.9) with boundary conditions (10) and (11) is given by [14]:

$$\frac{M(t)}{M_0} = 1 - \frac{6}{\pi^2} \sum_{n=1}^{\infty} \frac{1}{n^2} \exp\left[-n^2 \pi^2 \frac{t}{\tau}\right] \quad (5.13)$$

where the characteristic time constant  $\tau = a^2/D_{\text{eff}}$ . E.g., for a  $D_{\text{eff}}$  of  $10^{-13} \text{ m}^2/\text{s}$  and a particle radius of  $10^{-5} \text{ m}$ ,  $\tau$  would be 100 s. For short times this function can be approximated by

$$\frac{M(t)}{M_0} = \frac{6}{\sqrt{\pi}} \left[ \frac{t}{\tau} \right]^{\frac{1}{2}} - 3 \frac{t}{\tau} \quad (5.14)$$

For  $t/\tau < 0.01$ , with the diffusion layer developing in a thin outer shell of the particle sphere,  $M(t)$  is practically linear in  $t^{0.5}$ . For longer times, with  $t/\tau$  increasing to 0.1, the term in  $t$  counts as well and  $M(t)$  starts to level off. See references [14, 18] for more details.

### 5.3 Results and discussion

#### *Uptake kinetics*

The steady state rate of protein uptake after establishment of a diffusion layer in solution (i.e., after a few seconds) should equal the limiting flux of protein at the solution side of the gel-solution interface as given by Eq. (5.8). This limiting flux is proportional to the protein concentration in solution,  $c^*$ . We checked this by measuring the fluorescence intensity from a gel particle after addition of fluorescently labeled lysozyme for two different protein concentrations (0.7 and 1.4  $\mu\text{g/mL}$ ), at pH 3 as well as at pH 7. The results for the first 100 s are presented in Fig. 5.2. The slope of the curve for 1.4  $\mu\text{g/mL}$  protein concentration in Fig. 5.2A, converts to  $0.8 \times 10^{-19} \text{ mol s}^{-1}$  per particle using the calibration line of intensity vs. protein concentration [13]. This is close to the limiting diffusion flux, which for a radius of  $10^{-5} \text{ m}$  is easily computed to be  $10^{-19} \text{ mol s}^{-1}$  per particle (Eq. 5.8). The similarity demonstrates that the initial rate of protein uptake is determined by the diffusion transport in solution.

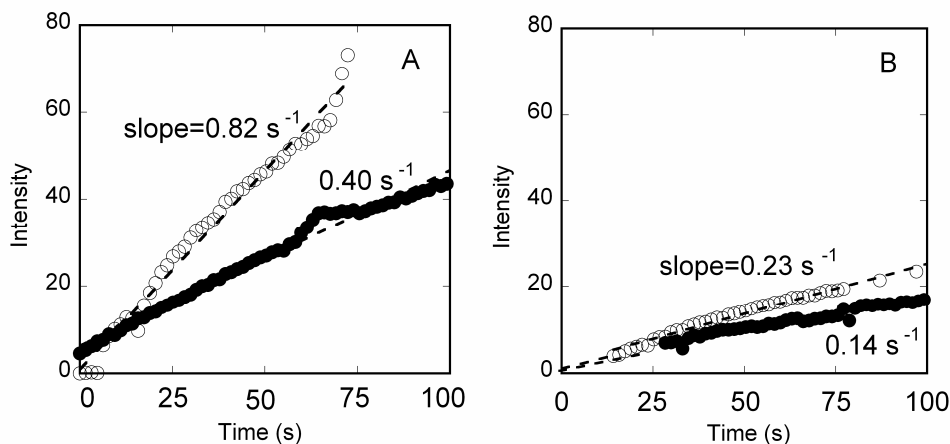


Figure 5.2. Fluorescence intensity (arbitrary units) of a gel particle as a function of time after addition of protein (initial 100 s). (A) At pH 3, ionic strength 0.01 M. (B) At pH 7, ionic strength 0.01 M. Protein concentration in solution: (●) 0.7  $\mu\text{g/mL}$ , (○) 1.4  $\mu\text{g/mL}$ . The dotted lines are linear fits of the data. The slope is proportional to the rate of the protein uptake.

At pH 3, increasing the protein concentration by a factor of two indeed results in an uptake rate that is twice as high (Fig. 5.2A). However, at pH 7 the uptake rate increases somewhat less than two times when the protein concentration is doubled (Fig. 5.2B). This can be explained from our previous finding that the binding strength of lysozyme to the microgel decreases with increasing pH [12]. Therefore the driving force for uptake in the initial regime (i.e., the protein concentration gradient at the solution side of the gel-solution interface) at pH 7 is lower than at pH 3. Therefore, at pH 7 the uptake kinetics deviates slightly from the limiting flux of the protein in solution toward the gel particles.

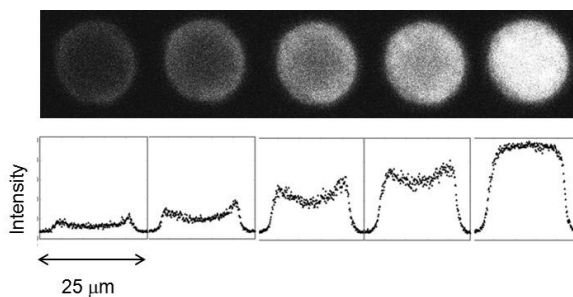


Figure 5.3 Time series of CLSM images and intensity profiles across the center of a gel particle for lysozyme uptake at pH 3 and ionic strength 0.01 M, at 60 s, 120 s, 180 s, 300 s, and 600 s after protein addition.

Fig. 5.3 shows the distribution of the lysozyme over the microgel particle at various times after protein addition at pH 3. The protein diffuses from the gel-solution interface

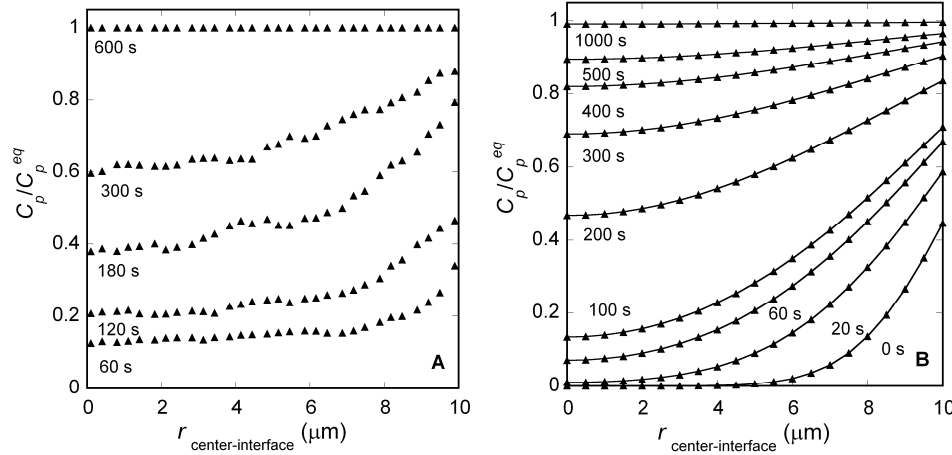


Figure 5.4 (A) Protein uptake concentration profiles in the gel particle (radius 10  $\mu\text{m}$ ), normalized to the equilibrium protein uptake  $c_p^{\text{eq}}$  at  $t = t_{\infty}$ . Uptake conditions: pH 3, ionic strength 0.01 M. (B)  $c_p/c_p^{\text{eq}}$  profiles obtained from numerical solutions of the diffusion equation considering the concentration gradient at the gel-solution interface and the accumulation of the protein inside the gel (Eqs.(5.3-5.7)). The ratio between bound and free protein inside the gel,  $R$ , was taken as 300; for the diffusion coefficient of the protein inside the gel,  $D_{p,g}$ , a value of  $3 \times 10^{-11} \text{ m}^2 \text{ s}^{-1}$  was used.

towards the gel center with a diffusion front. In the final situation the protein molecules are distributed rather homogeneously over the gel.

Fig. 5.4A shows the protein concentration, normalized to the equilibrium concentration in the gel  $c_p/c_p^{\text{eq}}$ , as a function to position  $r$  in the gel particle. Fig. 5.4B gives the normalized concentration profiles obtained from numerical solution of Eqs (5.4 - 5.7) based on the comprehensive uptake model taking into account the diffusion in the medium. With respect to the shape of the curves and the characteristic times, the numerical solutions and the experimental data are rather close, implying that the model is quite applicable to our data. For instance, the experimental protein uptake  $c_p/c_p^{\text{eq}}$  in the center of the particle is 0.4 at 200 s, 0.6 at 300 s and 1.0 at 600 s in Fig. 5.4A, which is consistent with the calculated values in Fig. 5.4B. However, near the outer boundary of the gel particle, the experimental concentration profiles are somewhat less steep than the calculated ones. The available data seem to suggest that in equilibrium protein distribution is fairly homogeneous throughout the gel particles, except for the outer shell (about 1  $\mu\text{m}$ ) of the gel particle (see e.g. Fig. 5.2 in Ref. [13]). This shell behaves like a transition layer of lower density with increased mobility of the protein. Taking into account such a gradual decrease of the density in the outer layer in this diffusion-based model, would greatly complicate the numerical simulation (see e.g. the paper of Duval[19] on diffusion and binding of metal ions in soft particles with spatially

inhomogeneous binding site distribution). In view of the uncertainties concerning the gel density as a function of position, it does not make sense to further refine the fits in Fig. 5.4. Such a refinement of the model would not lead to drastically different findings concerning time dependence of the diffusion-controlled protein uptake.

The numerical calculations of the concentration profiles as depicted in Fig. 5.4B, provide the best agreement for a ratio between bound and free protein inside the gel,  $R$ , on the order of a few hundreds. This result is in good accordance with lysozyme absorption isotherm data for our microgel at pH 3 and 0.01 M ionic strength [unpublished data], for which in the linear regime (below saturation) the ratio between the protein concentration in the gel particles and free protein in solution is several hundreds. The ensuing diffusion coefficient of free lysozyme in the gel  $D_{p,g}$  derived from the model is on the order of  $10^{-11} \text{ m}^2\text{s}^{-1}$ , well below its value in solution ( $10^{-10} \text{ m}^2\text{s}^{-1}$ ), which is expected since obstruction by the gel network increases the diffusion path length [20, 21].

We now focus on the effect of pH and salt concentration on the uptake kinetics over a longer time period.

In Fig. 5.5 the uptake kinetics is displayed for two concentrations of NaCl (0 M and 0.01 M, pH 7) and two pH values (pH 3 and pH 7, 0.01 M buffer). Fig. 5.5A shows that for 0.01 M NaCl the gel reaches equilibrium protein uptake faster than for the case without NaCl. However, the absolute fluorescence intensity at equilibrium (large  $t$ ) was found to be lower by a factor of 2 for 0.01 M than for 0 M NaCl, which is consistent with the earlier observation that equilibrium uptake decreases with increasing ionic strength [12, 13]. Therefore, although the initial slopes for 0.01 M and 0 M NaCl in Fig. 5.5A are practically the same, the absolute uptake rate is lower for 0.01 M than in the case of no added salt (the initial changes in fluorescence intensity were  $0.23 \text{ a.u. s}^{-1}$  and  $0.56 \text{ a.u. s}^{-1}$ , respectively). This is because the presence of NaCl reduces the affinity between the protein and the gel network, leading to a smaller protein concentration gradient in the solution during uptake.

Fig. 5.5B shows the uptake as a function of time at pH 3 and pH 7 at an ionic strength of 0.01 M. The final absolute fluorescence intensities, and therefore the equilibrium protein concentrations in the gel, were found to be approximately the same for the two pH values. The initial uptake rate is much higher for pH 3 than for pH 7. This is consistent with our previous finding that the binding affinity increases with decreasing pH [12]. It was concluded

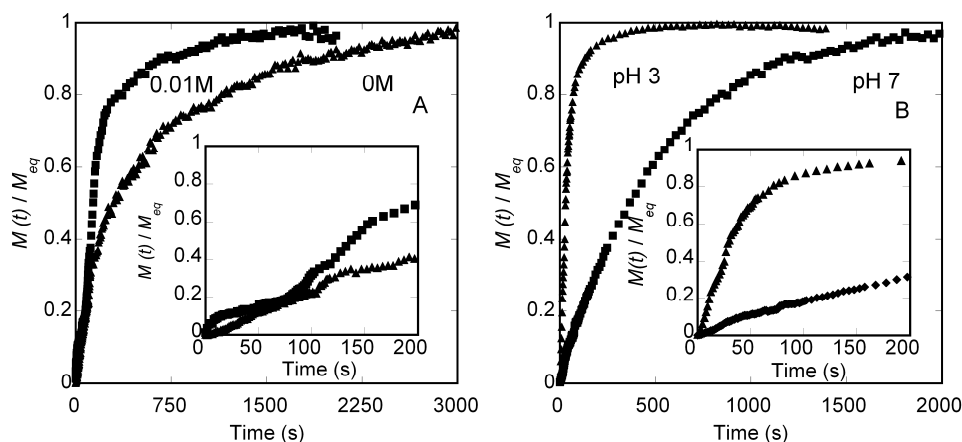


Figure 5.5 Protein uptake kinetics (i.e., fraction of protein taken up by a gel particle,  $M(t)/M_{eq}$ , as a function of time). Protein concentration in solution is  $0.7 \mu\text{g/ml}$ . (A) (▲) 0 M and (■) 0.01 M NaCl in water ( $\text{pH} \approx 7$ ); (B) ionic strength 0.01 M, (▲) pH 3 and (■) pH 7. The insets show the onsets of the curves, for (A) and (B) over the same time interval.

that the binding affinity is mainly determined by the charge on the protein, while the total uptake capacity is determined by charge compensation, i.e., the (negative) charge on the gel decreases with pH while the (positive) protein charge increases, so that less protein molecules can be accommodated in the gel at low pH.

### Release kinetics

For lysozyme bound inside the gel particles we identified several fractions of different binding strengths reflected by different exchange rates between bleached and unbleached fluorescently labeled lysozyme molecules [13]. It was found that increasing the salt concentration or the pH cause a shift in the distribution of the bound protein molecules towards more mobile fractions (i.e., more easily exchangeable fractions). Therefore protein release can be triggered by increasing the salt concentration and / or the pH. In this section, salt and pH triggered lysozyme release from the microgel is further investigated.

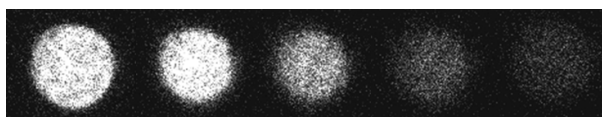


Figure 5.6 Time series of CLSM images taken during protein release from a microgel particle at pH 7 and ionic strength 0.035 M at time 0 s, 6 s, 60 s, 600 s, and 1800 s.

The release kinetics was determined by first saturating the gel particles (immobilized on the polylysine coated surface) with lysozyme in water. After removing the unabsorbed lysozyme

by flushing with water, the flow cell was flushed continuously with buffer of a specific ionic strength and pH. A time series of CLSM images of a gel particle was made to record the release process.

Fig. 5.6 shows that for solution conditions of 0.035 M NaCl and pH 7, the lysozyme is gradually released from the gel to the solution. The full protein concentration profiles at different times are shown in Fig. 5.7.

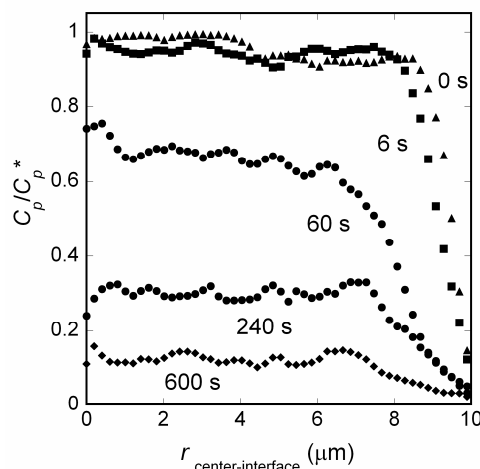


Figure 5.7 Protein concentration profiles (normalized to the initial protein concentration in the gel at  $t = 0$ ,  $c_p = c_p^*$ ). The microgel radius is 10  $\mu\text{m}$ . At  $t = 0$  the protein release was started by switching the ionic strength from 0 to 0.035 M at pH 7.

The concentration profile in the particle just before flushing with buffer (at  $t = 0$ ) shows a steep protein concentration gradient between the gel and solution. The fact that the initial concentration profile is not a step function between gel and solution, again reflects the heterogeneity of the gel cross-link density, which seems to be lower at the gel boundary (probably the heterogeneity extends over 1  $\mu\text{m}$ ). As soon as the buffer is flowing, the protein molecules are driven to leave the particle into the solution.

The temporal evolution of the profile in Fig. 5.7 shows that over the first 60 s close to 50% of the protein has already left the outer 3  $\mu\text{m}$  of the particle sphere. However, with increasing time the profile seems to remain flat without further growth of the depletion shell. This might point to a limited rate of release of the protein from the gel matrix, and/or a gradual decrease of the effective protein diffusion coefficient towards the heart of the gel particle. Further investigations of this behavior seem to be relevant for controlled-release applications.



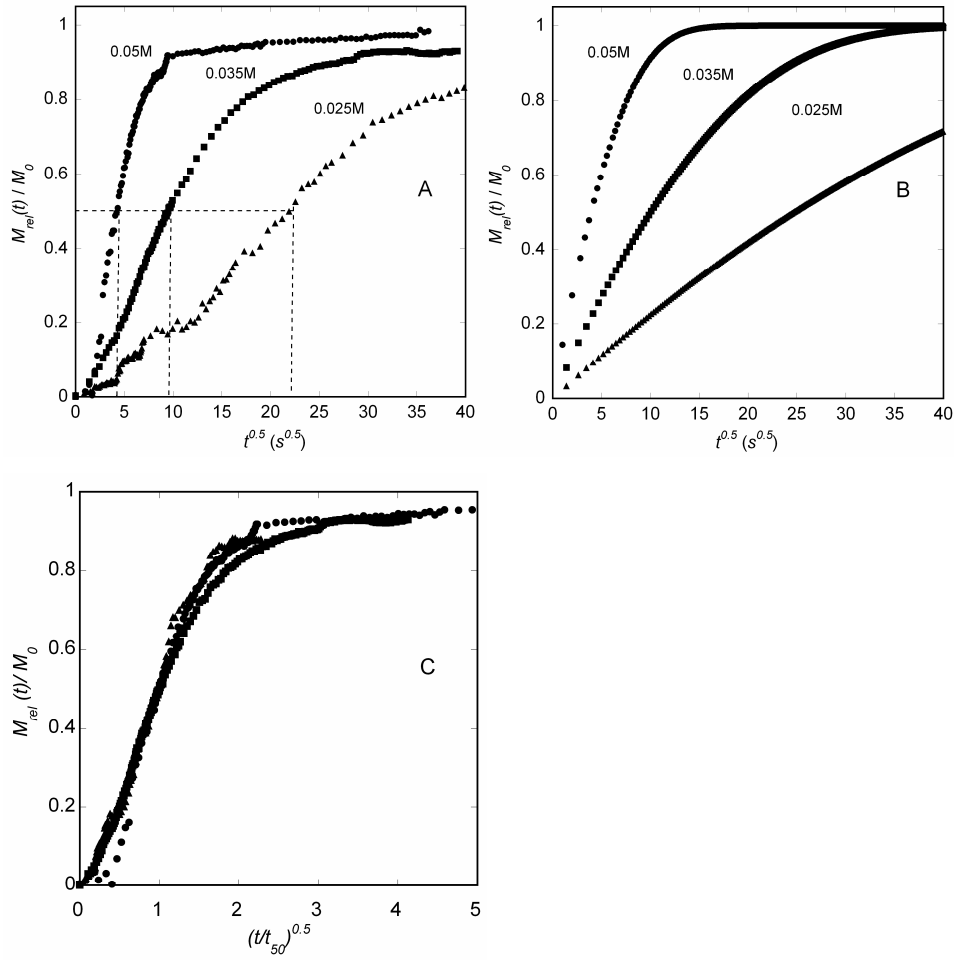


Figure 5.8 Release kinetics of lysozyme from the microgel at pH 7 and ionic strength ( $\blacktriangle$ ) 0.025 M ( $\blacksquare$ ) 0.035 M ( $\bullet$ ) 0.05 M. (A) Fraction of protein released  $M_{rel}(t)/M_0$  as a function of  $t^{0.5}$ . Dotted lines indicate for each ionic strength the characteristic time  $t_{50}$  at which 50% of the protein was released. (B) The modelling of release kinetics according to Eq. 5.13. (C) Fraction of protein released as a function of  $(t/t_{50})^{0.5}$ . The values for  $t_{50}$  are: 480 s at 0.025 M, 90 s at 0.035 M, and 18 s at 0.05 M.

The release kinetics data at different ionic strengths were fitted with Eq. (5.13), the solution of the diffusion equation for release under our specified conditions. The experimental data are shown in Fig. 5.8A, and the fits in Fig. 5.8B. It seems our data almost obey the  $t^{1/2}$  functionality, and the fits can be used as a first approximation for the characteristic diffusion times  $\tau$ .

In Fig. 5.8C the data are re-plotted as a function of  $(t/t_{50})^{1/2}$ , in which  $t_{50}$  is the characteristic time for each particular salt concentration at which 50% of the protein is released from the gel. In this way the release data for different salt concentrations give rise to one single master curve. This provides strong evidence that in all cases there is equilibrium between bound and free protein in the gel phase as assumed in the model, and that diffusion is indeed the limiting

step during protein release. This can be understood considering that in case of no equilibrium, at the start of the release process the concentration ratio of free and bound protein in the gel would become time and position dependent. Therefore,  $D_{\text{eff}}$  would no longer be a constant but decrease in time in a way dictated by the rate of desorption of the protein from the gel network. This effect would be dependent on the salt concentration (the stronger the binding, the stronger the time dependence of  $D_{\text{eff}}$ ) and therefore the normalized curves for different salt concentrations would not overlap (note that the time axis is normalized with respect to the characteristic diffusion time), showing that the diffusion model would not be valid.

From the characteristic times  $\tau$  the effective diffusion coefficients in the gel,  $D_{\text{eff}}$ , at the different ionic strengths can be derived. The magnitude of the diffusion coefficient of free protein molecules inside the gel was already estimated from the modeling of the protein uptake:  $D_{\text{p,g}} \approx 10^{-11} \text{ m}^2\text{s}^{-1}$ . Now the corresponding values for  $R = c_{\text{bound}}/c_{\text{free}}$  can be calculated as well through Eq. (5.12). The results are shown in Table 1. The ratio between bound and free amounts of protein in the gel phase decreases dramatically with increasing ionic strength, due to screening of the electrostatic attraction between protein and gel. It should be noted that the values in Table 1 are estimates, not exact data. Especially the uncertainty in the  $R$  values is high, since these are based on  $D_{\text{eff}}$  as well as on  $D_{\text{p,g}}$ , which are both only first approximations. For comparison, from the absorption isotherm of lysozyme to the microgel obtained at pH 7 and 0.05 M ionic strength [12] we find  $R$  to be in the range 100-200.

Table 5.1 Data obtained from the release kinetics at pH 7: the characteristic diffusion time  $\tau = a^2/D_{\text{eff}}$  and effective diffusion coefficient  $D_{\text{eff}}$  in the gel, and the ratio  $R = c_{\text{bound}}/c_{\text{free}}$ . The diffusion coefficient for the free protein molecules in the gel phase  $D_{\text{free}}$  is approximately  $10^{-11} \text{ m}^2\text{s}^{-1}$ , estimated from the protein uptake kinetics.

$I \text{ (M)}$	$\tau \text{ (s)}$	$D_{\text{eff}} \text{ (m}^2\text{s}^{-1}\text{)}$	$R$
0.025	$10^4$	$10^{-14}$	1000
0.035	$2 \times 10^3$	$5 \times 10^{-14}$	200
0.05	$5 \times 10^2$	$2 \times 10^{-12}$	50

The pH dependence of the release was investigated by measuring the release at pH 3 and pH 8 (0.01 M buffer) (data not shown). These two pH values were chosen because they correspond to the acid environment in the human stomach and the basic conditions in the small intestine or colon, relevant for possible applications as a carrier for intestine/colon specific drugs. It was found that at pH 3 no significant release takes place at the time scale of our experiments

(1 - 2 hours), except for a small instantaneous release of about 10 % just after switching to the buffer solution. This may be caused by release of free and loosely bound protein at the exterior of the particles. Because of the high affinity between lysozyme and the gel at low pH and ionic strength, the very slow release is in line with expectation. The protein loaded gel particles at pH 3 are stable for 24 hours in buffer. The long-time stability of the protein loaded gel particles at low pH deserves further study. At pH 8 and 0.01 M buffer a release curve was found comparable to the ones in Fig. 5.8, with a value for  $R$  of 250,  $D_{\text{eff}}$  of  $4 \times 10^{-14} \text{ m}^2 \text{ s}^{-1}$ , and a characteristic diffusion time  $\tau$  of 2500 s. Since at pH 7 and 0.025 M NaCl the characteristic time is higher (see Table 5.1) than this, the effect of the pH difference seems to outweigh the effect of the difference in ionic strength ( $\tau$  increases with decreasing pH and with decreasing ionic strength).

### *Amylase triggered lysozyme release kinetics*

Our microgel is composed of cross-linked starch polymer; 30% of the primary alcohol groups on the glucose units have been oxidized into carboxyl groups. Therefore, a large fraction of the alpha-1,4 glucose linkages is still degradable by amylase. When loaded with lysozyme, this protein should be released into the surrounding solution when the gel is enzymatically broken down. To test this, first the empty microgel particles were incubated with  $\alpha$ -amylase in water at room temperature. Optical microscopy images were taken to follow the gel degradation in time. Fig. 5.9 shows that the gel is gradually broken down by amylase and degradation is nearly complete after 1000 s. Then lysozyme loaded microgel particles were incubated with the same amount of amylase, and the release of the protein was monitored by CLSM. Fig. 5.10 shows that at the location of a microgel particle the protein fluorescence intensity decreases as a function of time. The protein release kinetics after adding amylase is depicted in Fig. 5.11. In the first 300 s the release rate is slow and this is probably because the amylase molecules need some time to access and adjust their conformation to the substrate. After about 500 s the rate increases. The release is complete and reaches a plateau after 1200 s when all the starch has been degraded. This result is comparable to the observation of Brandl et al. [22] that bovine serum albumin (BSA) molecules detach from a PEG-polypeptides hydrogel when there is an enzymatic degradation of that gel. It strongly supports our idea of using the starch microgel for antimicrobial packaging as mentioned in the introduction section. To further test the potential for such an application we perform microbiological experiments and will report on this in Chapter 6.

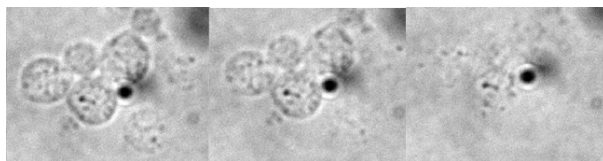


Figure 5.9 Optical light microscopy time series images of the degradation of empty gel particles in water at 0 s, 300 s, 1000 s after addition of amylase.

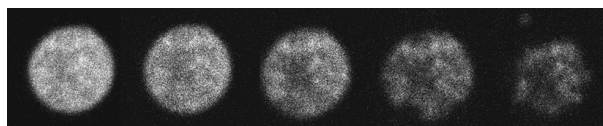


Figure 5.10 CLSM time series images of a protein loaded gel particle at 0 s, 300 s, 600 s, 800 s, 1000 s after addition of amylase.

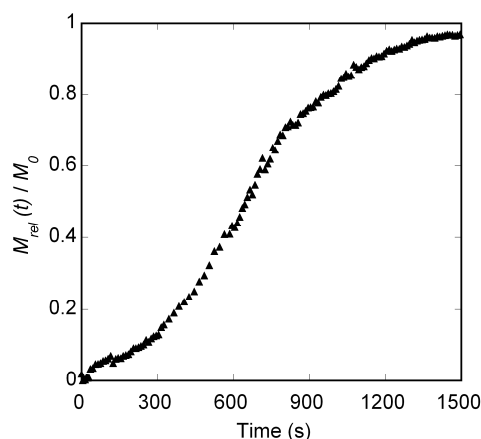


Figure 5.11 Fraction of protein released  $M_{rel}(t)/M_0$  as a function of time during enzymatic degradation of the gel particles by  $\alpha$ -amylase.

## 5.4 Concluding remarks

Our experimental data on lysozyme uptake and release kinetics in starch microgel particles can be very well modeled on the basis of diffusion equations, taking into account the equilibrium between protein bound to the gel network and protein free in the gel particles. The diffusion coefficient of lysozyme in the gel particles ( $D_{p,g}$ ) is found to be on the order of  $10^{-11} \text{ m}^2\text{s}^{-1}$ , an order of magnitude lower than in solution, due to binding of protein to the gel and obstruction by the gel network. From fitting of the release data at pH 7 the effective diffusion coefficient  $D_{eff}$  of the protein in the gel and the ratio concentration  $R$  between bound and free protein have been estimated. These quantities are extremely sensitive to the ionic strength, which is consistent with previously obtained data.

In addition, the time evolution of the experimental protein concentration profiles in the gel particle on release seems to reflect gel inhomogeneity (i.e., the particles are somewhat denser in the center than near the gel/solution interface). Further investigation of the influence of gel homogeneity on the release behavior is relevant for the use of the particles in controlled release applications.

Lysozyme is released from the gel particles at pH 8, but not at pH 3 (0.01 M NaCl). This provides opportunities for use of the microgel in food and pharma controlled-delivery applications, since a functional ingredient can be protected in the stomach, and released in the small intestine.

The enzyme  $\alpha$ -amylase degrades the oxidized starch microgel resulting into the release of their protein content into solution. This is an important result, since it demonstrates the feasibility of the use of the microgel in, for example, antimicrobial packaging. The presence of amylase producing bacteria would lead to degradation of the gel and subsequently the lysozyme released would kill the bacteria. In chapter 6 the antimicrobial activity of the lysozyme loaded gel particles tested on amylase-producing bacteria is in preparation.

## References

- [1] S.V. Vinogradov, Colloidal microgels in drug delivery applications, *Current Pharmaceutical Design*, 12 (2006) 4703-4712.
- [2] J.K. Oh, R. Drumright, D.J. Siegwart, K. Matyjaszewski, The development of microgels/nanogels for drug delivery applications, *Progress in Polymer Science*, 33 (2008) 448-477.
- [3] A.S. Hoffman, Hydrogels for biomedical applications, in: D. Hunkeler, A. Cherrington, A. Prokop, R. Rajotte (Eds.) *Bioartificial Organs Iii: Tissue Sourcing, Immunoisolation, and Clinical Trials*, New York Acad Sciences, New York, 2001, pp. 62-73.
- [4] E.J. Oh, K. Park, K.S. Kim, J. Kim, J.A. Yang, J.H. Kong, M.Y. Lee, A.S. Hoffman, S.K. Hahn, Target specific and long-acting delivery of protein, peptide, and nucleotide therapeutics using hyaluronic acid derivatives, *Journal of Controlled Release*, 141 (2010) 2-12.
- [5] P.J. Skrzyszewska, F.A. de Wolf, M.W.T. Werten, A. Moers, M.A. Cohen Stuart, J. van der Gucht, Physical gels of telechelic triblock copolymers with precisely defined junction multiplicity, *Soft Matter*, 5 (2009) 2057-2062.
- [6] Y.F. Poon, Y. Cao, Y.X. Liu, V. Chan, M.B. Chan-Park, Hydrogels Based on Dual Curable Chitosan-graft-Polyethylene Glycol-graft-Methacrylate: Application to Layer-by-Layer Cell Encapsulation, *Acs Applied Materials & Interfaces*, 2 (2010) 2012-2025.
- [7] M.V. Tsurkan, K.R. Levental, U. Freudenberg, C. Werner, Enzymatically degradable heparin-polyethylene glycol gels with controlled mechanical properties, *Chemical Communications*, 46 (2010) 1141-1143.
- [8] W.X. Wang, H. Liang, R.C. Al Ghanami, L. Hamilton, M. Fraylich, K.M. Shakesheff, B. Saunders, C. Alexander, Biodegradable Thermoresponsive Microparticle Dispersions for Injectable Cell Delivery Prepared Using a Single-Step Process, *Advanced Materials*, 21 (2009) 1809-1815.
- [9] F.H. Meng, W.E. Hennink, Z. Zhong, Reduction-sensitive polymers and bioconjugates for biomedical applications, *Biomaterials*, 30 (2009) 2180-2198.
- [10] F. Abreu, M.M.C. Forte, T.B.L. Kist, L.P. Honaiser, Effect of the preparation method on the drug loading of alginate-chitosan microspheres, *Express Polymer Letters*, 4 (2010) 456-464.
- [11] Y. Li, R. de Vries, T. Slaghek, J. Timmermans, M.A. Cohen Stuart, W. Norde, Preparation and Characterization of Oxidized Starch Polymer Microgels for Encapsulation and Controlled Release of Functional Ingredients, *Biomacromolecules*, 10 (2009) 1931-1938.
- [12] Y. Li, R. de Vries, J. M. Kleijn, T. Slaghek, J. Timmermans, M.A. Cohen Stuart, W. Norde, Lysozyme Uptake by Oxidized Starch Polymer Microgels, *Biomacromolecules*, 11 (2010) 1754-1762.
- [13] Y. Li, J.M. Kleijn, T. Slaghek, J. Timmermans, M. A. Cohen Stuart, W. Norde, Mobility of lysozyme inside oxidized starch polymer microgels, *Soft Matter*, 7 (2011) 1926-1935.
- [14] J. Crank, *The Mathematics of Difussion*, Clarendon Press, Oxford, 1975.
- [15] V.G. Levich, *Physicochemical hydrodynamics*, Prentice Hall, Englewood Cliffs, 1962.
- [16] J. Buffle, K. Startchev, J. Galceran, Computing steady-state metal flux at microorganism and bioanalytical sensor interfaces in multiligand systems. A reaction layer approximation and its comparison with the rigorous solution, *Physical Chemistry Chemical Physics*, 9 (2007) 2844-2855.
- [17] F. Brandl, F. Kastner, R.M. Gschwind, T. Blunk, J. Tessmar, A. Gopferich, Hydrogel-based drug delivery systems: Comparison of drug diffusivity and release kinetics, *Journal of Controlled Release*, 142 (2010) 221-228.

- [18] P.L. Ritger, N.A. Peppas, A simple equation for description of solute release I. Fickian and non-fickian release from non-swellable device in the form of slabs, spheres, cylinders or discs *Journal of Controlled Release*, 5 (1987) 23-36.
- [19] J.F.L. Duval, *Journal of Physical Chemistry A*, 113 (2009) 2275-2293.
- [20] A.H. Muhr, J.M.V. Blanshard, Diffusion in gels, *Polymer*, 23 (1982) 1012-1026.
- [21] E.M. Johnson, D.A. Berk, R.K. Jain, W.M. Deen, Diffusion and partitioning of proteins in charged agarose gels, *Biophysical Journal*, 68 (1995) 1561-1568.
- [22] F. Brandl, N. Hammer, T. Blunk, J. Tessmar, A. Goepferich, Biodegradable Hydrogels for Time-Controlled Release of Tethered Peptides or Proteins, *Biomacromolecules*, 11 (2009) 496-504.





---

# Chapter 6

## The antimicrobial activity of lysozyme-loaded oxidized starch microgel

---

### *Abstract*

The aim of this study is to determine the release of lysozyme from oxidized starch microgels and subsequently test its antimicrobial activity. The gels are made of oxidized potato starch polymers, which are chemically cross-linked by sodium trimetaphosphate (STMP). The microgel is negatively charged and interacts with positively charged lysozyme by electrostatic attraction. Application of the lysozyme-containing starch particles to environments contaminated with microbes, may lead to hydrolysis of the starch by microbial enzymes. As a result, lysozyme is released in the environment where it inhibits microbial growth. In this study, first bacteria were screened for amylase production and lysozyme sensitivity. Then, the bacteria were mixed with empty gel particles (i.e., without lysozyme) in a Nutrient Broth liquid medium to test whether the bacteria that can produce amylase are also able to degrade oxidized starch gel. Subsequently the amylase-producing lysozyme sensitive bacteria, *Bacillus licheniformis* 7558 and *Bacillus subtilis* 168, were selected for further quantification of the antimicrobial activity of the gel-lysozyme particles after incubation with these bacteria in Nutrient Broth liquid suspensions. The results prove that the starch microgel has a potential as antimicrobial carrier targeting amylase-producing and lysozyme-sensitive bacteria. The controlled antimicrobial delivery for killing undesired micro-organisms may find applications in food related systems, where amylase-producing bacteria may be abundantly present.

## 6.1 Introduction

Control of microbiological food safety is a very important issue in food industry and therefore innovation in antimicrobial technology has a high priority. Encapsulation of antimicrobial compounds is a promising option since it can effectively reduce undesirable interaction between these compounds and food components, and improves the stability and activity of antimicrobials in complex food systems. For example, encapsulation of Nisin and lysozyme in liposomes [1] enhances activity against *Listeria monocytogenes* [2] and *Escherichia coli* O157:H7 [3] chitosan-lysozyme films and coatings improve microbial safety of Mozzarella cheese [4], and incorporation of antimicrobial peptides into mesoporous silica films inhibits growth of both Gram-positive *Staphylococcus aureus* and Gram-negative *E. coli* bacteria [5]. However, only few of these carriers have a “release-on-demand” functionality for enclosed ingredients. We have developed a so-called “Bioswitch” microgel carrier [6-9] which consists of cross-linked negatively charged potato starch polymer. It can absorb and bind positively charged antimicrobial compounds, e.g., lysozyme, through electrostatic attraction. The antimicrobial activity can be switched on by amylase secretion from microorganisms, causing hydrolysis of the starch, and leading to release of lysozyme into the environment that subsequently hydrolyses cell walls of sensitive bacteria finally leading to cell death. Thus, the system detects and subsequently kills amylase-producing microorganisms.

Because of its biodegradability by  $\alpha$ -amylase, this starch gel carrier is targeted in particular against amylase-producing microorganisms. Amylase-producing microorganisms widely exist in nature. Several bacillus strains produce extracellular amylases and are of considerable industrial importance [10-12]. For instance, *Bacillus licheniformis* produces a thermostable  $\alpha$ -amylase, which is widely used for starch liquefaction [13]. Various lactobacillus (LAB) strains [14] are also capable of producing amylase. However, some of these amylase-producing microorganisms are pathogenic, e.g., *Aeromonas hydrophila* is a pathogenic bacteria in fish and *Guignardia citricarpa* is a plant pathogenic fungus that causes citrus diseases. Antimicrobial compounds encapsulated in starch microgel particles can specifically target and inactivate such amylase-producing pathogens. Several starch gels designed for this purpose have already been presented in literature [15-18]. However, our “Bioswitch” microgels (10-20  $\mu\text{m}$  in diameter) are novel with respect to their controlled degree of oxidation and cross-link density [6, 7] and, hence, their controlled swelling and controlled uptake of the functional ingredient.

Lysozyme is an antimicrobial protein that is naturally present in egg white, in plants and in animal secretions [1]. Its antimicrobial properties are associated with hydrolysis of peptidoglycan layers in the bacterial cell wall and also to membrane perturbation [19]. Our previous studies show that the starch microgel can accommodate a large amount of lysozyme [6], while the uptake and release kinetics can be tuned by varying the charge, the degree of oxidation and the cross-link density in the gel [7]. These features are important because they may also be applicable to other positively charged water-soluble antimicrobials.

The objective of this study is to test the antimicrobial activity of lysozyme-loaded oxidized starch gel particles. A selection of food spoilage and pathogenic gram-positive bacteria including *Bacillus. licheniformis* 7558 and *Bacillus. licheniformis* 6993, *Bacillus subtilis* 168, *Bacillus cereus* 14579 and *Bacillus. cereus* 10957, and *Listeria. monocytogenes* LR991 and *Listeria. monocytogenes* 001 were screened for their amylase-production and lysozyme sensitivity. The selected bacteria were used for quantification of the antimicrobial activity of the lysozyme-gel particles. Our study opens a new approach to using lysozyme containing gels in antimicrobial applications.

## 6.2 Material and Methods

### *Materials*

Native potato starch was kindly provided by AVEBE, the Netherlands. The oxidation catalyst 2,2,6,6-tetramethyl-1-piperidinyloxy (TEMPO) was purchased from Merck, Germany. The cross-linker sodium trimetaphosphate (STMP) and the globular protein lysozyme (from chicken egg white, Mw = 14.4 kDa) were supplied by Sigma-Aldrich. The fluorescent dye, Alexa Fluor 488 carboxylic acid succinimidyl ester (mixed with isomers), was purchased from Invitrogen. Alexa Fluor 488 labelled lysozyme was prepared as described previously [8]. *B. licheniformis* 7558 and *B. licheniformis* 6993 were obtained from TNO Quality of Life, Netherlands. The bacterial strains *B. subtilis* 168, *B. cereus* 14579 and *B. cereus* 10987, *L. monocytogenes* LR991 and *L. monocytogenes* 001 were kindly provided by the Food Microbiology department of Wageningen University, Netherlands. Brain Heart Infusion (BHI) medium is from Bacton Dickinson, France. (Composition BHI in Appendix) Agar bacteriological (Agar no.1), Nutrient Broth (NB), Nutrient Agar (NA) were purchased from Oxoid, England. (Composition NB and NA in Appendix) Iodine solution (Color gram 2 (R2-F) Stabilized Lugol) is obtained from Biomerieux, France. Solutions were all prepared using sterilized distilled water. All experiments were replicated at least twice.

### ***Microgel preparation***

The spherical microgel particles (diameter 10 - 20  $\mu\text{m}$ ) of cross-linked oxidized starch polymer were synthesized by inverse emulsion polymerization. First the primary alcohol groups on the starch polymer were oxidized into carboxyl groups; the degree of oxidation was 30%. To form the gel a 0.20 cross-linker to polymer weight ratio was used. For more details on the oxidation of the starch polymers and preparation of the microgel particles we refer to Chapter 2 [6] and 4 [8].

### ***Encapsulation of lysozyme by DO30 microgel***

We suspended 40 mg of the dry gel particles [6, 7] in 4 mL sterilized distilled water (pH 7, no salt), added 1 mL of 50 mg/mL protein solution and gently stirred for 2 hours (enough time to reach equilibrium). Subsequently, the samples were divided over 4 tubes and centrifuged at 10,000 rpm for 5 minutes and the concentration of lysozyme in the supernatant was determined by UV spectrophotometry. The sediment of protein-gel particles was separated from the supernatant to remove the unabsorbed lysozyme. The protein absorbed in equilibrium (mg protein/mg dry gel) in the microgel particles was calculated from mass balance. It is around 1.2 mg protein / mg dry gel. The experiment was performed in a sterilized environment in a microbiology hood.

### ***Enzyme induced protein release***

Gel particles were first saturated with fluorescent (Alexa Fluor 488) labeled protein for 2 hours. Then 100  $\mu\text{L}$  of an amylase solution in water ( $10^5 \times$  dilutions of original 120 KNU/g enzyme activity) was added to the protein loaded gel particle. (1 KNU - kilo Novo Unit, is defined as the amount of enzyme which breaks down 5.26 g of starch in one hour). The degradation of the gel was followed by optical microscopy. A time series of fluorescence images was used to monitor the protein release.

### ***Assay of bacterial amylase production***

Bacterial strains were stored at  $-80^\circ\text{C}$  in the presence of 26% (v/v) glycerol. Before each experiment, strain cultures were grown overnight in BHI broth at  $30^\circ\text{C}$  while shaking (200 rpm). The overnight cultures (around  $10^6$  CFU/mL) were spot-inoculated on BHI-Agar plates containing 1% of soluble starch (starch plates). Starch plates were incubated for 24 hours at  $30^\circ\text{C}$ . Colonies were scraped off/washed out from the plate with sterilized water and 2ml of

Lugol's iodine was poured on the starch plates. A clear hydrolysis zone indicates degradation of starch by amylase produced by the bacteria. Results are shown in Figure A6.1 in Appendix.

#### ***Visualization of starch gels degraded by amylase-positive bacteria***

100  $\mu$ L overnight culture of amylase-positive bacterial strains cultivated in BHI broth (around  $10^6$  CFU/mL) was mixed with 100  $\mu$ L concentrated spherical DO30% microgel particles [8, 9] in 1 mL NB liquid medium. The mixtures were incubated in a shaker incubator at 30 °C. Pictures of the starch gel particles were taken for all strains after 24 hours incubation at 100  $\times$  magnification. For *B. licheniformis* 7558, a time series pictures were taken after 0h, 3h, 6h, 9h, 12h, 24h incubation.

#### ***Lysozyme-sensitivity of bacterial strains***

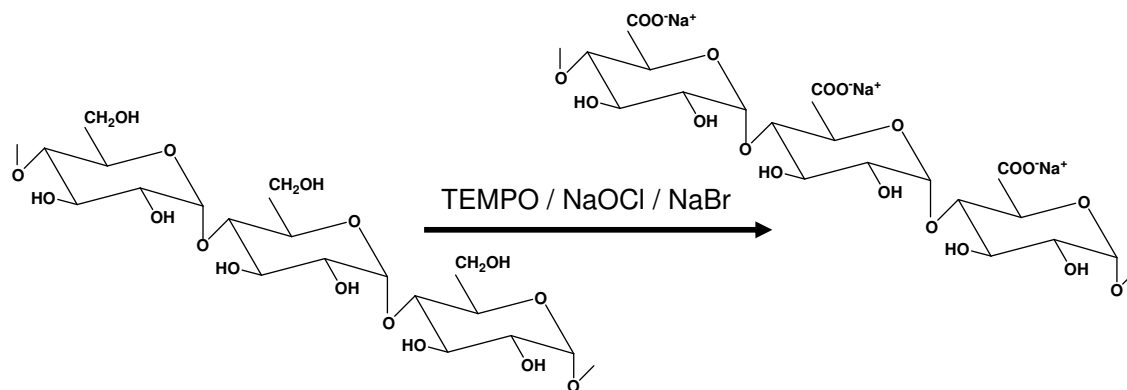
100  $\mu$ L overnight culture of bacterial strains in BHI broth (around  $10^6$  CFU/mL) were spread evenly on BHI-Agar plates to obtain a uniform bacterial lawn. A hole (5 mm in radius) was made in each plate. 200  $\mu$ L 50 mg/mL lysozyme solution was added into the hole. For lysozyme-sensitive bacteria, an inhibition zone will occur around the hole after 24 hours incubation at 30 °C. Results were shown in Figure A6.2 in Appendix.

#### ***Determination of antimicrobial activity of starch gel-lysozyme particles in liquid suspension***

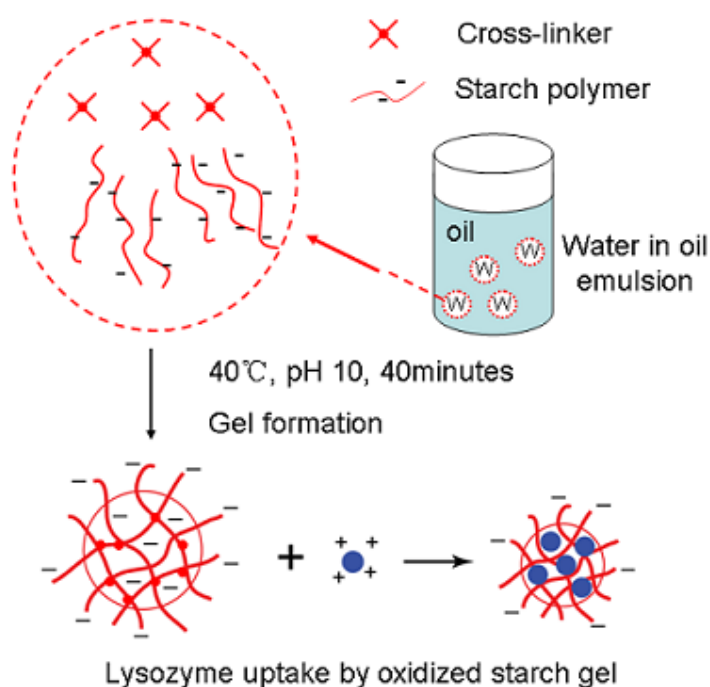
A low salt NB (3 g /L NaCl) liquid medium was prepared in order to prevent the salt-induced protein release from starch gel particles. 0.03-0.10M NaCl was used to find out the optimal salt concentration for bacterial growth. The results indicate that 0.05 M (3 g/L) NaCl is the most suitable salt concentration. 200  $\mu$ L overnight cultures of bacterial strains grown in BHI broth (around  $10^6$  CFU/mL) was added into 20 mL NB liquid medium as a control. Protein-gel particles (12 mg protein / 10 mg gel), 12 mg lysozyme and 10 mg gel particles were separately added into three separated beakers containing 20mL NB medium, and subsequently mixed with 200  $\mu$ L bacterial overnight cultures. The mixtures and the control were placed in a 30 °C shaker incubator (200 rpm). After 0 h, 3 h, 6 h, 12 h, 24 h, 27 h, and 30 h incubation, 100  $\mu$ L of each sample was diluted with 900  $\mu$ L NB medium and then the optical density (OD) at 600 nm was measured. The optical density of the bacterial suspensions at this wavelength is roughly proportional to the number concentration of bacterial cells [2]. The reduced OD indicates inhibition of bacterial growth due to the lysis of bacterial cell walls. The optical density of the starch gel particles themselves is very low and does not interfere with the optical density of the bacteria.

### 6.3 Results and discussion

#### *Optimum starch microgel for amylase-triggered bacterial inhibition*



Scheme 6.1 TEMPO / NaOCl / NaBr oxidation of starch amylose to the corresponding polyuronic derivatives.



Scheme 6.2 Preparation of oxidized starch microgel by inverse (W/O) emulsion polymerization; encapsulation of oppositely charged ingredient by the starch microgel.

A natural biopolymer-based release-on-demand Bioswitch microgel that consists of cross-linked oxidized potato starch polymers has been developed [20]. As it is shown in Scheme 6.1, the primary alcohol groups at the 6-position on the starch polymer (e.g., amylose) were selectively oxidized into carboxyl groups, by TEMPO-mediated oxidation [21,

22]. In this way, starch polymers of 30%, 50%, 70% and 100% degree of oxidation (DO) were prepared. The DO was controlled by the amount of sodium hypochlorite added during oxidation. Spherical microgel particles were prepared by chemically cross-linking the oxidized starch polymer with sodium trimetaphosphate (STMP) at pH 10 in the water droplets of a water-in-oil (W/O) emulsion (Scheme 6.2) [8]. The oxidized starch microgel carries negative charges which are able to interact with positively charged ingredients (e.g., proteins) through electrostatic attraction. The swelling and protein uptake behavior are responsive to environmental parameters such as pH and salt concentration [6, 7]. Uniquely, the starch gel can be degraded by enzymatic attack by amylase, which switches on the release of the functional ingredients from the gel. Advantages of the Bioswitch microgel are the controlled charge and cross-link density, and, hence, controlled swelling and uptake capacity.

The natural biopolymer potato starch is not well-defined, nevertheless it can be used to make microgels with well-defined properties. As shown in Figure 6.1A, the maximum charge density  $Q_{\max}$  (obtained from proton titrations [7]) of various oxidized polymers in solution increases linearly with increasing DO. Gels attain the same charge density as the corresponding dissolved polymers except at high DO-values, at which the charge density is somewhat reduced due to the polyelectrolyte effect. Figure 6.1B shows that the maximum lysozyme uptake  $\Gamma_{\max}$  (the plateau value of the protein absorption isotherm [7]) increases linearly with the charge density  $Q_{\text{gel}}$  of the gel. Thus, the maximum amount of protein absorbed can be tuned by controlling the DO of starch gels. Highly oxidized amylose is difficult to digest by amylase. DO70% and DO100% starch gel were found to be non-degradable by  $\alpha$ -amylase, and these gels are therefore not suitable for the Bioswitch system. The gel having a low degree of oxidation, DO30%, and a low cross-link density (cross-linker to polymer weight ratio 0.10) was selected as the suitable carrier, since it is easily degraded by bacteria that produce amylase. This gel is used throughout this chapter.

Lyon et al. have reported different kinds of innovative environmental multi-responsive hydrogels for targeted drug delivery and microlenses for biosensing [23-25]. Hovgaard and Brøndsted [26] have found that degradation of their dextran hydrogel by dextranase leads to the release of encapsulated drugs. Our starch microgel does not only show stimuli-responsive behavior, but it can also be degraded by  $\alpha$ -amylase[9]. Figure 6.1C shows that fluorescently labeled lysozyme is released after degradation of a gel particle by  $\alpha$ -amylase. It is therefore expected that bacterial amylase can trigger the release of encapsulated antimicrobial compounds from the starch gel

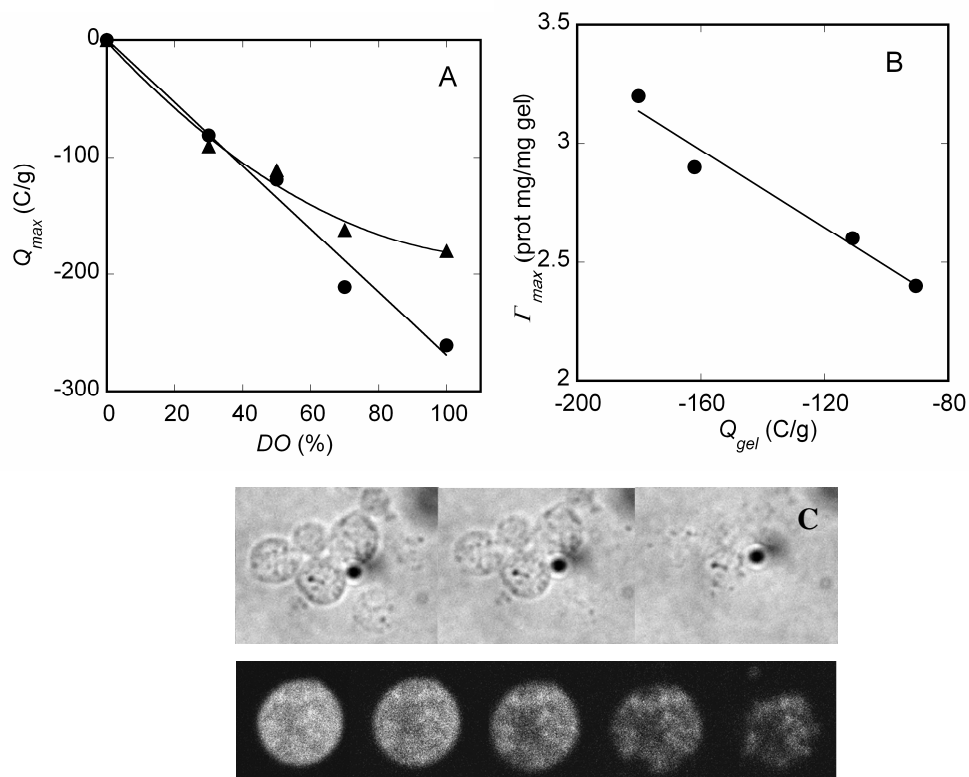


Figure 6.1 (A) Maximum charge density  $Q_{max}$  obtained by proton titration as a function of degree of oxidation (DO) for cross-linked ( $\blacktriangle$ ) and not cross-linked ( $\bullet$ ) starch polymer. (B) Maximum lysozyme uptake  $\Gamma_{max}$  as a function of charge density  $Q_{gel}$  of the microgels. (C) Top: optical light microscopy time series images of the degradation of empty DO30% gel particles in water at 0 s, 300 s, and 1000 s after addition of amylase. Bottom: fluorescence CLSM time series images of a protein loaded gel particle at 0 s, 300 s, 600 s, 800 s, and 1000 s after addition of amylase. The lysozyme was fluorescent labeled with Alexa Fluor 488.

### Screening for amylase-producing and lysozyme sensitive bacteria

In order to measure the antimicrobial activity of the starch gel encapsulated lysozyme (gel-lysozyme) system, firstly, bacteria that can produce amylase and/or are sensitive to lysozyme were screened. The amylase-producing property of bacteria was determined by the iodine test: starch amylose forms helices where iodine molecules assemble, causing a dark purple/black color. In case of amylase-producing bacteria, clear zones surrounding the bacterial colonies can be observed, due to degradation of the amylose into smaller units, such that iodine cannot bind. Several bacterial strains were incubated in a starch-agar medium plate at 30 °C for 24 hours. Then iodine solution was applied to the plates. As shown in Figure A6.1 in Appendix, a clear zone occurs around the spots where amylase-producing bacteria have been growing. After 24 h incubation at 30°C lysozyme sensitivity of selected strains was



reflected in the appearance of an inhibition zone near the spot on BHI agar plate where lysozyme solution was applied (see Figure A6.2 in Appendix). The results for amylase production and lysozyme sensitivity are summarized in Table 6.1. Four strains were selected for further investigation of the inhibition effect of the starch gel-lysozyme particles.

Table 6.1 Amylase-production and lysozyme-sensitivity of selected bacteria.

Test Strains	Amylase-producing [a]	Lysozyme sensitive [b]
<i>B. licheniformis</i> 7558	+	+
<i>B. licheniformis</i> 6993	-	+
<i>B. subtilis</i> 168	+	+
<i>B. cereus</i> 14579	+	-
<i>B. cereus</i> 10987	-	-
<i>L. monocytogenes</i> LR991	-	+
<i>L. monocytogenes</i> 001	-	+

[a] The amylase-producing property is measured by starch medium plate and iodine test. The results are shown in Figure A6.1 in Appendix.

[b] The lysozyme sensitivity is determined by a BHI-agar plate assay. Results are shown in Figure A6.2 in the Appendix.

*B. licheniformis* 7558 and *B. subtilis* 168 were selected as the target strains because of their ability to produce amylase and their growth inhibition by lysozyme. *B. licheniformis* 6993 was selected as a control strain, because it cannot degrade starch but is sensitive to lysozyme, and *B. cereus* 14579 as another control because it degrades starch but is insensitive to lysozyme.

#### **Visualization of starch gel degradation by amylase-positive bacteria**

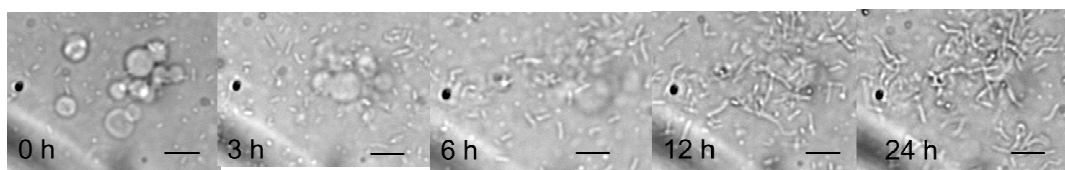


Figure 6.2 Time series of degradation of DO30% starch gel by *B. licheniformis* 7558 after 0 h, 3 h, 6 h, 12 h, and 24 h of incubation at 30 °C. The scale bars corresponds to 10 μm.

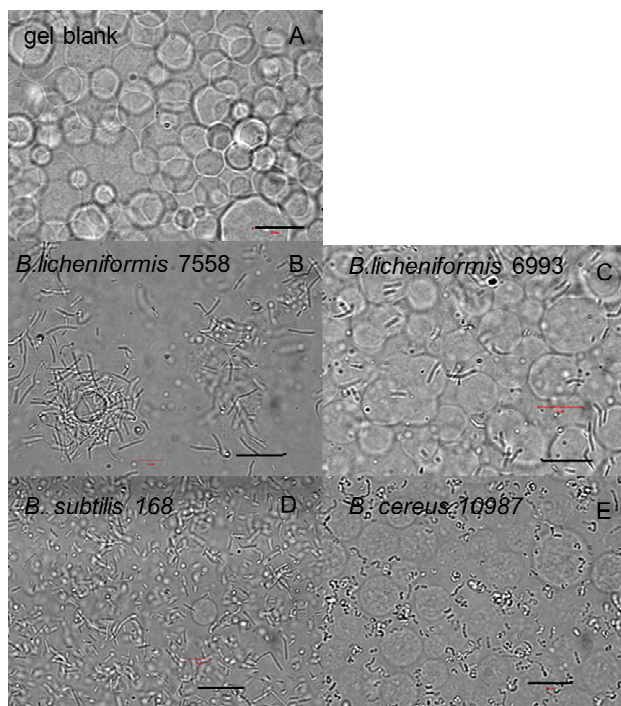


Figure 6.3 Optical images of bacterial strains mixed with DO30% starch microgel particles in Nutrient Broth (NB) liquid medium after 24 hours of incubation at 30 °C, no lysozyme added. The concentration of gel particles and amount of bacteria added are equal for all the samples. (A) Gel blank: only gel particles; (B) *B. licheniformis* 7558 (amylase +) and gel particles; (C) *B. licheniformis* 6993 (amylase -) and gel particles; (D) *B. subtilis* 168 (amylase +) and gel particles ; (E) *B. cereus* 10987 (amylase -) and gel particles. The scale bars indicated are 20  $\mu\text{m}$ .

Although the iodine test shows that some bacterial strains hydrolyze starch in solution, the ability of those strains to degrade the cross-linked oxidized starch still needs to be proven. About  $10^7$  cells  $\text{mL}^{-1}$  of each strain were mixed with  $10^{-1}$  diluted DO30% microgel particles in NB liquid medium. Optical microscopic images were made after 24 hours incubation at 30 °C to qualitatively judge degradation of the gel particles. As an example, the kinetics of gel degradation by *B. licheniformis* 7558 is shown in Figure 6.2. A given gel particle concentration was applied to the selected bacterial strains and after 24 hours incubation at 30 °C. Their ability to degrade the gel particles was judged from the optical images displayed in Figure 6.3 B-E, by comparison with the image in Figure 6.3A for the blank sample (without bacteria). Figure 6.3B and 6.3D show that *B. licheniformis* 7558 and *B. subtilis* 168 are able to degrade the gel particles. As shown in Figure 6.3C and 6.3E, *B. licheniformis* 6993 and *B. cereus* 10987 can not degrade the starch gel. These results are consistent with the iodine experiments for the amylase induced degradation of dissolved starch.

### ***Determination of the antimicrobial activity of starch gel-lysozyme in liquid suspension***

The antimicrobial activity of gel-lysozyme particles may be effectively and accurately determined in a suspension containing NB liquid medium in which microscopic gel particles and bacteria are intimately mixed. NB liquid medium contains 50 mM NaCl which may lead to some release of protein from the gel particles, due to salt-screening effect of electrostatic attraction between the starch gel and lysozyme [7]. The amount of protein released after 24 hours immersion of the gel-lysozyme particles in the NB liquid medium was measured by UV spectrophotometry and showed that only 2% protein of initial amount of protein in the gel is released. In the next 24 h no further release of lysozyme was observed (see Figure 6.4). Hence passive protein release in NB liquid medium is only very limited and can be neglected.

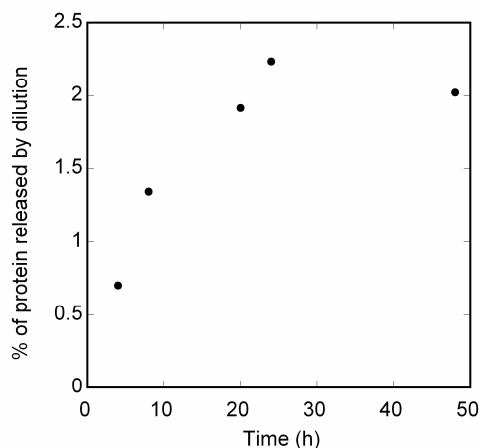


Figure 6.4 Percentage of lysozyme released from oxidized starch microgel particles in NB liquid medium during shaking and incubation without bacteria. The total amount of protein absorbed in the gel is 1.2 mg prot/mg gel. In the end about 2% of the total amount of absorbed protein was released (lysozyme concentration is 25  $\mu\text{g/mL}$ ).

The antimicrobial activity of starch gel-lysozyme particles on bacterial growth is measured by optical density (OD) as a function of time. The OD value of bacterial suspension at 600nm is roughly proportional to the number concentration of bacterial cells [2]. The growth inhibition is indicated by a low OD value due to lysis of bacterial cell walls. The four selected strains in Figure 6.5 were used to assess the antimicrobial activity of starch gel encapsulated lysozyme particles. The OD values were determined for bacterial suspensions in the presence of free lysozyme, gel encapsulated lysozyme, gel without lysozyme and compared with the control (only bacteria in the medium). For the bacterial suspensions containing free lysozyme, complete inhibition occurred for all strains (Figure 6.5A-C) except *B. cereus* 14579 (Figure 6.5D). As shown in Figures 6.5B and 6.5C, the optical densities in

the presence of free lysozyme approached those of encapsulated lysozyme and remained at a low level over time.

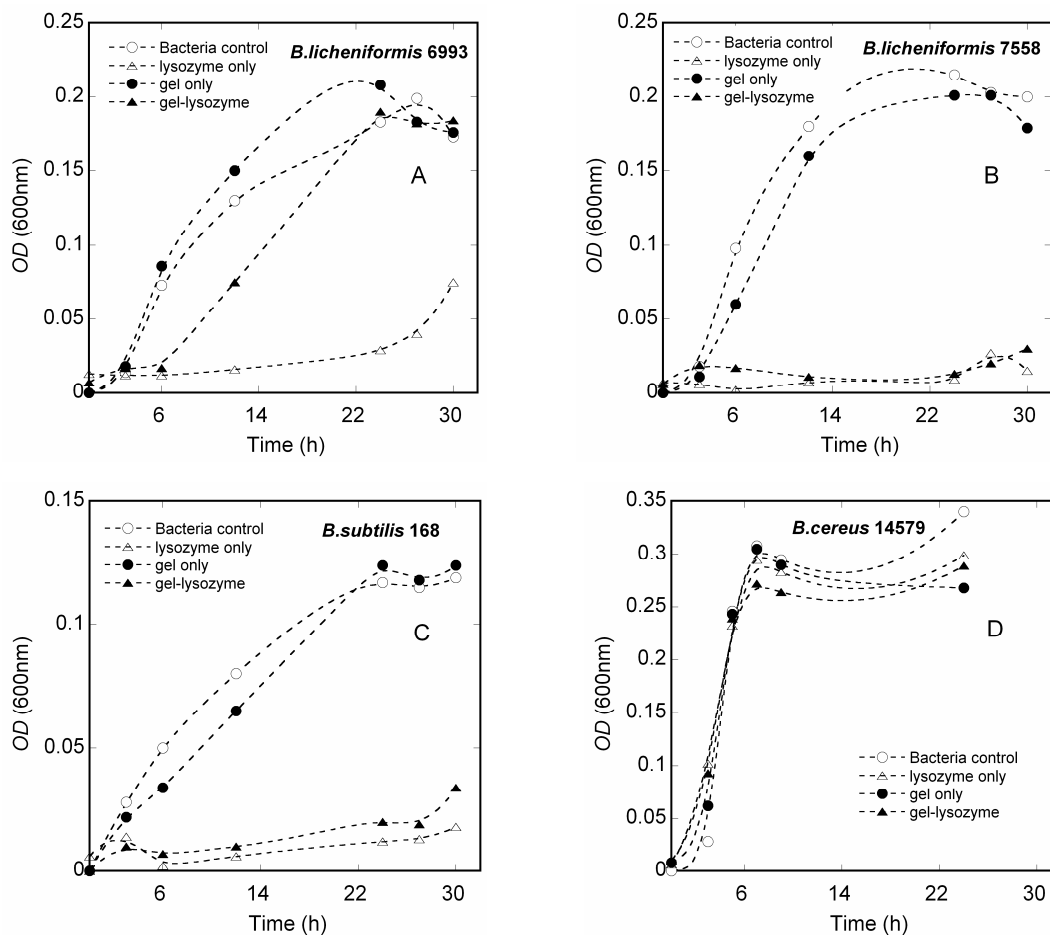


Figure 6.5 Bacteria growth in suspensions as determined by optical density (OD) measurements at 600 nm. (A) *B. licheniformis* 6993, amylase (-), lysozyme sensitive (+). (B) *B. licheniformis* 7558, amylase (+), lysozyme sensitive (+). (C) *B. subtilis* 168, amylase (+), lysozyme sensitive (+). (D) *B. cereus* 14579, amylase (+), lysozyme sensitive (-). The optical density in the figure is obtained from 10 times diluted samples from the original suspensions. The dotted lines are only meant as a guide for the eye.

This result indicates that the growth of the amylase-positive and lysozyme-sensitive bacteria *B. licheniformis* 7558 and *B. subtilis* 168 were inhibited by the presence of the lysozyme-loaded gel particles. The inhibition effect was nearly as effective as in the case free lysozyme was added. These results prove that the starch gel was degraded by the bacterial amylase, and the released lysozyme killed bacteria in the medium. In the case empty gel particles were added to the bacterial suspensions, the growth was found to be nearly the same as in the control that only contains bacterial cells. It proves that the empty starch gel particles have no antimicrobial activity.

Figure 6.5A shows that starch gel-lysozyme particles did not effectively inhibit the amylase-negative *B. licheniformis* 6993 although it is killed by free lysozyme in the medium. It shows that the slight amount (about 2%) of salt-induced release lysozyme is diluted in the suspension down to sub-lethal concentrations. The gel-lysozyme particles do not have antimicrobial activity to amylase-negative bacteria. The liquid suspension method shows that the lysozyme containing starch gel particles can be potentially used in food systems that are often more or less liquid-like. It proves that the gel-lysozyme particles are specific to amylase-producing bacteria. It detects the amylase-producing bacteria and subsequently kills those that are sensitive to lysozyme.

## 6.4 Concluding remarks

We have prepared oxidized starch-based microgels capable of encapsulating lysozyme that are easily degraded by bacterial amylase, thereby releasing the lysozyme. We selected a microgel with a relatively low degree of oxidation (DO30%) to test the antimicrobial activity of the gel-lysozyme system.

The results show that degradation of the starch particles is a pre-requisite for the lethal activity of the gel-lysozyme particles, since only the amylase-positive lysozyme sensitive bacteria are killed. Thus, our system is able to diagnose the presence of amylase-producing microorganisms followed by eradication of the lysozyme sensitive species.

Similarly, the oxidized starch gel system can be used to encapsulate other positively charged antimicrobial compounds that will be effectively released by amylase activity. The system thus shows potential to deliver antimicrobials to target undesired micro-organisms in food applications.

## References

- [1] L.M. Were, B.D. Bruce, P.M. Davidson, J. Weiss, Size, stability, and entrapment efficiency of phospholipid nanocapsules containing polypeptide antimicrobials, *Journal of Agricultural and Food Chemistry*, 51 (2003) 8073-8079.
- [2] L.M. Were, B. Bruce, P.M. Davidson, J. Weiss, Encapsulation of nisin and lysozyme in liposomes enhances efficacy against *Listeria monocytogenes*, *Journal of Food Protection*, 67 (2004) 922-927.
- [3] T.M. Taylor, B.D. Bruce, J. Weiss, P.M. Davidson, *Listeria monocytogenes* and *Escherichia coli* O157 : H7 inhibition in vitro by liposome-encapsulated nisin and ethylene diaminetetraacetic acid, *Journal of Food Safety*, 28 (2008) 183-197.
- [4] J. Duan, S.L. Park, M.A. Daeschel, Y. Zhao, Antimicrobial chitosan-lysozyme (CL) films and coatings for enhancing microbial safety of Mozzarella cheese, *Journal of Food Science*, 72 (2007) M355-M362.
- [5] I. Izquierdo-Barba, M. Vallet-Regi, N. Kupferschmidt, O. Terasaki, A. Schmidtchen, M. Malmsten, Incorporation of antimicrobial compounds in mesoporous silica film monolith, *Biomaterials*, 30 (2009) 5729-5736.
- [6] Y. Li, R. de Vries, T. Slaghek, J. Timmermans, M.A. Cohen Stuart, W. Norde, Preparation and Characterization of Oxidized Starch Polymer Microgels for Encapsulation and Controlled Release of Functional Ingredients, *Biomacromolecules*, 10 (2009) 1931-1938.
- [7] Y. Li, R. de Vries, J.M. Kleijn, T. Slaghek, J. Timmermans, M.A. Cohen Stuart, W. Norde, Lysozyme Uptake by Oxidized Starch Polymer Microgels, *Biomacromolecules*, 11 (2010) 1754-1762.
- [8] Y. Li, J.M. Kleijn, T. Slaghek, J. Timmermans, M.A. Cohen Stuart, W. Norde, Mobility of lysozyme inside oxidized starch polymer microgels, *Soft Matter*, 7 (2011) 1926-1935.
- [9] Y. Li, Z. Zhang, H.P. van Leeuwen, M.A. Cohen Stuart, W. Norde, J.M. Kleijn, Uptake and release kinetics of lysozyme in and from an oxidized starch polymer microgel, *Soft Matter*, DOI:10.1039/C1SM06072D
- [10] N.T. Mai, D.T. Giang, N.T.N. Minh, V.T. Thao, Thermophilic amylase-producing bacteria from vietnamese soils, *World Journal of Microbiology & Biotechnology*, 8 (1992) 505-508.
- [11] R.P. John, D. Gangadharan, K.M. Nampoothiri, Genome shuffling of *Lactobacillus delbrueckii* mutant and *Bacillus amyloliquefaciens* through protoplasmic fusion for L-lactic acid production from starchy wastes, *Bioresource Technology*, 99 (2008) 8008-8015.
- [12] C. Meenakshi, K. Narender, A. Vikrant, S. Karupothula, B. Shobhana, S. Sushma, Detection of Alpha - Amylase Producing Bacteria (*Bacillus sp.* 5250) from soil: Isolation and Optimization of Various Conditions of Growth, *Research Journal of Biotechnology*, 4 (2009) 50-56.
- [13] P. Joyet, M. Guéneau, H. Heslot, Cloning of a thermostable [alpha]-amylase gene from *Bacillus licheniformis* and its expression in *Escherichia coli* and *Bacillus subtilis*, *FEMS Microbiology Letters*, 21 (1984) 353-358.
- [14] C. Vishnu, G. Seenayya, G. Reddy, Direct conversion of starch to L(+) lactic acid by amylase producing *Lactobacillus amylophilus* GV6, *Bioprocess Engineering*, 23 (2000) 155-158.
- [15] A. Salam, J.J. Pawlak, R.A. Venditti, K. El-tahlawy, Synthesis and Characterization of Starch Citrate-Chitosan Foam with Superior Water and Saline Absorbance Properties, *Biomacromolecules*, 11 (2010) 1453-1459.
- [16] G.F. Mehyar, Z.Q. Liu, J.H. Han, Dynamics of antimicrobial hydrogels in physiological saline, *Carbohydrate Polymers*, 74 (2008) 92-98.

- [17] M.H. Ofman, C.A. Campos, L.N. Gerschenson, Effect of preservatives on the functional properties of tapioca starch: analysis of interactions, *Lebensmittel-Wissenschaft Und-Technologie-Food Science and Technology*, 37 (2004) 355-361.
- [18] S. Nam, M.G. Scanlon, J.H. Han, M.S. Izydorczyk, Extrusion of pea starch containing lysozyme and determination of antimicrobial activity, *Journal of Food Science*, 72 (2007) E477-E484.
- [19] B. Masschalck, D. Deckers, C.W. Michiels, Lytic and nonlytic mechanism of inactivation of gram-positive bacteria by lysozyme under atmospheric and high hydrostatic pressure, *Journal of Food Protection*, 65 (2002) 1916-1923.
- [20] H.M.W.M. Thijssen, R. C. ;Timmermans, J. W. ;Van Veen, J. J. F. , Inducible release vehicles, Eur.Patent EP1628529, 2006.
- [21] A.E.J. De Nooy, A.C. Besemer, H. vanBekkum, Highly selective nitroxyl radical-mediated oxidation of primary alcohol groups in water-soluble glucans *Carbohydrate Research*, 269 (1995) 89-98.
- [22] A.E.J. De Nooy, Selective Oxidation of Primary Alcohol Groups in Polysaccharides, Technical University of Delft, Delft, The Netherlands, 1997.
- [23] Z.Y. Meng, G.R. Hendrickson, L.A. Lyon, Simultaneous Orthogonal Chemoligations on Multiresponsive Microgels, *Macromolecules*, 42 (2009) 7664-7669.
- [24] G.R. Hendrickson, L.A. Lyon, Bioresponsive hydrogels for sensing applications, *Soft Matter*, 5 (2009) 29-35.
- [25] G.R. Hendrickson, M.H. Smith, A.B. South, L.A. Lyon, Design of Multiresponsive Hydrogel Particles and Assemblies, *Adv. Funct. Mater.*, 20 (2010) 1697-1712.
- [26] L. Hovgaard, H. Brøndsted, Dextran hydrogels for colon-specific drug-delivery, *Journal of Control. Release*, 36 (1995) 159-166.

## Appendix

### *Medium composition*

#### **Brain Heart Infusion (BHI) ( 1 L)**

Calf Brains, Infusion from	200gm	7.7gm
Beef Heart, Infusion from	250gm	9.8gm
Protease peptone		10.0gm
Dextrose		2.0gm
Sodium Chloride		3.0gm
Disodium phosphate		2.5gm
pH		7.4± 0.2

#### **Nutrient Broth (NB) ( 1 L)**

Lab Lemco powder	1.0gm
Yeast Extract	2.0gm
Sodium Chloride	3.0gm
pH	7.4± 0.2

#### **Nutrient Agar (NA) ( 1 L)**

Lab Lemco powder	1.0gm
Yeast Extract	2.0gm
Sodium Chloride	3.0gm
Agar	15.0gm
pH	7.4± 0.2



### Screening of amylase-producing bacteria

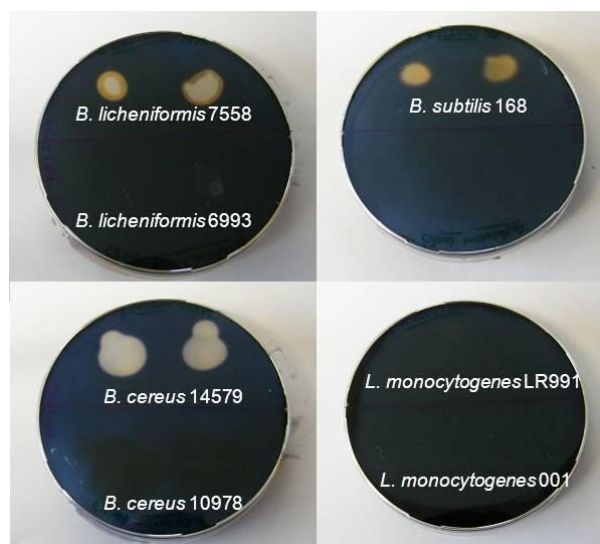


Figure A6.1. Amylase production assay by bacterial strains on starch agar plates by iodine test. If the starch is degraded by bacteria amylase, it will show a yellow spot around the bacteria colonies after pouring iodine solution into the plates. The iodine test was performed after incubating bacteria on a starch medium for 24 hours at 30 °C.

### Screening of lysozyme-sensitivity bacteria

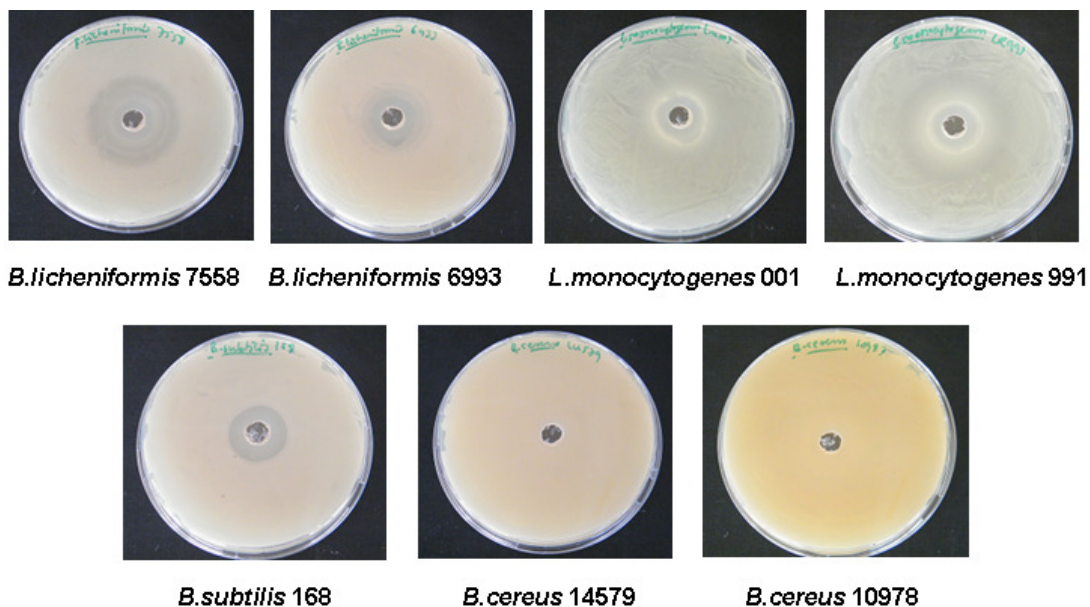


Figure A6.2. Lysozyme sensitivity test by growing bacterial strains on BHI-Agar plates with 200  $\mu$ L 50 mg/mL lysozyme solution added in the hole. The inhibition zone around the hole shows that bacteria were killed. The photos were taken after 24 hours of incubation at 30 °C.



---

# Chapter 7

## The stabilization of lysozyme-loaded starch microgel by polyelectrolytes

---

### *Abstract*

In this chapter the addition of biocompatible polyelectrolytes (chargeable polyamino acids) to oxidized starch microgel particles has been studied. The aim was to form a polyelectrolyte complex layer at the outer shell of the microgel particles to slow down the release of functional ingredients from the gel and make this process less sensitive to salt. Firstly, the distribution of positively charged poly-L-lysine (PLL) of two different molecular weights ('small', 15-30 kDa, and 'large', 30-70 kDa) in the negatively charged gel particles was measured. The small PLL distributes homogenously throughout the gel particles, but the large PLL forms a shell, i.e., its concentration at the outer layer of the particles was found to be much higher than in their core. This shell formation does not occur at a relatively high salt concentration (0.07 M). The large PLL was selected for further study. Unexpectedly, it was found that upon addition of PLL to lysozyme-loaded gel particles, the protein is exchanged by PLL. The exchange rate increases with increasing pH, in line with the increasing electrostatic attraction between the gel and the polyelectrolyte. Therefore, it was decided to use also a negatively charged polyamino acid, poly-L-glutamic acid (PGA) to form together with PLL a stable polyelectrolyte complex shell around the gel particles. This approach turned out to be successful and the PLL/PGA complex layer effectively slows down the release of lysozyme from the microgel particles at 0.05 M salt. In addition, it was found that the PLL/PGA layer protects the gel particle from degradation by  $\alpha$ -amylase.

Submitted for publication: Y. Li, W. Norde, M.A. Cohen Stuart, J.M.Kleijn, The stabilization of lysozyme-loaded starch microgel by polyelectrolytes

## 7.1 Introduction

In the field of advanced delivery systems for controlled uptake and release, there is a growing need for devices that can deliver their loaded ingredients in a well-tailored time-controlled fashion. Nowadays, most researchers focus on designing carrier systems, without paying sufficient attention to optimizing and controlling the release rate of the enclosed substances from the carriers.

In Chapters 2-6 [1-4], we reported on a biodegradable microgel (diameter 10-20  $\mu\text{m}$ ) based on natural starch polymer. The microgel consists of covalently cross-linked negatively charged polymers, which interact with positively charged functional ingredients (e.g. lysozyme) through electrostatic interaction. It was shown that release of lysozyme from the gel can be triggered by increasing the pH and/or salt concentration [3]. The release kinetics at various salt concentrations shows that the protein is fully released within an hour at a NaCl concentration as low as 0.035 M. The salt sensitivity of the starch gel particles is considered quite high, and the time scale for release is too short to meet the requirement in most applications. Deposition of a layer of polyelectrolytes around the microgel particle may be an effective approach to decrease the rate of lysozyme release.

The layer-by-layer (LbL) stepwise electrostatic assembly of oppositely charged species is nowadays a useful approach to coat substrates and to make well-defined architectures. Various kinds of charged species, for example, polyelectrolytes [5], nanoparticles [6], nanotubes [7] and lipids [8] have been used to build LbL structures. Polyelectrolytes are widely used to build LbL layers. Some polyelectrolytes made of polyamino-acids, i.e., poly (l-lysine) (PLL), poly (l-glutamic acid) (PGA), and natural polyelectrolytes (e.g., hyaluronan (HA), alginate, chitosan, collagen) allow, for example, to create biomimetic architectures [9-12].

The aim of this study is to evaluate the possibilities to create a polyelectrolyte complex layer on the surface of the starch microgel particles, in order to modulate the release of lysozyme from the particles. Firstly, we applied only positively charged poly-L-lysine (PLL) of two different molecular weights, which can form complexes with the starch gel and observed how these molecules distribute inside the microgel particles. Secondly, we investigated the uptake of PLL by the starch gel at various pH values and salt concentrations with and without preloading the gel with lysozyme. Finally, we immobilized the PLL at the outer layer of the gel particles by adding poly-L-glutamic acid (PGA) just after the addition of PLL to the gel particles; in this way a PLL/PGA complex layer was formed at the surface of

the microgel particles. The effect of such a complex layer on the release kinetics of lysozyme from the gel particle by salt and  $\alpha$ -amylase has been monitored.

## **7.2 Material and Methods**

### ***Materials***

Spherical microgel particles (diameter 10 - 20  $\mu\text{m}$ ) of cross-linked oxidized starch polymer were synthesized by inverse emulsion polymerization. For details on the oxidation of the starch polymers and preparation of the microgel particles we refer to Li et al. [1, 3] (Chapters 3 and 4 of this thesis). Lysozyme (from chicken egg white,  $M_w = 14,400$  g/mole), FITC-labeled poly-L-lysine (15-30 kDa and 30-70 kDa), and poly-L-glutamic acid (50 kDa) were supplied by Sigma-Aldrich. Lysozyme was labeled using an Alexa Fluor<sup>®</sup>594 protein labeling kit (Invitrogen). Heat-stable  $\alpha$ -amylase (Termamyl<sup>®</sup> 120L, Type L, activity 120 KNU/g) was purchased from Novo Nordisk. Solutions were prepared using Millipore water with a specific resistance of 18.3 M $\Omega$ /cm. All experiments were performed at room temperature.

### ***Fluorescence confocal laser scanning microscopy***

A confocal microscope (Carl Zeiss Axiovert 200 microscope, Zeiss, Germany) equipped with an LSM 5 Exciter configuration, a 40 $\times$ /0.60 objective, an Argon laser set at 488 nm and a He-Ne laser at 543 nm were used. Measurements were performed in a flow cell (Ibidi, Germany).

In a number of experiments gel particles were fixed at the flow cell surface to be able to observe the same particle(s) during the measurements. For this the negatively charged cell surface was coated with positively charged (non-labeled) poly-lysine by absorption from a 0.1% poly-lysine (PLL) solution (150 kDa, from Sigma-Aldrich) in water for two hours. Subsequently, unabsorbed poly-lysine was flushed away and a dispersion of negatively charged microgel particles in water was added for attachment to the surface. After one hour unattached gel particles were rinsed out of the cell.

### ***Interaction of poly-lysine and microgel as a function of salt concentration***

Dispersions of starch microgel particles were mixed with 25  $\mu\text{g/mL}$  FITC-labeled poly-lysine solutions having different molar mass distributions, i.e., 15-30 kDa (denoted as ‘small’) and 30-70 kDa (denoted as ‘large’) and of different salt concentration (0 - 0.5 M NaCl). 2D images were taken after 2 hours of equilibration.

### ***Re-swelling of PLL containing gel particles by increasing the salt concentration***

FITC-labeled PLL containing microgel particles were fixed on the surface of the flow cell and were flushed with NaCl solutions of increasing salt concentration (from 0 to 2 M NaCl). For each salt concentration 2D images of the particles were taken after reaching equilibrium.

### ***Poly-lysine uptake kinetics by empty gel particles***

One gel particle attached to the flow cell surface was brought into focus. Then 100  $\mu$ L of an FITC-labeled poly-lysine solution (25  $\mu$ g/mL) was added to the cell and the PLL uptake was monitored. (Recording of fluorescence images, 0.5 s/image, was already started before adding the labeled PLL to observe the kinetics from the very beginning.) Uptake kinetics was determined at pH 3 and 7 (at 0.01 M ionic strength) and at different NaCl concentrations (0 and 0.10 M) at a pH value of about 6 (unbuffered).

### ***Poly-lysine uptake by lysozyme-loaded gel particles***

Starch gel particles were saturated with Alexa Fluor 594-labeled lysozyme. After removing the unabsorbed lysozyme, 25  $\mu$ g/mL FITC-labeled PLL (30-70 kDa) was added into the cell at pH 3 and 7 (at 0.01 M ionic strength). Both the fluorescence intensities of the labeled protein and PLL were measured continuously.

### ***Deposition of a poly-lysine/poly-glutamic acid complex layer around the microgel***

Lysozyme containing starch gel particles were fixed on the flow cell surface, whereafter 100  $\mu$ L 50  $\mu$ g/mL FITC-PLL (30-70 kDa) was supplied to the flow cell. Fluorescence intensity of both lysozyme (orange) and PLL/PGA layer (green) were measured in real time. After 20 seconds a PLL layer appeared around the gel-lysozyme particle; then, 100  $\mu$ L of a 50  $\mu$ g/mL poly-glutamic acid solution was added into the cell. The PLL/PGA layer coated gel-lysozyme particles were flushed with water for 2 hours to check their stability under dilution.

### ***Lysozyme release from PLL/PGA stabilized gel particles***

Uncoated and PLL/PGA complex coated gel-lysozyme particles were flushed with 50 mM NaCl solution and the fluorescence intensity of the lysozyme inside the gel was measured continuously to follow the protein release. For amylase-induced lysozyme release, 100  $\mu$ L 10 times diluted  $\alpha$ -amylase solution (activity 12 KNU/g) was added to the gel-lysozyme particles and the lysozyme fluorescence intensity was monitored.

## 7.3 Results and Discussion

### *Effect of the mass of poly-lysine on the interaction with starch microgel*

First of all, we studied the interaction between the starch gel and poly-lysine of two different molecular weight distributions, i.e., 15-30 kDa and 30-70 kDa.

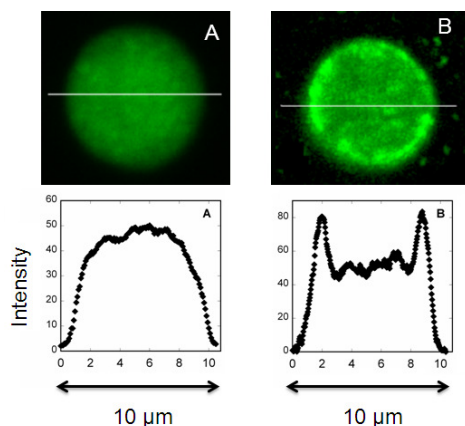


Figure 7.1. Distribution of poly-lysine in an oxidized starch microgel particle after 2 hours of absorption. (A) 'Small' PLL (15-30 kDa); (B) 'large' PLL (30-70 kDa). No salt added, pH about 7.

After mixing poly-lysine with starch gel in water, absorption of PLL was allowed to occur for 2 hours. As shown in Figure 7.1, the small PLL distributed more homogeneously across the gel particle than the large PLL. For the case of the large PLL, a layer with a higher intensity formed at the outside the microgel, reflecting a higher concentration, and a more diluted PLL phase appeared in the gel core. It suggests that the interaction of the large PLL with the microgel is much stronger than that of the smaller PLL, which causes some degree of quenching of the PLL position when it reaches the particle surface. It was found that upon absorption of PLL the microgel particles shrink. For the large PLL the degree of de-swelling is much more severe than for the small PLL. This may be due to strong binding which exerts a pressure on the gel particle, causing the gel particle to de-swell. The PLL in the shell slowly migrates to the centre of the gel particle: the shell becomes less pronounced overnight and disappears after two days. This behavior is in agreement with literature where it has been reported that a complex between poly-lysine and a slightly cross-linked poly (acrylic acid) hydrogel, which initially formed at the surface of the gel, propagated inward into the highly swollen core [13]. There, the core-shell formation was considered as a phase separation of concentrated cross-linked polymer and oppositely charge peptides at the particle-complex interface and a diluted phase of starch/poly-lysine complex in the gel core. Bysell et al. [14]

investigated the interaction between poly-lysine and a poly(acrylic acid) microgel; they also found that larger peptides concentrated in a surface layer around the gel particles, and that smaller ones evenly distributed throughout the microgel particles. Their interpretation was that high molecular weight PLL (170 kDa) is larger than the effective mesh size in the microgel particle, so that it is too large to penetrate through the entire gel. However, we found this conclusion only true for compact molecules like proteins that are not very flexible. In our study the large PLL has an average size (hydrodynamic radius) of around 25 nm, which strongly exceeds the pore size (pore diameter 4-25 nm) of our microgel, but it still can enter the gel. Flexible molecules like poly-lysine may adjust their shape upon entering the pores. Whether or not encapsulation takes place is determined by the balance of attraction between the ingredient and the gel, and the loss of conformation entropy due to the deformation.

To study the influence of ionic strength on interaction between microgel and PLL, PLL and gel particles were mixed at various salt concentrations for 2 hours. As demonstrated in Figure 7.2, for both sizes of PLL, the saturated gel particles aggregate when the salt concentration is above 0.1 M. For the large PLL, extensive clusters of gel-PLL particles occurred at 0.5 M NaCl. Probably this is due to bridging between gel-PLL particles. When their positive charges are screened by salt, the long tails of PLL may stretch out of the gel particles and form bridges between gel-PLL particles. For the small PLL, which is distributed homogeneously inside the gel particle at all salt concentrations, bridging is less likely to occur. It is observed in Figure 7.2 that shell formation does not occur for the large PLL at salt concentrations beyond 0.07 M. It seems that salt prevents PLL shell formation on the gel surface, by screening the electrostatic attraction, thus facilitating the diffusion of PLL into the gel. This might suppress the formation of bridges; on the other hand, bridging may occur immediately after mixing, before the long PLL chains have entered the particles completely. Bysell et al. [15] found that when the salt concentration is increased from 0.02 M to 0.2 M, the collapse of a microgel particle by high molecular weight PLL (170 kDa) is reduced.



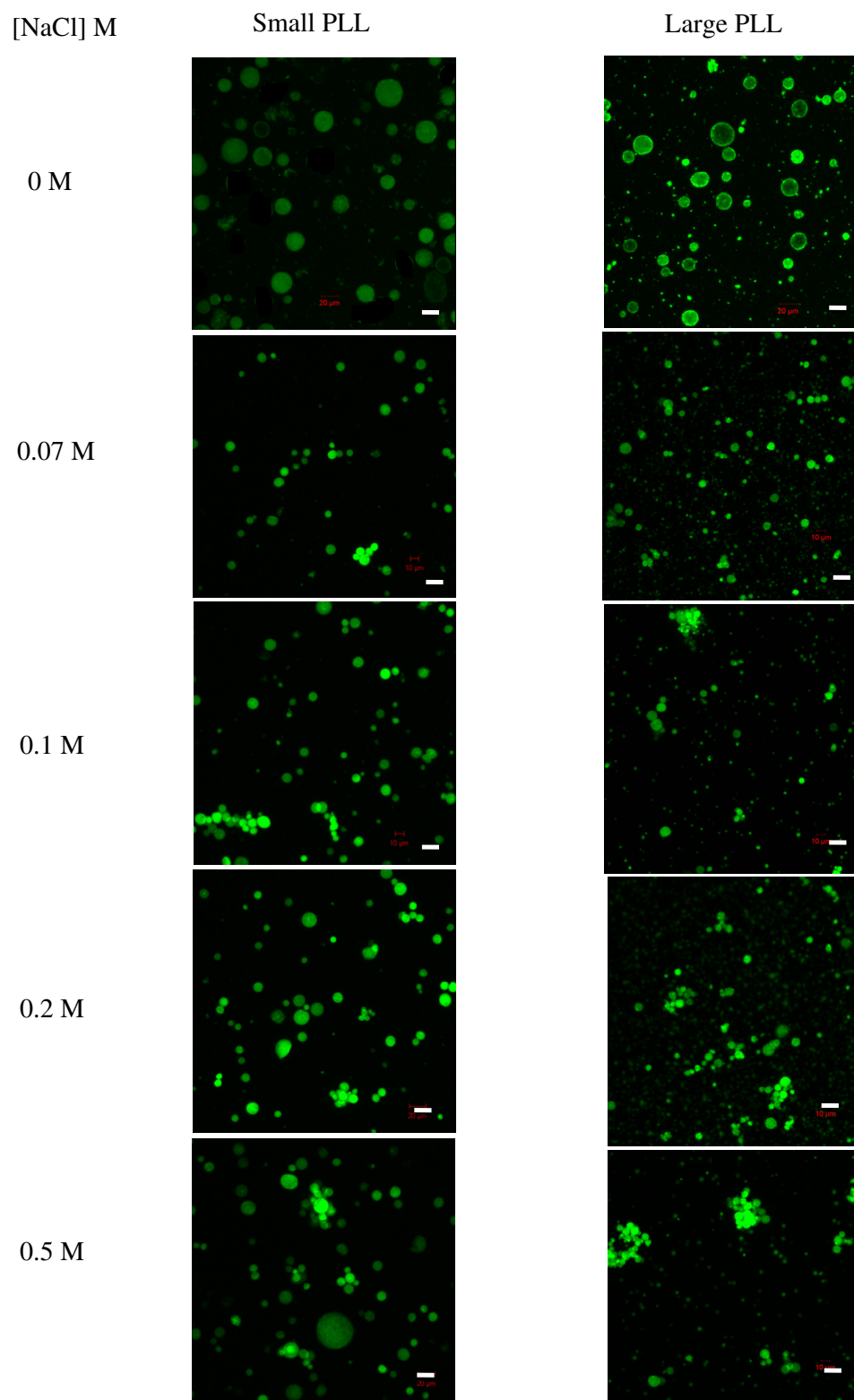


Figure 7.2. Fluorescence CLSM images of poly-lysine containing gel (gel-PLL) particles at various salt concentrations (0-0.5 M NaCl) for (left) small PLL (15-30 kDa) and (right) large PLL (30-70 kDa). The PLL and gel particles were equilibrated at each salt concentration for 2 hours. Scale bar = 20  $\mu\text{m}$ .

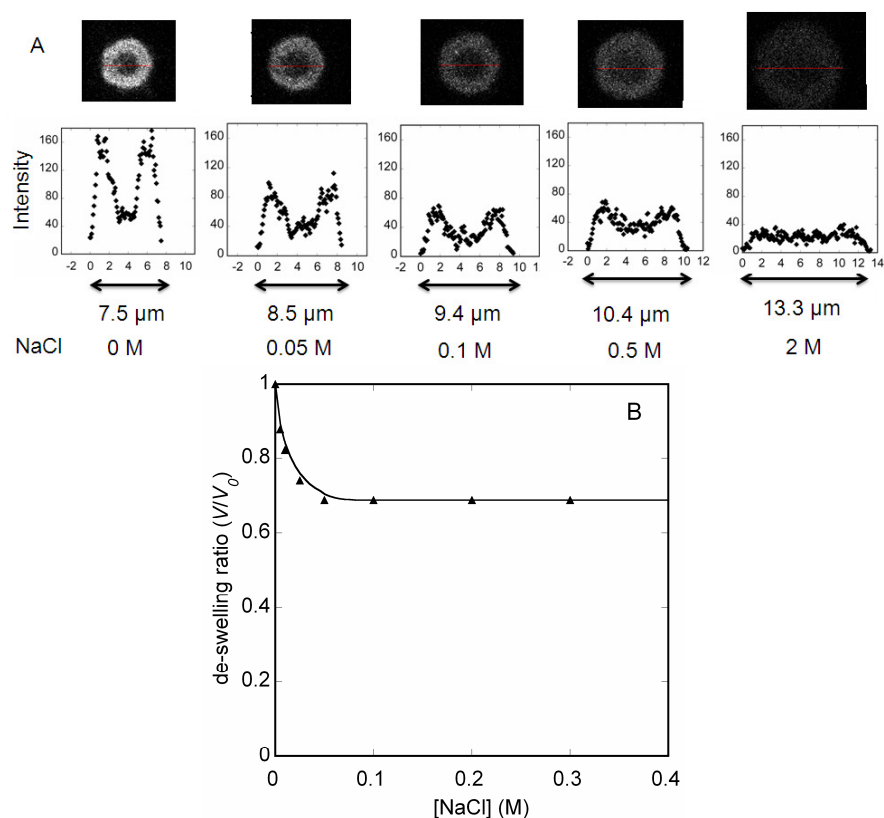


Figure 7.3. (A) Re-swelling of a gel-PLL particle (30-70kDa) by increasing the salt concentration from 0 M to 2 M, pH 7. The diameter ( $\mu\text{m}$ ) of the gel-PLL particle at the different NaCl concentrations is indicated in the figure. (B) De-swelling ratio of an empty gel particle as a function of NaCl concentration at pH 7.

In view of our previous studies [2, 3], where it was found that salt induces protein release from the gel by screening the electrostatic interaction between the two, it is expected that the interaction between PLL and gel is also weakened by increasing salt concentration. As shown in Figure 7.3A, at 0 M NaCl concentration a thick PLL (30-70 kDa) shell formed around the particle due to strong attraction. This gel-PLL particle was flushed with buffers of gradually increasing salt concentration (0 – 2 M). Figure 7.3A shows how the intensity of the PLL shell layer gradually decreases with increasing salt concentration with a concomitant re-swelling of the gel particle. Surprisingly, the gel-PLL particle re-swells rather than de-swells when the salt concentration is increased. The de-swelling ratio ( $V/V_0$ , with  $V$  the volume of the particle and  $V_0$  its volume at 0 M salt) of empty gel particles as a function of salt concentration is presented in Figure 7.3B; the empty gel particle shrinks by increasing the salt concentration and above 20 mM NaCl its volume remains constant. Apparently, the negative charges on the

gel are effectively screened at 20 mM NaCl solution and the gel particle behaves like being uncharged. In the first step of the measurements on the PLL loaded gel particle the salt concentration was increased to 50 mM, above which no further shrinkage of the (empty) gel particle occurs. However, salt still decreases the electrostatic attraction between gel and poly-lysine, causing release of PLL from the gel. The gel is relieved from the pressure exerted by the PLL and re-swells. Re-swelling at high salt concentration did not occur for small PLL, confirming that the interaction between small PLL and microgel is less strong.

### *Uptake of poly-lysine by lysozym-loaded microgel particles*

The above results indicate that PLL having the higher molar mass, 30-70 kDa, interacts more strongly with starch gel particles than the smaller PLL of 15-30 kDa, leading to the formation of a more or less quenched shell on the microgel surface. Such a layer may be able to slow down the release of lysozyme from the gel.

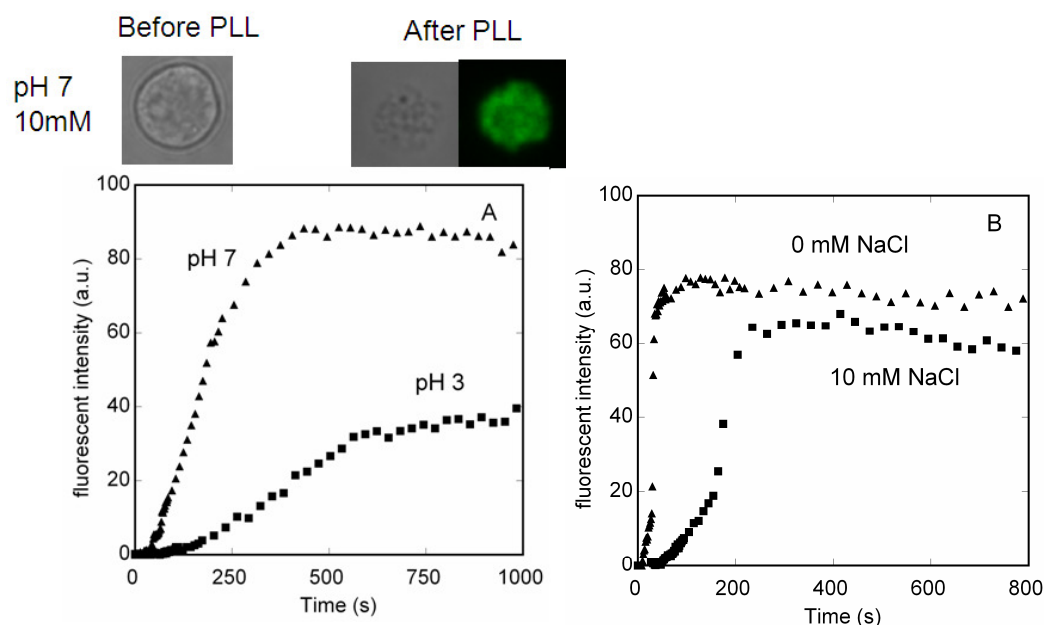


Figure 7.4. Fluorescence intensity of poly-lysine (30-70 kDa) in oxidized starch microgel as a function of time (A) at pH 3 and pH 7, ionic strength 10 mM; the average de-swelling ratio  $V/V_0$  at pH 7 is 60% and at pH 3 is 85%; (B) at pH 6, 0 M and 10 mM NaCl; the average de-swelling ratio for 0 M is 51% and for 10 mM is 70%.

The uptake kinetics of PLL in the gel particles was measured at two different pH values and two salt concentrations. As shown in Figure 7.4A, at 10 mM NaCl both the uptake rate

and uptake capacity for PLL of the starch gel are higher at pH 7 compared to pH 3. Chapter 3 [2] shows that the binding affinity between the gel and an oppositely charged species is primarily determined by the component with the lowest charge density. Compared to PLL (having a constant and high charge density at pH < 9 [14]), the gel is the most weakly charged species. The negative charge on the starch microgel increases with increasing pH. This explains why the uptake capacity and binding affinity is higher at pH 7 than at pH 3. For the same reason the PLL uptake by a poly (acrylic acid) (PAA) microgel was found to be higher at pH 7 than at pH 5.5 [14, 16]. The uptake rate of PLL at 0 M NaCl is much higher than that at 10 mM at pH 6, as shown in Figure 7.4B. This is mainly due to screening of the electrostatic interactions by the salt. In addition, the de-swelling ratio (volume after poly-lysine uptake/volume before poly-lysine uptake) seems strongly influenced by the binding strength of PLL to the gel: it de-swells more at conditions where PLL is more strongly attracted. (see Figure Caption of Fig.4)

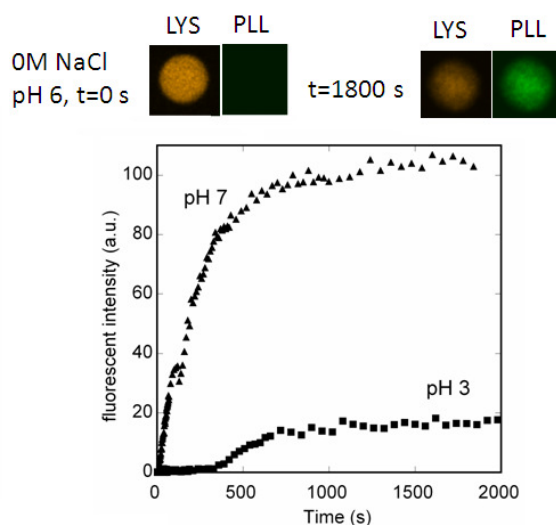


Figure 7.5. Exchange of fluorescently labeled poly-lysine (PLL; 30-70 kDa) (green) with lysozyme (LYS) (orange) preloaded in oxidized starch microgel. The graph shows the fluorescence intensity of PLL as a function of time at pH 3 and pH 7, and 10 mM ionic strength. The average de-swelling ratio  $V/V_0$  as a result of the exchange is 45% at pH 7 and 68% at pH 3.

Alexa Fluor 594-labeled lysozyme was preloaded inside microgel particles in a 10 mM NaCl solution. An FITC-labeled poly-lysine (30-70 kDa) solution was added to the suspension of the lysozyme-gel particles in order to build a PLL layer at the gel surface. However, it was found that the PLL exchanges with the lysozyme inside the gel rather than

building a stable layer around the gel particle. As shown in Figure 7.5, the exchange rate is higher at pH 7 than at pH 3, which is comparable to the poly-lysine uptake kinetics shown in Figure 7.4A. Like in the uptake experiments, the gel particle de-swells more at pH 7. Poly-lysine is a more highly charged and is a more flexible molecule than lysozyme. Therefore, it is able to enter the gel and exchange with the lysozyme. PLL shell formation does not occur; apparently in the presence of lysozyme the interaction between the less negatively charged gel-lysozyme particles and PLL is reduced and PLL is not trapped at the outer layer of the gel particles.

***Deposition of a poly-lysine/poly-glutamic acid complex layer around lysozyme-loaded gel particles***

From the results presented above, it is derived that PLL alone is not able to build a polyelectrolyte layer around lysozyme-loaded gel particles. However, complexing positively charged PLL with negatively charged poly-glutamic acid (PGA) may prevent PLL entering the gel particle. The PLL/PGA complexes were made by mixing equal concentrations of PLL and PGA of nearly equal molar mass, in order to reach a charge ratio of 1:1, which is found to be the optimum charge ratio for complex formation [17].

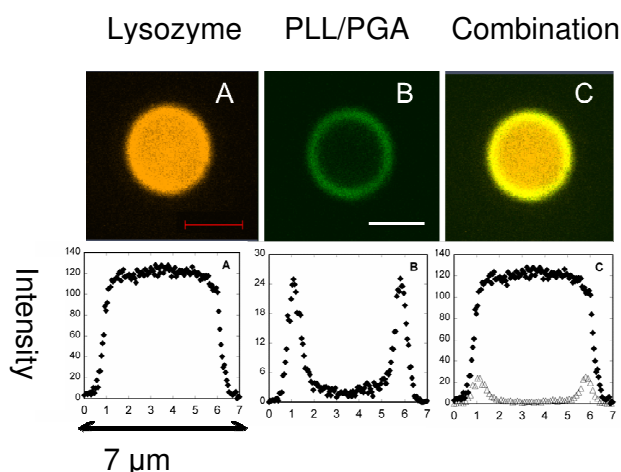


Figure 7.6. Deposition of a poly-lysine/poly-glutamic acid (PLL/PGA) layer on a lysozyme-loaded gel particle (pH 6, no salt added). Fluorescence 2D images and intensity profiles obtained from different channels are presented in (A) Alexa Fluor 594-labeled lysozyme distribution inside microgel, and (B) FITC-PLL/PGA complex layer distribution around microgel.(C) Combined image of (A) and (B). The scale bar represents 5 μm.

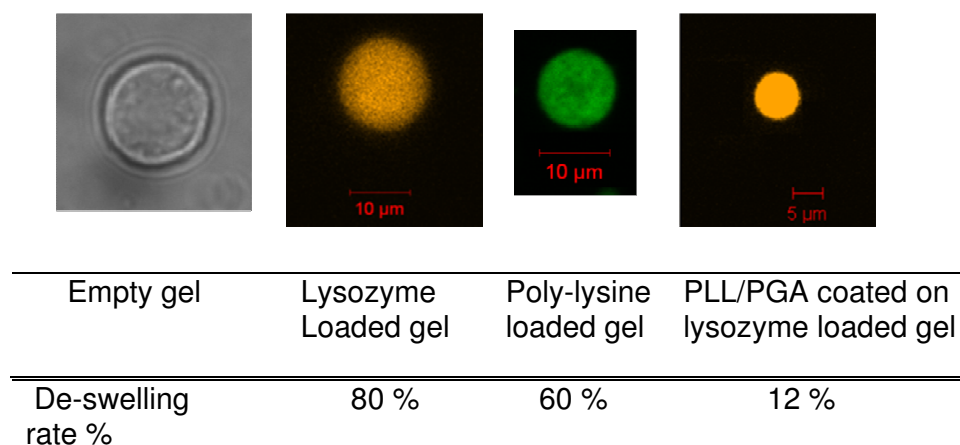


Figure 7.7. De-swelling ratio (volume after absorption/volume of empty gel particle) of a gel particle (1) after uptake of lysozyme and (2) after uptake of PLL, and (3) of a gel-lysozyme particle after deposition of a PLL/PGA layer.

Two different channels were used to simultaneously observe the Alexa Flour 594-labeled lysozyme (excitation wavelength 543 nm; fluorescence orange) and the FITC-PLL/PGA complexes (excitation wavelength 488 nm: fluorescence green): see Fig. 7.6. A gel particle was first saturated with lysozyme in water and subsequently 0.1 mg/mL poly-lysine (30-70 kDa) was added. A thin poly-lysine layer around the gel-lysozyme particle formed after 5 seconds. Immediately 0.1 mg/mL unlabeled poly-glutamic acid (50 kDa) was added to gel-lysozyme particle. Fig. 7.6A represents the image obtained from the 543 nm channel showing a homogeneous distribution of lysozyme throughout the gel particle coated with PLL/PGA complexes. Fig. 7.6B (488 nm channel) shows that the PLL/PGA complexes are accommodated in the outer layer of the particle. Fig. 7.6C gives the combined images. The PLL/PGA layer effectively prevents the migration of poly-lysine into the center of the gel particle. Upon flushing with water the fluorescence intensities of the complex layer and the lysozyme inside the gel remained constant for several hours (results not shown).

The starch gel is a soft polymer network containing nearly 90% water [1], so it tends to collapse when it absorbs substances that are electrostatically attracted to the network. The stronger the attraction, the more the particles shrink. As shown in Figure 7.7, the de-swelling ratio ( $V/V_0$ ) is 60% for poly-lysine absorption and 80% for lysozyme absorption. At the same pH and ionic strength, the charge density of PLL is higher than that of lysozyme. Therefore the interaction between PLL and the gel is stronger than that between lysozyme and the gel, leading to more de-swelling. Coating a lysozyme-loaded particle with PLL/PGA leads to a

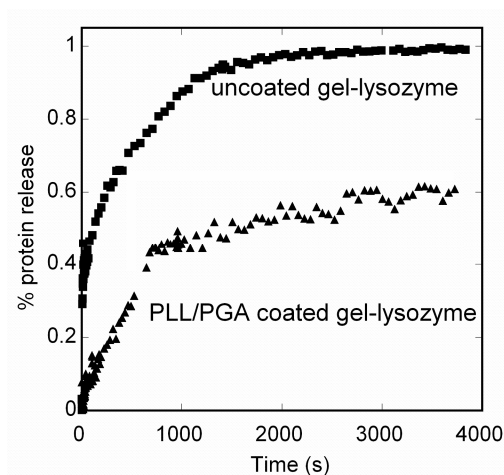


Figure 7.8. Release kinetics of lysozyme from starch gel at 50 mM NaCl for uncoated gel-lysozyme particles and PLL/PGA coated gel-lysozyme particles at pH 6.

very strong shrinkage of the particle to 12% of its original size of an empty gel particle. This may be caused by the formation a compact PLL/PGA complex, therewith contracting the PLL around the gel particle upon PGA addition.

Chanel A: Lysozyme    Chanel B: PLL/PGA

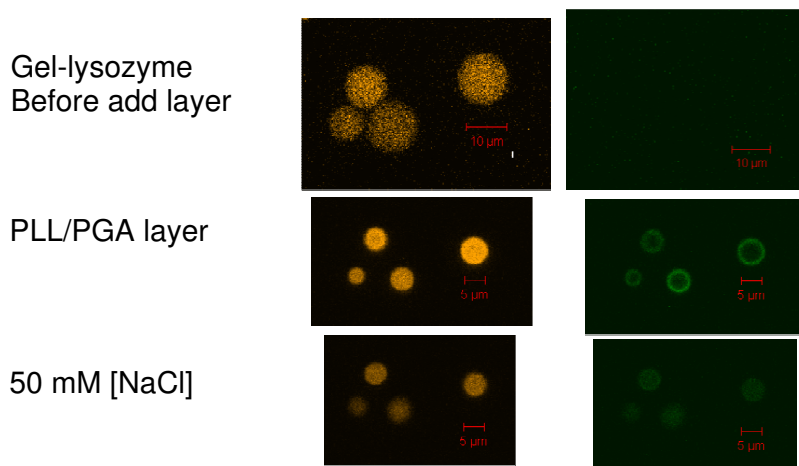


Figure 7.9. Fluorescence 2D images of PLL/PGA layers around lysozyme preloaded gel particles. The images are displayed in two channels, for lysozyme (orange, left) and for the PLL/PGA layer (green, right). The upper images are obtained from lysozyme saturated gel particles before PLL/PGA addition; the middle images show the same particles after coating with PLL/PGA; the lower images show the PLL/PGA layer coated gel-lysozyme particles after flushing with 50 mM NaCl for one hour.



As shown in Figure 7.8, the uncoated starch gel is salt sensitive and at 50 mM NaCl all the absorbed protein is released within one hour. This is unwanted in cases requiring slow and gradual release. However, after deposition of the PLL/PGA layer at the gel-lysozyme particle surface, the protein release is slowed down and after one hour 60% of the total absorbed protein is released.

Figure 7.9 displays the images of (1) lysozyme containing gel particles, (2) de-swelling of these gel-lysozyme particles after deposition of a PLL/PGA layer on their surface, and (3) the effect of adding 50 mM NaCl. The decrease in the green fluorescence intensity in 50 mM NaCl points to dissociation of the PLL/PGA layer, after which the lysozyme can be released. Thus, in this way the salt-induced release rate of protein from the gel is controlled by the rate of dissociation of the PLL/PGA complex. By carefully choosing the polyelectrolytes to form the shell on the gel particles, the stability of the polyelectrolyte complex with respect to salt concentration and pH and therefore the rate of release of the component from the gel can be tuned.

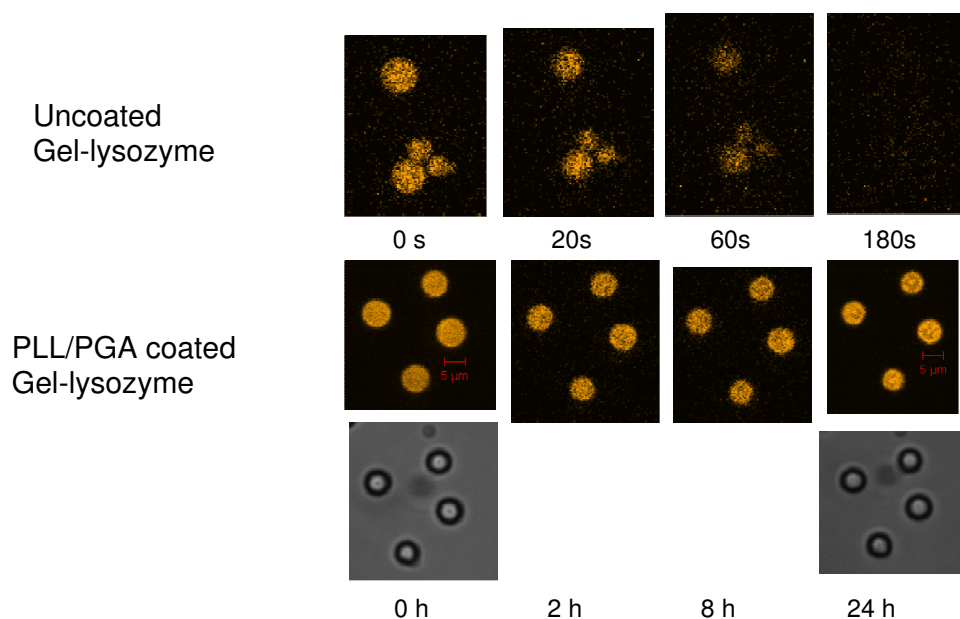


Figure 7.10. Fluorescence times series images of amylase-degradation of uncoated and PLL/PGA coated lysozyme-loaded gel particles. No salt is added at pH 7.



In Chapter 5, we demonstrated the degradation of the starch gel by  $\alpha$ -amylase after which lysozyme is set free. However, after deposition of a PLL/PGA layer, the gel-lysozyme particles become protected against amylase degradation for at least 24 hours, which is shown in Fig. 7.10. Probably, the PLL/PGA shell is too dense to be passed by  $\alpha$ -amylase, which is a larger protein (diameter 6 nm) than lysozyme. This is useful for applications where gel particles have to be protected from enzymatic degradation. Alternatively, by degradation of the starch core, for instance by using a smaller sized amylase that is able to penetrate the PLL/PGA layer or by applying a less dense polyelectrolyte complex, hollow capsules may be produced. Such capsules could be applied in drug delivery systems [18].

## 7.4 Concluding remarks

The aim of the study described in this chapter was to stabilize oxidized starch microgel particles by deposition of a (biocompatible) polyelectrolyte layer at their surface in such a way that the release of functional ingredients is slowed down and less sensitive to the salt concentration.

It was found that relatively small poly-L-lysine molecules (15-30 kDa) do not form a shell and readily distribute homogeneously throughout the microgel particles. Larger PLL molecules (30-70 kDa) do form a shell below salt concentrations of 0.07 M, although on a timescale of about a day they migrate to the core of the particles. Increasing the salt concentration causes bridging between the particles, leading to aggregation. Moreover, when applied to lysozyme-loaded gel particles, they do not form a shell at all and displace the lysozyme from the gel network. Therefore, it was concluded that complex formation between PLL and the gel network is not sufficient to form a stable shell layer that serves our purpose.

Adding a second polyelectrolyte, i.e. negatively charged poly-L-glutamic acid (50 kDa), just after addition of the positively charged PLL (30-70 kDa) to the lysozyme-loaded gel particles, was found to be a successful approach. The results show that a stable PLL/PGA layer is formed on the gel surface. The release of lysozyme from the PLL/PGA coated microgel at 0.05 M salt is effectively slowed down. In fact, the release as a function of salt concentration seems to be determined by the stability of the polyelectrolyte complex. Therefore the release kinetics of functional ingredients from the starch gel as a function of pH and salt concentration may be tuned by choosing specific polyelectrolytes to form the shell on the gel particles.

Furthermore it was found that after PLL/PGA layer deposition the gel particles are protected against enzymatic degradation.

## References

- [1] Y. Li, R. de Vries, T. Slaghek, J. Timmermans, M.A. Cohen Stuart, W. Norde, Preparation and Characterization of Oxidized Starch Polymer Microgels for Encapsulation and Controlled Release of Functional Ingredients, *Biomacromolecules*, 10 (2009) 1931-1938.
- [2] Y. Li, R. de Vries, J.M. Kleijn, T. Slaghek, J. Timmermans, M.A. Cohen Stuart, W. Norde, Lysozyme Uptake by Oxidized Starch Polymer Microgels, *Biomacromolecules*, 11 (2010) 1754-1762.
- [3] Y. Li, J.M. Kleijn, T. Slaghek, J. Timmermans, M.A. Cohen Stuart, W. Norde, Mobility of lysozyme inside oxidized starch polymer microgels, *Soft Matter*, 7 (2011) 1926-1935.
- [4] Y. Li, Z. Zhang, H.P. van Leeuwen, M.A. Cohen Stuart, W. Norde, J.M. Kleijn, Uptake and release kinetics of lysozyme in and from an oxidized starch polymer microgel, *Soft Matter*, DOI:10.1039/C1SM06072D
- [5] K.H. Kyung, S. Shiratori, Nanoscale Texture Control of Polyelectrolyte Multilayer Using Spray Layer-by-Layer Method, *Jpn. J. Appl. Phys.*, 50 (2011).
- [6] G. Machado, A.F. Feil, P. Migowski, L. Rossi, M. Giovanela, J.D. Crespo, L. Miotti, M.A. Sortica, P.L. Grande, M.B. Pereira, R.R.B. Correia, Structural control of gold nanoparticles self-assemblies by layer-by-layer process, *Nanoscale*, 3 (2011) 1717-1723.
- [7] D. Lee, T.J. Cui, Layer-by-Layer Self-Assembly of Single-Walled Carbon Nanotubes with Amine-Functionalized Weak Polyelectrolytes for Electrochemically Tunable pH Sensitivity, *Langmuir*, 27 (2011) 3348-3354.
- [8] S. Moya, E. Donath, G.B. Sukhorukov, M. Auch, H. Baumler, H. Lichtenfeld, H. Mohwald, Lipid coating on polyelectrolyte surface modified colloidal particles and polyelectrolyte capsules, *Macromolecules*, 33 (2000) 4538-4544.
- [9] M. Dimitrova, Y. Arntz, P. Lavalle, F. Meyer, M. Wolf, C. Schuster, Y. Haikel, J.C. Voegel, J. Ogier, Adenoviral gene delivery from multilayered polyelectrolyte architectures, *Adv. Funct. Mater.*, 17 (2007) 233-245.
- [10] M.C. Du, W.X. Song, Y. Cui, Y. Yang, J.B. Li, Fabrication and biological application of nano-hydroxyapatite (nHA)/alginate (ALG) hydrogel as scaffolds, *J. Mater. Chem.*, 21 (2011) 2228-2236.
- [11] T. Imoto, T. Kida, M. Matsusaki, M. Akashi, Preparation and Unique pH-Responsive Properties of Novel Biodegradable Nanocapsules Composed of Poly( $\gamma$ -glutamic acid) and Chitosan as Weak Polyelectrolytes, *Macromol. Biosci.*, 10 (2010) 271-277.
- [12] S. Boddohi, J. Almodovar, H. Zhang, P.A. Johnson, M.J. Kipper, Layer-by-layer assembly of polysaccharide-based nanostructured surfaces containing polyelectrolyte complex nanoparticles, *Colloid Surf. B-Biointerfaces*, 77 (2010) 60-68.
- [13] V.A. Kabanov, V.B. Skobeleva, V.B. Rogacheva, A.B. Zezin, Sorption of proteins by slightly cross-linked polyelectrolyte hydrogels: Kinetics and mechanism, *J. Phys. Chem. B*, 108 (2004) 1485-1490.
- [14] H. Bysell, M. Malmsten, Visualizing the interaction between poly-L-lysine and poly(acrylic acid) microgels using microscopy techniques: Effect of electrostatics and peptide size, *Langmuir*, 22 (2006) 5476-5484.
- [15] H. Bysell, P. Hansson, M. Malmsten, Transport of poly-L-lysine into oppositely charged poly(acrylic acid) microgels and its effect on gel deswelling, *J. Colloid Interface Sci.*, 323 (2008) 60-69.
- [16] H. Bysell, M. Malmsten, Interactions between Homopolypeptides and Lightly Cross-Linked Microgels, *Langmuir*, 25 (2009) 522-528.

- [17] F. Weinbreck, R.H. Tromp, C.G. de Kruif, Composition and structure of whey protein/gum arabic coacervates, *Biomacromolecules*, 5 (2004) 1437-1445.
- [18] B.G. De Geest, C. Dejumat, M. Prevot, G.B. Sukhorukov, J. Demeester, S.C. De Smedt, Self-rupturing and hollow microcapsules prepared from bio-polyelectrolyte-coated microgels, *Advanced Functional Materials*, 17 (2007) 531-537.



---

# Chapter 8

## General discussion

---

This chapter deals with answering the following questions: What did I learn during this investigation? How does my work contribute to the knowledge on protein-polymer gel interaction? What aspects need to be improved? What is the application perspective?

## 8.1 What did I learn during this investigation?

The aim of this research is to clarify the mechanism of the interaction between negatively charged starch microgels and oppositely charged proteins (lysozyme) at various environmental conditions to control the effects of pH, salt concentration and amylase degradation on protein uptake and release. A preparation method for spherical microgel particles with a narrow size distribution is useful for producing well-defined microgels. Relevant physical-chemical properties of various gels can be tuned for different applications. For example, oxidized starch microgels having degrees of oxidation (DO) of 30% and 50%, which are amylase-degradable, can be used in applications that require the degradation of the gel; in highly oxidized starch gels (DO70%, DO100%) encapsulated ingredients are protected from enzymatic degradation, but their release from the gel may be triggered by high pH or high salt concentration. Neutral pH and low salt concentration are considered optimum uptake conditions and are applicable for all positively charged ingredients. Releasing incorporated ingredients with high binding affinity is extremely difficult, due to restricted mobility of these molecules inside the microgel particle. Any trigger such as high pH and high salt concentration that shifts the mobility distribution towards more mobile fractions, drives the release of encapsulated ingredients.

Some aspects are still unclear, in particular with respect to the effect of the degree of oxidation of the microgel. It was found that highly oxidized starch microgel (e.g., DO100%) has a relatively low swelling capacity. This indicates that highly oxidized starch polymers are cross-linked more efficiently than slightly oxidized starch polymer, even though the cross-linker sodium trimetaphosphate (STMP) mainly reacts with the primary alcohol groups on the starch, i.e., amylose. Slightly oxidized starch gels (e.g., DO30%) contain starch polymer with more remaining primary alcohol groups, which are supposed to build more cross-links and, hence, result in a high cross-link density. However, the results show the opposite. This may be due to a surplus of active primary alcohol groups, leading to side reactions such as substitution rather than cross-linking. Organic chemistry would be a useful tool for further studying this aspect. In addition, it was not possible to make spherical microgel particles with the DO100% polymer by the same inverse-emulsion polymerization method used for making spherical DO30% microgels.

## **8.2 How does my work contribute to the knowledge on protein-polymer gel interaction?**

This dissertation contributes to the knowledge of the interaction between negatively charged cross-linked polymer (e.g., natural polysaccharides used in our experiments) and oppositely charged ingredients (e.g. proteins). Although the potato starch polymer, used in our experiments, is not well-defined compared to most synthetic polymers, the results show that it is very well possible to have good control over the physical- chemical properties of the microgels made of this polymer. Below are some aspects which are important for controlling the (protein) uptake and release properties of the cross-linked polymer gel.

### ***Prerequisites for encapsulated ingredients***

The different ingredients that were successfully incorporated into the negatively charged starch microgel are positively charged proteins (lysozyme, myoglobin,  $\alpha$ -lactalbumin and bovine serum albumin), peptides like poly-lysine (three different sizes: 30, 50, 150 kDa), and the neutral polymer dextran (size ranges 4 - 250 kDa). The prerequisites for the ingredients to be loaded into starch microgel are the following. First of all, they should be hydrophilic, since the gel is hydrophilic. For instance, the polycyclic antimicrobial peptide Nisin could not be incorporated into the starch gel, because Nisin is a quite hydrophobic molecule. Secondly, the size of the ingredients to be encapsulated is crucial. For compact molecules that are hard to deform, such as globular proteins, the size should be smaller than the pore size of the gel. Flexible molecules may adjust their shape upon entering the pores; hence, even though their size (e.g., hydrodynamic radius) is larger than the gel pores they may be absorbed by the gel. More precisely, whether or not encapsulation takes place is determined by the balance of attraction between the ingredient and the gel and the loss of conformation entropy due to the deformation. Most importantly, for charged ingredients, a pH far below their pI and a low ionic strength is preferred to ensure strong electrostatic attraction. For non-charged ingredients, a high pH and a low ionic strength are more favourable since the gel tends to collapse at low pH and high ionic strength.

### ***Interaction between starch microgel and oppositely charged proteins/peptides***

This dissertation focuses on the interaction between a starch gel and an oppositely charged protein, i.e., lysozyme. In addition, interactions between the gel and oppositely charged poly-lysine molecules have been studied as well. For these systems it is shown that the main driving force for encapsulation is the electrostatic interaction between

proteins/peptides and gel. The binding affinity, protein uptake capacity and de-swelling rate are the main aspects we investigated. First of all, the binding affinity is controlled by the charge density of both the protein and the gel, being mainly determined by the most weakly charged species of the two. For instance, for interaction between lysozyme and gel the binding affinity is high at low pH, since lysozyme is the most weakly charged compound; for interaction between poly-lysine and gel the affinity is high at high pH because the gel is the most weakly charged species. In case of a fixed charged density on the gel, the binding affinity is higher for the ingredient that has a higher charge density. Thus, the affinity for poly-lysine is higher than for lysozyme because poly-lysine is more positively charged. The binding affinity is a very important parameter since high affinity implies low mobility of enclosed molecules inside the gel. Any condition that decreases the binding affinity may trigger the release of the incorporated substance from the gel particles. Secondly, the protein uptake capacity (i.e., saturation absorbance) is mainly determined by the charge stoichiometry. The uptake capacity reaches a maximum at conditions where the charge ratio between gel and lysozyme is 1:1. Lastly, the de-swelling of the microgel as result of the uptake of lysozyme is found to be closely related to the binding strength. The gel shrinks more when the interaction is stronger. For example, it de-swells more at pH 3 than pH 7. The strong binding of protein causes the gel network to shrink. It has been reported in literature that protein-gel interaction results in a weakly swollen shell and a highly swollen core of the protein-gel complex. We also found initial binding of protein in the outer part of the gel particles, but subsequent diffusion into the gel leads to a homogeneous distribution of the protein in the gel. Only in case of interaction with highly charged poly-lysine we observed permanent absorption in the outer gel layer. It suggests that shrinkage of the gel due to uptake of the oppositely charged compound determines further transport into the gel. In turn, the tendency to shrink decreases with increasing mechanical strength of the gel.

### **8.3 What aspects need to be improved?**

Many aspects need to be improved in order to reach real applications. A disadvantage of the DO30% gel is its high salt sensitivity. Our study shows that incorporated lysozyme is released within one hour at 25 mM NaCl. However, the ionic strength in most practical systems, like food, biofluids etc, is often higher. Therefore, decreasing the salt sensitivity and slowing down the speed of release are necessary to improve the system.

Deposition of a polyelectrolyte complex on the surface of the protein-load microgel particle may add a useful feature to these systems. Our preliminary experiments have shown



that one single layer of poly-l-lysine/poly-l-glutamic acid effectively slows down the rate of salt-induced release of lysozyme from microgel. Besides, it prevents the DO30% gel from being degraded by amylase. Hence, incorporated ingredients are protected in a (microbial) amylase containing environment.

Another aspect that could be improved is downscaling of the gels: monodisperse nanogels are of interest for pharmaceutical application, because nano-sized particles may be taken up by cells. The uptake and release processes are easily controlled for monodisperse gel particles. Of course, the toxicity of oxidized starch gel should be checked beforehand.

Linkage of a functional group to the starch gel can provide the gel with multi-functionality. For example, folic acid (recognizes cancer cells) can be covalently bound to the carboxyl groups of starch by a di-amine linker. This provides the gel a targeting function. Furthermore, photodegradable polymers may be included in the gel, allowing a light-switchable gel structure transition by which uptake and release of functional ingredients may be tuned.

## **8.4 What would be the application perspectives?**

As we know from the amylase degradation experiment, DO30% and DO50% polymer gels are degradable, DO70% is slightly degradable, and DO100% is non-degradable. Therefore, we can use DO30% and DO50% microgels for applications requiring substances to be released by enzymatic degradation (e.g. antimicrobial particles or digestion in human body fluid). DO70% and DO100% microgels are suitable for applications requiring high stability, and the ingredients enclosed can be protected from enzymatic degradation, but released by a salt and/or pH shock.

The swelling capacity of the various gels varies significantly. Highly swellable DO30% gels with the lowest cross-link density are able to absorb 100 times their weight in the form of water. They may be used as a hygrometer. The humidity of the air may be calculated from the amount of water absorbed by the gel. Further application could be delivery of water to plants in arid areas. The water in the gel is protected against evaporation and drainage into the soil but the capillary action in the plant roots may be able to extract the water from the gel.

The gel could also be used as a “taste masker” for food or medicine. Some ingredients, e.g., medical peptides, have an undesirable bitter taste. As these peptides are positively charged they can be readily absorbed by starch gel, thus masking the bitter flavour.



---

# Summary

---

This dissertation describes a systematic study on oxidized starch microgel particles. It begins with the preparation and characterization of oxidized starch gels in terms of some important physical-chemical properties, with the aim to select an optimum gel for further investigation of protein uptake. The gel with the highest degree of oxidation DO100% is chosen for lysozyme uptake because of its high protein uptake capacity and low swelling capacity. In addition, DO30% gels have been used in many experiments, since DO30% starch allows for preparation of well-defined spherical microgel particles and because it is enzymatically degradable. The two main aspects of interest are the protein binding affinity and protein saturation. Neutral pH and low salt concentration are found to be the optimum protein uptake conditions for high protein saturation.

For more detailed studies, spherical microgels with a narrow size distribution have been made by optimizing the preparation process. The mobility of lysozyme molecules inside those microgel particles has been investigated. The main conclusion is that high salt and high pH increase the mobility of lysozyme in the gel particles. It implies that high pH and high salt concentration are potential triggers for lysozyme release from the gel. Subsequently, the kinetics of protein release by high pH and high salt concentration is presented. Finally, the antimicrobial activity of lysozyme containing starch gel particles against some bacterial strains is determined. Each aspect mentioned above is described in more detail below.

## **1. Properties of oxidized starch microgel particles**

Oxidized starch microgels of a wide range of cross-link density (weight ratios of cross-linker to polymer  $R_{\text{cross-linker/polymer}}$  0.1 - 0.4) and degree of oxidation (30% - 100%) were prepared by chemically cross-linking TEMPO-oxidized starch polymers. In **Chapter 2** the basic physical-chemical properties such as swelling capacity, charge density, electrophoretic mobility and protein uptake capacity of our oxidized starch microgel particles are established. The results indicate that we have a good chemical control over the charge density of the microgels, which is in good agreement with the expected degree of oxidation (DO). The cross-link efficiency was found to depend on the DO of the polymers, with highly charged polymers leading to more densely cross-linked microgels. The swelling capacity increases with increasing pH and decreasing salt concentration. The uptake of the globular protein lysozyme by the microgels increases with increasing DO and decreasing cross-link density. A highly charged microgel (DO100%) with intermediate cross-link density ( $R_{\text{cross-linker/polymer}}$  0.20) is found to optimally absorb lysozyme. Intermediate cross-link density is optimal

because highly cross-linked gels have too small pores, and low cross-link density gels swell enormously, which is undesirable for most applications.

## 2. Protein uptake by microgel

The microgel DO100% with cross-link density  $R_{\text{cross-linker/polymer}}$  0.20, showing optimum lysozyme uptake, is selected for further investigation. In **Chapter 3** the interaction between protein and the selected microgel has been studied in terms of protein uptake capacity, binding affinity, gel de-swelling behaviour, and charge regulation between protein and gel.

The results can be schematically summarized in the cartoons shown in Figure 1.

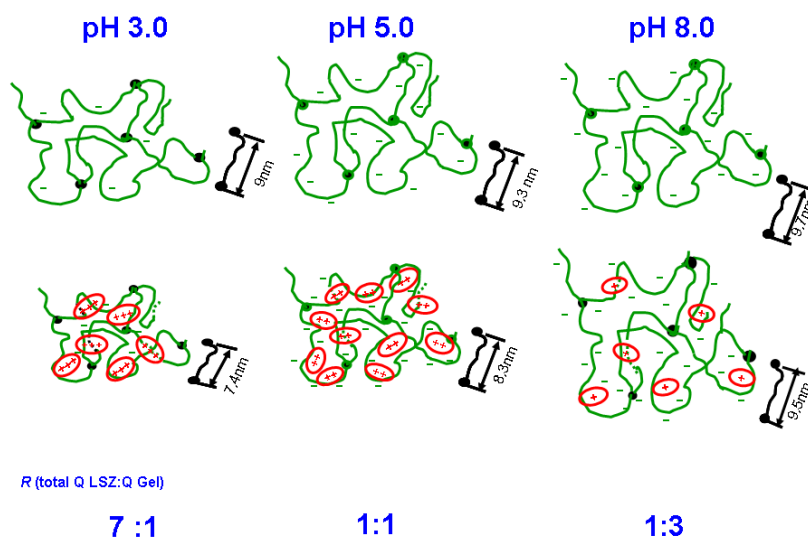


Figure 1. Schematic representation of the DO100% microgel before and after absorbing lysozyme at pH 3.0, 5.0 and 8.0, and ionic strength 0.20 M. Indicated is the average distance between two cross-links (the mesh size), and the total charge ratio  $R$  between the bound protein and the gel, neglecting charge regulation. The number of protein molecules represents the saturation protein uptake  $\Gamma_{\text{sat}}$ ; +++ indicates a high charge density on the protein molecules, + a low charge density. For clarity, the counterions are not included in this sketch.

The cartoons compare the empty gel (upper row) with the fully protein-saturated gel (lower row) at pH 3, 5 and 8 and an ionic strength of 0.2 M. The electric charge density on the gel increases over the pH range 3 - 5, while the average mesh size is only slightly dependent on pH. It indicates that the repulsion among charged polymers in the network contributes little to the swelling of the gel.

The shrinkage of the gel network upon protein uptake increases with decreasing pH. It is caused by the electrostatic attraction between the protein and the gel. Our results suggest that the binding strength depends more on the charge of protein rather than on that of the gel. Lysozyme carries more charges at low pH and therefore the binding is the strongest and the gel shrinks most.

For most applications protein uptake capacity should be high and one should be able to control the binding affinity. For our system the protein uptake capacity at low salt concentration is mainly determined by the charge ratio between protein and microgel and increases with increasing pH. For higher salt concentrations an optimum pH for protein uptake is observed, which shifts to lower pH values with increasing salt concentration. The binding affinity, on the other hand, seems to be dominated by the charge density on the protein and decreases with increasing pH. As a result, lysozyme binds with low affinity at high pH and high salt concentration and is under these conditions easily released by dilution. In contrast, at low pH and low salt concentration lysozyme binds so strongly that dilution does hardly result in any protein release. Therefore, at intermediate pH (around pH 5) there is an optimal balance between protein uptake capacity and binding affinity. Protein release can be triggered by increasing the pH and/or ionic strength.

### **3. Protein mobility inside microgel**

The optimum conditions for protein uptake have been determined in **Chapter 3**; the next step is to investigate protein release. In **Chapter 4**, the mobility of protein molecules inside microgel particles has been studied systematically. The mobility of the protein inside the gel reflects its binding strength to the polymer network, and this, in turn, is important for (triggering) its release.

To study the mobility of lysozyme in an oxidized starch microgel, we successfully prepared well-defined spherical microgels with a narrow size distribution (10 - 20 $\mu$ m in diameter) by emulsion polymerization (see Figure 2A). The newly prepared microgel particles have the same physical-chemical properties as the gel particles obtained following the original preparation method. As is shown in Figure 2B, lysozyme molecules distribute homogeneously over the microgel particles. Figure 2C shows fluorescence recovery after photobleaching (FRAP) in a microgel particle loaded with fluorescently labelled lysozyme. The recovery of the fluorescence the bleached area is measured as a function of time. The exchange rate of bleached with unbleached protein molecules is a measure for their mobility. By fitting the FRAP data with a model based on exchange between bleached and unbleached protein

molecules inside the gel, we identified three protein fractions of different mobility. The protein molecules that have the lowest mobility are strongly bound to the gel. This is attributed to binding of these molecules to multiple sites of the microgel. Increasing the salt concentration (NaCl) or the pH causes a shift in the distribution towards the more mobile fractions (Figure 3). This is consistent with the earlier uptake and release measurements, described in **Chapter 3**, which showed that the binding affinity decreases with increasing salt concentration and pH.

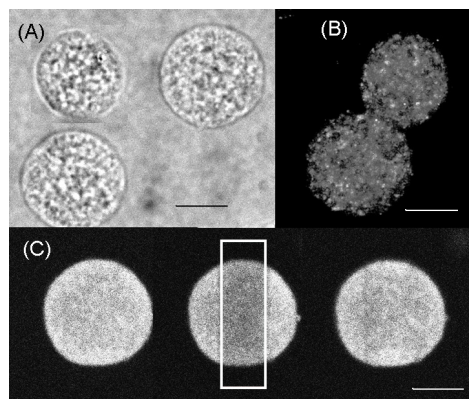


Figure 2 (A) Image of empty microgel particles in water by optical microscopy. (B) 3D image of microgel particles loaded with Alexa-488 labelled lysozyme by fluorescence confocal laser scanning microscopy (CLSM). The scale bars in all figures represent 10  $\mu\text{m}$ . (C) Left: Fluorescence CLSM image of a protein loaded microgel particle before bleaching. Middle: image immediately after photo bleaching (only the part indicated by the rectangle was bleached). Right: image after fluorescence recovery (full recovery takes about 5 minutes).

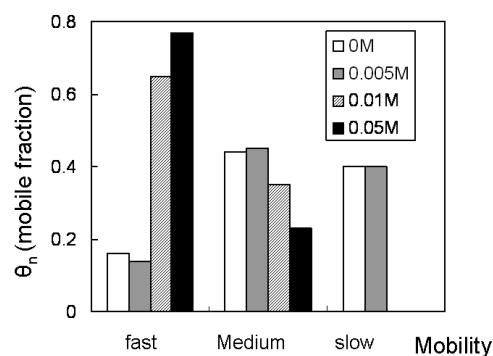


Figure 3. Fractions of bound protein in the gel with different mobilities at pH 7. The low, medium and high mobility fractions are defined by the order of magnitude of the exchange rate  $kC_p$  (respectively  $0.001 \text{ s}^{-1}$ ,  $0.01 \text{ s}^{-1}$  and  $0.1 \text{ s}^{-1}$ ;  $C_p$  is the protein concentration in solution). The results show that the fraction with low mobility has disappeared at high NaCl concentration.

Our model reasonably explains the mechanism of protein mobility inside the microgel, indicating that embedded ingredients with charge properties comparable to those of lysozyme can be protected at low salt concentration and low pH. Increasing the salt concentration or the pH triggers the release.

#### 4. Protein release from microgel

Mobility experiments in **Chapter 4** revealed that high pH and high salt concentration are effective triggers for protein release. Therefore, in **Chapter 5**, the pH and salt-triggered release kinetics are analysed. Figure 4 shows time series of 2D images of protein uptake and protein release (by salt and degradation of the starch gel by amylase).

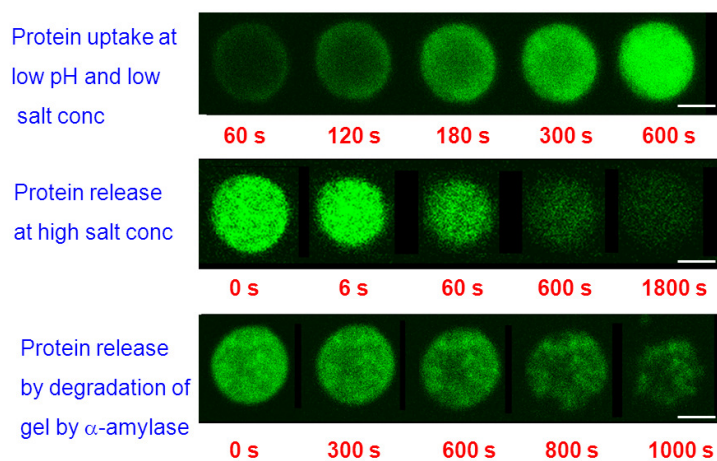


Figure 4. (Top) Uptake kinetics of lysozyme in oxidized starch microgel at pH 3, 10 mM ionic strength. (Middle) Release kinetics of lysozyme at pH 7, 35 mM ionic strength. (Bottom) Release kinetics of lysozyme by  $\alpha$ -amylase in water. The scale bar represents 10  $\mu\text{m}$ .

We modelled the lysozyme uptake in the starch microgel particles on the basis of diffusion theory, taking into account the exchange equilibrium between protein bound to the gel network and free protein in the gel pores. In line with our studies in **Chapter 3** and **4**, the uptake rate increases with decreasing pH and decreasing salt concentration. In case of strong affinity of the protein to the gel, the initial uptake rate is completely determined by diffusion in the medium and therefore by the protein concentration and diffusion coefficient in the solution. The diffusion coefficient of free lysozyme in the gel particles ( $D_{p,g}$ ) is found to be on the order of  $10^{-11} \text{ m}^2\text{s}^{-1}$ , an order of magnitude lower than in solution, due to obstruction by the gel network (including bound protein molecules).



In the release experiments the protein concentration gradient in the medium can be neglected since the protein loaded gel particle is flushed with buffer. The release data for various NaCl concentrations (25, 35, 50 mM) at pH 7 are fitted with Crank's mathematical solution of a substance released from a spherical matrix by Fickian diffusion, holding for the case where diffusion in the medium can be ignored. The release kinetics are essentially invariant with salt concentration when plotted as a function of normalized time,  $t/\tau$ , with  $\tau$  the characteristic diffusion time in the gel. This strongly suggests that the diffusion model is applicable. The time evolution of the protein concentration profiles in the gel seems to reflect this inhomogeneity (the particles are somewhat denser in the centre than near the gel/solution interface). Further investigation of the influence of gel homogeneity on the release behaviour is relevant for the use of the particles in controlled release applications. From the fit, the effective diffusion coefficient  $D_{eff}$  of the protein in the gel, and the concentration ratio  $R$  between bound and free protein have been estimated. These quantities are extremely sensitive to the ionic strength, which is consistent with obtained data on affinity between protein and gel (**Chapter 3**) and mobility of the protein in the gel (**Chapter 4**).

The lysozyme can be released from gel particles at pH 8, 0.01M NaCl but not at pH 3, 0.01M NaCl. This provides opportunities for use of the microgel in food and pharma controlled-delivery applications, since the functional ingredient can in principle be protected in the stomach (low pH), and released in the small intestine (high pH).

We showed that  $\alpha$ -amylase can degrade the oxidized starch microgel (DO30%) leading to release of its protein content into solution. This is an important result, since it demonstrates the feasibility of the use of lysozyme loaded gel particles in, for example, antimicrobial packaging.

## 5 Applications

In view of the observation in **Chapter 5** that degradation of the gel by  $\alpha$ -amylase results into the release of lysozyme, it is expected that the presence of amylase-producing bacteria leads to the release of lysozyme that subsequently kills the bacteria. The aim of **Chapter 6** is to determine the antimicrobial activity of lysozyme containing starch gel particles. DO30% microgel is selected as the gel matrix as it is easily degraded by bacterial amylase.

A preliminary test on bacteria growing on a BHI agar plate indicates that near spots where lysozyme-loaded gel particles are applied also bacteria that do not produce amylase are killed. This may be due to salt-induced release of a very small fraction, i.e., about 2%, of the encapsulated lysozyme in the direct limited region around the application spots. Mixing gel-

lysozyme particles with bacteria in liquid suspension is considered to be a more accurate method to determine the antimicrobial activity of the gel-lysozyme particles. The results show that bacteria that produce amylase and are sensitive to lysozyme, are killed by lysozyme that is released after degradation of the starch gel, whereas the growth of amylase-negative bacteria is not inhibited by the gel-lysozyme particles.

Similarly, the starch gel systems may be used to encapsulate other positively charged antimicrobial compounds, which will be effectively released by amylase activity. It offers great potential for using such systems to diagnose the presence and, subsequently, inhibit proliferation of undesired micro-organisms in food and drugs, and to prevent bacterial infections in processing equipment and biomedical materials.

## **6 Optimization of the system**

The results in **Chapter 5** indicate that protein release by increasing the salt concentration is quite fast (see minutes time scale), which is not always desirable in application. To slow down the protein release from the gel, we successfully built a poly-lysine/poly-glutamic acid complex layer around lysozyme-loaded microgel. This is described in **Chapter 7**. It was found that the layer also protects the gel-lysozyme particles against amylase-degradation. This is extremely useful for applications where the release kinetics have to be controlled, and the incorporated functional ingredients have to be protected from enzymatic degradation.

## Samenvatting

Het doel van het werk beschreven in dit proefschrift was het bepalen van de eigenschappen en bindingskarakteristieken van een nieuw ‘release-on-command’ microgel gemaakt van biopolymeren, genaamd ‘Bioswitch’. Het microgel bestaat uit gecrosslinkte negatief geladen aardappelzetmeelpolymeren en kan daardoor positief geladen functionele ingrediënten opnemen. Deze studie behelst met name de opname en het vrijkomen van het eiwit lysozym (positief geladen beneden pH 10) als functie van de pH en de zoutconcentratie en het effect van amylase, een zetmeelafbrekend enzym.

Allereerst komt de bereidingswijze en karakterisering van het microgel aan de orde. Gevarieerd zijn de oxidatiegraad (OD) van het zetmeel en de cross-linkdichtheid van het gelnetwerk. Deze bepalen de mate van zwelling van de deeltjes in waterige oplossingen, de ladingsdichtheid, de elektroforetische mobiliteit en de eiwitopnamecapaciteit. Vanwege zijn hoge opnamecapaciteit en relatief lage zwelling, is gekozen om verder te werken met het microgel met de hoogste graad van oxidatie, DO100%, en een gewichtsverhouding tussen cross-linker en polymeer van 0.2. Daarnaast zijn veel experimenten uitgevoerd met DO30% microgelen met dezelfde cross-linkerdichtheid, omdat hiervan gemakkelijk goedgedefinieerde bolvormige deeltjes (diameter 10 - 20  $\mu\text{m}$ ) te maken zijn.

Bij opname verdeelt lysozym zich tamelijk homogeen over het microgel. Eiwitopname gaat gepaard met een volumeverkleining van de geldeeltjes. Dit is het gevolg van de elektrostatische attractie tussen het positief geladen eiwit en de negatief geladen gelmatrix. De bindingssterkte tussen eiwit en gel blijkt vooral bepaald te worden door de ladingsdichtheid van het eiwit. Hierdoor zijn de binding en de volumeverkleining het sterkst bij lage pH (ver beneden het iso-elektrisch punt van lysozym). De opnamecapaciteit van het gel wordt voornamelijk bepaald door *ladingscompensatie*: de totale lading van de maximaal opgenomen hoeveelheid eiwit per volume-eenheid gel komt ongeveer overeen met de ladingsdichtheid van het gel. Hierdoor neemt de *opnamecapaciteit* toe met de pH: als de pH toeneemt, neemt de positieve lading op het eiwit af en de negatieve lading van de gel toe, zodat er meer eiwitmoleculen nodig zijn om de lading van het gel te compenseren. De *bindingsaffiniteit* tussen eiwit en gel neemt echter af met toenemende pH, doordat deze vooral gevoelig is voor de lading van het eiwit. Een neutrale pH waarde en lage zoutconcentraties zijn de beste condities voor opname van lysozyme. Afgifte van het eiwit kan getriggered worden door een verhoging van de pH en/of zoutconcentratie. Dit schept mogelijkheden om het microgel te gebruiken voor controlled delivery van functionele ingrediënten in het maagdarmkanaal: het

ingredient wordt beschermd door het gel in de maag (lage pH) en komt vrij in de dunne darm (hoge pH).

De snelheid van uitwisseling tussen vrije en gebonden eiwitmoleculen in het gel is gemeten met CLSM (confocal laser scanning microscopie) in combinatie met FRAP (fluorescence recovery after photobleaching). Er werden een aantal fracties eiwitmoleculen met verschillende mobiliteit (bindingssterkte) gevonden (pH 7). Door verhogen van de zoutconcentratie verschuift de verdeling over deze fracties naar de minder sterk gebonden fracties; bij verlagen van de pH naar pH 3 is er een verschuiving naar de sterker gebonden fracties. Bij lage eiwitconcentraties waarbij het gel nog niet verzadigd is, zijn de eiwitmoleculen zowel bij lage als hoge zoutconcentratie (0 – 0.1 M) gemiddeld sterker gebonden dan bij hoge eiwitconcentratie, waarschijnlijk doordat de moleculen gebonden zijn aan meer bindingsplaatsen op het gel.

De kinetiek van lysozymopname en -afgifte is bestudeerd met CSLM en de resultaten zijn geanalyseerd met een model gebaseerd op diffusie, rekening houdend met de evenwichtsuitwisseling van vrij en gebonden eiwit in de gelmatrix. De met dit model berekende concentratieprofielen van lysozym in de geldeeltjes bij opname van het eiwit komen goed overeen met de experimenteel gevonden profielen. Bij lage pH en lage zoutconcentratie (sterke binding van het eiwit) wordt de limiterende flux van eiwit op het gel/oplossingsgrensvlak volledig bepaald door diffusie vanuit het omringende medium. Uit de afgiftekinetiek bij pH 7 (gemeten onder condities waarbij er geen eiwit zit in de omringende oplossing) is de effectieve diffusiecoëfficiënt van lysozym in het gel afgeleid en de verhouding tussen gebonden en vrij eiwit in de gelmatrix. Deze waarden zijn extreem gevoelig voor de zoutconcentratie.

Amylase breekt het microgel volledig af waardoor lysozym vrijkomt in de oplossing. Dit schept mogelijkheden voor toepassing van het microgel ter voorkoming van de groei van amylase-producerende bacteriën in bijvoorbeeld de levensmiddelensector of infecties van biomaterialen. Om dit verder na te gaan zijn een aantal bacteriestammen gescreend op hun vermogen om amylase te produceren en hun gevoeligheid voor lysozym. Het met lysozym geladen microgel blijkt inderdaad dodelijk te zijn voor amylase-producerende lysozymgevoelige bacteriën, terwijl bacteriën die geen amylase produceren en/of ongevoelig zijn voor lysozym niet in hun groei belemmerd worden.

De afgifte van lysozyme bij verhogen van de zoutconcentratie gebeurt relatief snel (op de tijdschaal van hooguit tientallen minuten). Daarom is als laatste onderdeel van deze studie onderzocht of door middel van een schil van polyelektrolietcomplex (positief geladen poly-L-

lysine en negatief geladen poly-L-glutaminezuur) de afgifte van functionele ingrediënten door het gel afgeremd kan worden. Dit blijkt het geval te zijn en bovendien is gevonden dat de polyelektrolietlaag rond de deeltjes bescherming biedt tegen afbraak door amylase.



DO [%]	Degree of Oxidation
$\kappa^{-1}$ [nm]	Debye length
$R_{\text{cross-linker/polymer}}$ [-]	weight ratio of cross-linker to polymer
$SW_v$ [-]	equilibrium volumetric swelling ratio
$SW_w$ [-]	equilibrium weight swelling ratio
$Q_{\text{max}}$ [C g <sup>-1</sup> ]	maximum charge density when all charged groups are dissociated
$Q_{\text{gel}}$ [C g <sup>-1</sup> ]	charge density of starch gel
$Q_{\text{prot}}$ [C g <sup>-1</sup> ]	charge density of the protein
$Q_{\text{LSZ}}$ [C g <sup>-1</sup> ]	charge density of the lysozyme
$N_b$ [-]	maximum number of protein molecules that can bind to the gel
$pK_{a,\text{eff}}$ [-]	effective intrinsic $pK_a$ value of the dissociation of the COOH groups on starch polymer
$pH_{\text{opt}}$	the pH when the saturation protein uptake is the maximum at certain salt concentration
$\rho_{\text{fix}}$ [C m <sup>-3</sup> ]	fixed charge density
$\lambda^{-1}$ [nm]	softness (relates to gel permeability)
$\mu$ [m <sup>2</sup> s <sup>-1</sup> V <sup>-1</sup> ]	electrophoretic mobility (electrophoretic velocity per unit field strength)
$\eta$ [Pa s]	viscosity of solvent
$\gamma$ [Nm <sup>-4</sup> s]	effective friction coefficient for the solvent in the microgel
$\Gamma$ [-]	lysozyme uptake (gram protein per gram dry gel)
$\Gamma_{\text{max}}$ ( $\Gamma_{\text{sat}}$ ) [-]	maximum lysozyme uptake (the plateau value of absorption isotherm)
$C_{\text{salt}}$ [M]	salt concentration in solution (usually means [NaCl])
$C_{\text{int, max}}$ [M]	maximum internal salt concentration for microgels
$K_{\text{aff}}$ (d $\Gamma$ /d $C_{\text{prot}}$ ) [L g <sup>-1</sup> ]	binding affinity (the initial slope of the protein absorption isotherm)
$P_{\text{release}}$ [%]	percentage of protein released from microgel by dilution
$v_e$ [mol cm <sup>-3</sup> ]	effective cross-link density of polymer gel
$V_1$ [cm <sup>3</sup> mol <sup>-1</sup> ]	molar volume of the solvent
$V_2$ [-]	volume fraction of polymer in the swollen gel
$\chi$ [-]	polymer-solvent Flory-Huggins interaction parameter
$\rho_p$ [g cm <sup>-3</sup> ]	Density of the dry polymer in gel

$M_c$ [g mol <sup>-1</sup> ]	average molecular weight between cross-links
$\zeta_{empty}$ [nm]	mesh size of the empty gel
$\zeta_{filled}$ [nm]	mesh size of the microgel after protein uptake
$v/v_0$ [-]	de-swelling ratio of polymer gel
$Z_p$ [-]	number charges per protein molecule
$D_{eff}$ [m <sup>2</sup> s <sup>-1</sup> ]	effective diffusion coefficient for the protein in the gel particle
$D_0$ [m <sup>2</sup> s <sup>-1</sup> ]	diffusion coefficient of protein in solution
$\theta_u$ [-]	fractions of unbleached bound protein
$\theta_b$ [-]	fractions of bleached bound protein
$C_{prot}$ [g L <sup>-1</sup> ]	protein concentration in solution
$C_{p,b}$ [g L <sup>-1</sup> ]	bleached protein concentrations in solution
$C_{p,u}$ [g L <sup>-1</sup> ]	unbleached protein concentrations in solution
$kC_p$ [s <sup>-1</sup> ]	exchange rate constant of unbleached protein with bleached protein
$M(t)$ [g]	protein uptake at time $t$
$M_{eq}$ [g]	amount of protein in the gel when equilibrium uptake is reached
$M_{rel}(t)$ [g]	amount of protein released from the gel at time $t$
$M_0$ [g]	initial amount of protein in the gel (at $t = 0$ )
$R$ ( $c_{bound}/c_{free}$ ) [-]	ratio between bound and free protein in the gel
$D_p$ [m <sup>2</sup> s <sup>-1</sup> ]	diffusion coefficient of the protein molecules in solution
$D_{p,g}$ [m <sup>2</sup> s <sup>-1</sup> ]	diffusion coefficient of the protein molecules in gel
$C_p$ ( $c_{bound} + c_{free}$ ) [g L <sup>-1</sup> ]	sum of the bound protein and freely dissolved protein concentrations
$C_p^{eq}$ [g L <sup>-1</sup> ]	protein concentration inside the gel when reach the final equilibrium
$C_p^*$ [g L <sup>-1</sup> ]	initial total protein concentration inside the gel phase before releasing
$\tau$ [s]	characteristic diffusion time
$J_p$ [mol m <sup>-2</sup> s <sup>-1</sup> ]	steady state protein supply flux from the medium to the particle
$a$ [μm]	the radius of the starch microgel particle
OD [-]	optical density/absorbance at certain wavelength
OPSP	oxidized potato starch polymer
TEMPO	2, 2, 6, 6-tetramethyl-1-piperidinyloxy
STMP	Sodium trimetaphosphate
PLL	poly-L-lysine
PGA	poly-L-glutamic acid



## Acknowledgement

Yuan (缘) in Chinese means encountering someone in your life is a very valuable opportunity. Meeting you during my six years stay in The Netherlands is the greatest fortune I have ever had in my life. Thanks to all of you.

First of all, I would like to express my gratitude to my promoter, Willem Norde. Thank you for providing me with the opportunity to start a PhD and your trust in me even though I do not have a strong background in physical chemistry. I am especially thankful for your encouragement in any of my small progresses. It brings me the confidence when I am not certain about myself.

Secondly I would like to thank my supervisor, Martien Cohen Stuart. I am grateful for your comprehensive knowledge and creative ideas. I am very much thankful that you always stand at the side of your students and protect them as a father in a family. Thank you for uniting everyone so well as a group, so that I can always feel at home.

And I am also grateful to my daily supervisor, Mieke Kleijn. You are such a nice and kind lady who seldom refuses to help me, even things like taking my passport in Berlin. I am most thankful for your time and carefulness on revising my manuscripts. It would not have been possible to complete this dissertation without your help.

I also would like to thank my daily supervisor during the first two years of my PhD, Renko de Vries. You taught me how to write a paper, how to do scientific research and how to think. You brought me to the world of physical chemistry. You helped me with my first steps, so that later I could walk smoothly.

Also thanks to Herman van Leeuwen, thanks for your patience every time when you answered my questions. Without you, I could not have worked out the problems of protein diffusion inside the gel.

I am also grateful to Jasper van der Gucht, you were always there answering my questions and giving me inspiring ideas. I also want to thank Dimtry Ershov for helping me to sort out how to use the Confocal Laser Scanning Microscopy.

I am thankful for the help of Ted Sleghek and Johan Timmermans, the supervisors from TNO Quality of Life, our collaborating institute. Thanks for providing assistance with the oxidation of the starch polymers and the preparation of the starch gels.

Thanks to Sachin Kadam and Tjakko Abee for cooperation on the microbiology test of the starch particles.

Thanks to my supervisor of my MSc thesis, Kees de Kruif. You showed me a wonderful world of Colloid Science, which I decide to further explore during my PhD and future career.

It is the time to thank all my nice colleagues at the group of Physical Chemistry and Colloid Science (FYSKO), my second home in the Netherlands. Because of you, I feel very happy when I am at work. The four years at FYSKO is the most unforgettable and happiest period of my life. Special thanks to Josie Zeevat, who always listens to me and gives me a hug when I am feeling sad. Also thanks to Mara Winkels for ordering chemicals and telling gossips. Thanks to Anita ter Haar who helped me to fill in my tax form. Remco Fokkink helped me with lots of questions. Anton Korteweg helped me move and build my sweet apartment in Wageningen. Ronald Wegh kindly solved my computer problems. Willem Threels taught me how to use the first equipment of my PhD. Now I would like to thank all the FYSKO children, Frans Leermakers, Paulina Skrzyszewska, Soumi Banerjee, Katarzyna Zielinska, Yunus Saricay, Armando Hernandez Garcia, Emilia Hilz, Dimtry Ershov, Liyakat Mujawar, Harke Pera, Lennart Beun, Thao Pham, Monika Golinska, Christian Buchcic, Surender Dhayal, Jacob Bouman, Sabine Akerboom, Cecilia Bernardini, Johan Bergsma, Pascal van der Veecken, Kathelijne Wintraecken, Junyou Wang, Huanhuan Feng, Zhang Qiang, Liu Bingtao....I could not stop laughing and being funny when I am with you guys. Thank you very much for bringing me so much happiness!!! I will never forget the fun we had together.

A special word of gratitude, finally, to my nicest officemates and my “parafilms”, Marc Lemmers and Evan Spruijt. Marc, thank you that you were always there to listen to my complaints. Evan, thanks for your kind help and nice company.

Also, I would like to thank my thesis reading committee: Per Hansson, Wim Hennink, Marcel Zwietering and Raewyn Town. Thanks for your time and taking part in this special day for me.

Andre Godkewitsch, thank you very much for your encouragement and wise suggestions. Your kind words gives me so much power.

Hein van Valenburg, my MSc coordinator and my good friend. It is my best luck to have you as my first supervisor in The Netherlands. I am thankful for your continuous support , encouragement and advice for my future.

Participating the Chinese Association in The Netherlands as a volunteer was a fruitful experience I had in my life. I would firstly like to thank the members in CASSW (Chinese Association of Students and Scholars in Wageningen) when I held the Chair. All of you helped me organizing so many wonderful activities: Lin Huning, Zhang Ningwen, Tang Yun,

Wang Yiding, Sun Beibei, Kang Ning, Zhang Xiaxia, Liu Chun Jie, Jiang Yuki, Qian didi, He Hanzi, Chen Xiaotong, Shang Haolv, Liu Jixin, Shi Zhuyan, Li Yang, Ye Zhenwei, Han kun, Deng Shixuan, Li Jimeng and Sun Zhaozheng. Secondly I would like to thank the colleagues when I am working in ACSSNL (Association of Chinese Students and Scholars in The Netherlands): Yu Miao, Li Chen, Mao Ziqian, Rao Xiangyu, Liu Fangbin, Li Jiayang, Xiang Fei and Yang Peng. Most importantly, I would like to thank Rien Bor, for his support to our Chinese Association. I am also grateful to Luo Ping, Zhang Xiaodong and Xia lei, who are the officers working in the Education Section of the Chinese Embassy in The Netherlands.

Thanks to all my good friends in The Netherlands; because of you, I am not alone here. Firstly I want to thank my old friends who I knew six years ago when I just arrived at Wageningen: Koko Wei, Gao Ran, Li Pengpeng, Jiang Jing, Zhu Ming, Xiao Yinghua, Cai Hengzhe, Wang Xingxin, Zheng Xiaowei, Liu Xiao, Huang Huiyan, Liu Huaifeng, Nie Haisheng, Chen Xu and Guan Xiaoyu. I also would like to thank the “Female PhD Organization”: Wu Jing, Lu Jing, Li Hui, Li Jia, Feng Yan and Liu Wenling. You are all beautiful, smart and lovely girls (including me!); thanks for spending time with me, playing “Mahjong”, shopping and having a nice weekend together. Many thanks to other friends I knew later, who helped me and with whom I spent happy times: Lu Xifeng, Wang Junli, Tian Lijin, Luo Jing, Wang Si, Yi Liya, Wang Lizheng, Dai Yue, Song Yang, Ning Lei, Li Min, Lu Yu, Bing Xiaoyun, Wang Xiaolin, Li Feng, Zhang Yuan, Chen Tie, Liang Dan and Jin Shuqing. Special thanks to Chen Xia, Zhang Yali, Zhao Jingjing and Yan Yun, thanks for your support from China.

Thanks to Prof. Zhang Liye who came from China to The Netherlands and “interviewed” me in June this year.

Finally, my deepest gratitude to my parents for their endless and unconditional love, making me full of courage and happiness. Thanks to my dearest father, Li Mingjian; you are such a selfless man that gives your daughter everything you have. Thanks to my mother, Gu Yanhua; you are always there to give me wise and warm words at the other side of the telephone.

I would like to thank everybody else who came or was willing to come to Wageningen today (21<sup>st</sup> of October, 2011), to celebrate with me this particular day.

*Yuan Li (李媛)*

*Wageningen,  
October 2011*



## Curriculum Vitae



Yuan Li was born on the 6<sup>th</sup> of April 1982 in Lanzhou, Gansu province in the northwest of China. After receiving her Bachelor of Science degree in Food Science and Nutritional Engineering at China Agricultural University in Beijing in 2005, she came to The Netherlands to pursue a Master of Science program in Food Technology, specializing in Dairy Science and Technology at Wageningen University. In 2006 she submitted her Master thesis on alpha-lac nanotubes with Prof. C. G. de Kruif at Nizo Food Research, Ede. Thereafter, she did an Internship at DSM Food Specialist in Delft on a project involving the synthesis of a functional polysaccharide for infants. She received her Master of Science degree in 2007 and in the same year she started her PhD research in the Laboratory of Physical Chemistry and Colloid Science at Wageningen University. This research was about using oxidized starch microgels as a novel carrier for encapsulation and release of functional ingredients. The results are presented in this thesis.



## List of publications

Y. Li, R. de Vries, T. Slaghek, J. Timmermans, M.A. Cohen Stuart, W. Norde, Preparation and Characterization of Oxidized Starch Polymer Microgels for Encapsulation and Controlled Release of Functional Ingredients, *Biomacromolecules*, 10 (2009) 1931-1938.

Y. Li, R. de Vries, J.M. Kleijn, T. Slaghek, J. Timmermans, M.A. Cohen Stuart, W. Norde, Lysozyme Uptake by Oxidized Starch Polymer Microgels, *Biomacromolecules*, 11 (2010) 1754-1762.

Y. Li, J.M. Kleijn, T. Slaghek, J. Timmermans, M.A. Cohen Stuart, W. Norde, Mobility of lysozyme inside oxidized starch polymer microgels, *Soft Matter*, 7 (2011) 1926-1935.

Y. Li, Z. Zhang, H.P. van Leeuwen, M.A. Cohen Stuart, W. Norde, J.M. Kleijn, Uptake and release kinetics of lysozyme in and from an oxidized starch polymer microgel. Accepted in *Soft Matter*, DOI:10.1039/C1SM06072D.

Y. Li, S. Kadam, T. Abee, T. M. Slaghek, J. W. Timmermans M.A. Cohen Stuart, W. Norde, J.M.Kleijn, Antimicrobial starch microgel to detect and kill amylase-producing microorganism. Submitted to *Food Hydrocolloids*.

Y. Li, M.A. Cohen Stuart, W. Norde, J.M.Kleijn, The stabilization of lysozyme-loaded starch microgel by polyelectrolytes. Submitted to *Langmuir*.

B. Trappmann, J. E. Gautrot, J. T. Connelly, Y. Li, M. L. Oyen, M. A. Cohen Stuart, H. Boehm, J. P. Spatz, F. M. Watt, W. T. S. Huck. Extracellular matrix tethering rather than substrate stiffness regulates epidermal stem cell fate. Submitted to *Nature Materials*.





## **Overview of completed training activities**

### ***Courses***

Summer School: POLYAMPHI, The Netherlands, 2007

Summer school: Scattering methods, Bombannes (France), 2008

Winter school: Physical chemistry, Han-sur-Lesse (Belgium), 2008

Techniques for writing and presenting a scientific paper, Wageningen, 2008

Colloid Science, Wageningen, 2008

Chemistry and physics of supramolecular systems, Wageningen, 2008

Advanced soft matter, Wageningen, 2008

### ***Conferences and Colloquia***

Polysaccharides as Food Colloids and Biomaterials: Fundamentals and Applications, Wageningen, 2007

EFFoST/EHEDG Joint Conference, Lisbon (Portugal), 2007<sup>+</sup>

6<sup>th</sup> meeting industrial platform CRC, Wageningen, 2008\*

Dutch Polymer Days, Lunteren (The Netherlands), 2008

23<sup>rd</sup> European colloid and interface science conference, Antalya(Turkey), 2009\*

3<sup>rd</sup> Delivery of functionality in complex food system, The Netherlands, 2009<sup>+</sup>

11<sup>th</sup> European symposium on controlled drug delivery, The Netherlands, 2009<sup>+</sup>

20<sup>th</sup> Polymer network group meeting, Goslar (Germany), 2010<sup>+</sup>

85<sup>th</sup> ACS colloid and surface science symposium, Montreal (Canada), 2011\*

\*=oral contribution, +=poster

### ***Other meetings and activities***

PhD Competence Assessment, Wageningen, 2007

PhD trip 2009, Swiss and France

PhD trip 2011, Southeast Asia

Group meetings 2007-2011

**Cover image:** the rainbow belts symbolize the paths to deliver the drugs which are encapsulated inside the microgel particles. In the end the released drugs go to the center of the rainbow circle, which means that they arrive at the target place to bring health. The cover is designed and made by Wang Danyu, a friend of mine.

**Printing:** GVO drukkers en vormgevers B.V. / Ponsen en Looijen, Ede, NL